

# Cohesive Sediment Erosion Induced By Coandă-Effect-Based Polymetallic-Nodule Collector

# Small-scale experiments

Ву

# M. Suleman

To obtain the degree of Master of Science at the Delft University of Technology,

September 2023

This thesis is confidential and cannot be online published before 08-09-2025

#### Graduation committee:

Dr.ir. Said Alhaddad Daily Supervisor
Dr.ir. Alex Kirichek Chairman
Prof.dr.ir. Cees van Rhee Supervisor
Dr.ir. Claire Chassagne Supervisor



# Preface

This master's thesis delves into the intricate study of cohesive sediment erosion by a Coandă-Effect-Based Polymetallic-Nodule Collector. As the final phase of the Master Structural Engineering program at Delft University of Technology, this research marks a significant milestone in my academic journey.

I express my heartfelt gratitude to my esteemed graduation committee, whose unwavering support and guidance played a pivotal role in shaping this thesis. My sincere appreciation goes to Dr.ir. Alex Kirichek, who not only served as a committee member but also facilitated the essential funding for this research. Unfortunately, we bid farewell to the esteemed Prof. dr. ir. Cees van Rhee, who was a valuable member of the committee and who is dearly missed. Special recognition is extended to dr. ir. Said Alhaddad, my daily supervisor, whose invaluable mentorship led to the attainment of the most accurate results throughout this research. I am deeply grateful to dr. ir. Claire Chassagne, who graciously accepted to join the committee after the passing of dr. Cees, thereby ensuring continuity and comprehensive evaluation.

I would like to extend my gratitude to Andre van den Bosch, Chantal Willems, and Ed Stok for their assistance during the experimental phase. Their expertise and collaboration greatly contributed to the successful execution of the experiments.

To my family and friends, I am profoundly thankful for their unwavering support and encouragement throughout this challenging yet rewarding journey. A special thank you is reserved for Anas Abbasi, Anass Kariouh, Dennis Ronckers, and Diaa Abbasi, whose assistance and camaraderie were invaluable during the experiments.

Mohammed Suleman

Delft, September 2023

## **Abstract**

The increasing demand for rare minerals, such as lithium, cobalt, and copper, driven by the growth of the world population and the transition towards sustainable energy technologies, has become a pressing concern. These minerals are crucial for electrifying the transportation sector through electric vehicle production and are in high demand for the thriving high technology industry. However, their scarcity and high prices due to supply shortages necessitate alternative sources to meet these demands. In recent years, deep-sea mining has emerged as a promising solution to address the growing need for rare minerals. The vast potential reserves in the ocean floor offer an enticing opportunity for exploration and extraction. However, deep-sea mining comes with its engineering and environmental complexities that require thorough investigation and understanding. This research delves into the experimental study of a Coandă-Effect-Based Collector, aiming to understand its behaviour regarding water entrainment and cohesive sediment erosion. The focus is on understanding the collection mechanism to minimize clay pickup and maintain low clay concentration in the discharged mixture. This is vital in mitigating the impact of deep-sea mining activities on the marine environment.

The study explored the influence of various operating parameters, including the collector's forward velocity, jet velocities, and bottom clearance, on these processes. The results revealed intriguing trends in water entrainment behaviour, with a larger bottom clearance leading to a lower flow rate in the collection duct. However, discrepancies were observed in comparison to previous studies, emphasizing the complexity of the collection mechanism and the need for a comprehensive understanding of influencing factors. Additionally, the study analysed the erosion depth of the clay bed under different conditions. It was found that the collector's forward velocity is inversely proportional to the erosion depth, while an increased jet velocity resulted in a larger erosion depth. Furthermore, the bottom clearance of the collector contributed to a greater erosion depth. These findings align with previous studies conducted on non-cohesive sediment erosion. Moreover, Clay erosion primarily occurs due to the jetting mechanism. This study investigated the correlation between erosion depth and both impingement force and dynamic pressure. The results showed that a logarithmic function describing the relationship between impingement force and erosion depth did not adequately fit the data. This observation contrasts with the findings of Alhaddad & Helmons (2023) for sand erosion, where a clear logarithmic correlation between erosion depth and impingement force was established. In contrast, a higher erosion depth was linearly linked to increased dynamic pressure. Furthermore, the investigation introduced the concept of the secondary jet duct's impact on water entrainment. Surprisingly, the flow rate in the collection duct increased with the presence of the secondary jet duct, even when it had zero flow rate. A hypothesis was formulated, suggesting that the duct enhances the development of a horizontal flow pattern, leading to higher velocities under the collector head and more water being directed towards the collection duct. Besides, Front velocities and the velocity of the turbidity current exhibited minimal variations, suggesting a consistent spillage plume behaviour across various operating parameters.

In conclusion, this research provides valuable insights into water entrainment and cohesive sediment erosion in the context of the Coandă-Effect-Based Collector. The findings emphasize the significance of operating parameters and shed light on the complexities of the collection mechanism. Future studies should explore additional data collection to understand the influence of the secondary jet duct better and employ reliable methods for measuring clay concentrations in the discharged water. Overall, these findings have important implications for optimizing collector design and mitigating the environmental impact of nodules mining activities.

# Contents

Pre	face			iii
Ab	stract			V
1.	Intro	duct	ion	1
-	l.1.	Gen	eral Background	1
-	1.2.	Prob	olem Description	6
:	1.3.	Rese	earch Objective	8
2	L.4.	Rese	earch Methodology	9
2	1.5.	Stru	cture of The Final Report	10
2.	Coh	esive	Sediment	11
2	2.1.	Clay	of The Clarion Clipperton Zone (CCZ)	11
2	2.2.	Eros	ion	12
2	2.3.	Aggı	regation	13
2	2.4.	Sett	ling Velocity	14
2	2.5.	Con	solidation and Erosion Resistance	15
3.	Jets	and <sub>l</sub>	plumes	16
3	3.1.	Jetti	ng	16
3	3.2.	Plun	nes and Turbidity Currents	17
4.	Coai	ndă-E	Effect-Based Collector	19
4	<b>1.1</b> .	Wat	er entrainment	19
4	1.2.	Spill	age	20
4	1.3.	Eros	ion of Sand	20
4	1.4.	Scali	ing	21
5.	Ехре	erime	ental Research	22
į	5.1.	Ехре	erimental Setup	22
į	5.2.	Instr	rumentation	23
į	5.3.	Test	Procedure and Data Acquisition	28
į	5.4.	Clay	Characterization	34
	5.4.2	1.	Composition of Clay	34
	5.4.2	2.	Shear strength	35
	5.4.3	3.	Particle size distribution	35
	5.4.4	1.	Bulk Density of clay	36
	5.4.5	5.	Solid content	36
6.	Resu	ılts		37
(	5.1.	Wat	er Entrainment	37
6	5.2.	Clav	Erosion	40

	6.2.1.	General Description of Clay Erosion	. 40
	6.2.2.	Forward Velocity	. 40
	6.2.3.	Bottom Clearance	. 42
	6.2.4.	Main and Secondary Jet Velocities	. 44
	6.2.5.	Time Effects on Clay Erosion	. 46
	6.2.6.	Reproducibility of Experiments	. 47
	6.3. Ana	lysis of Clay Erosion	. 48
	6.3.1.	Impingement Force	. 48
	6.3.2.	Dynamic Pressure	. 50
	6.3.3.	Erosion Patterns	. 52
	6.3.4.	Scaling	. 53
	6.3.5.	CCM Results	. 54
	6.4. Seco	ondary Jet Duct	. 55
	6.4.1.	Water Entrainment	. 55
	6.4.2.	Clay Erosion	. 57
	6.5. Turk	pidity Currents	. 59
7.	Conclusio	ons	. 62
8.	Discussio	n and Recommendations	. 65
Re	eferences		. 67
A.	Experiment	al Setup	. 70
В.	Water Er	ntrainment	. 74
	B1. Influence	ce of The Different Parameters	. 74
	B2. Influence	ce of The Secondary Jet Duct	. 75
C.	Clay Bed Er	osion	. 76
	C1. Prepara	tion of Clay	. 76
	C2. Conduc	ted Experiments	. 77
	C3. CCM Re	sults	. 78
	C4. Pictures	of Eroded Clay Bed after Experiments	. 79
D.	Turbidity co	urrents	. 87
	D1. x-t Diag	rams of Turbidity Currents	. 87
	D2. Vertical	Velocity Profiles	. 90

# 1. Introduction

# 1.1. General Background

The need for rare minerals (e.g., lithium, cobalt and copper) is increasing since new technologies and energy transition are dependent on these minerals. Hereby, the growth of the world population and the aim to reduce carbon emissions are important factors. These minerals are critical for electrifying the transportation sector through the production of electric vehicles. The high prices of these minerals due to high demand and supply shortage force the European countries to search for alternatives since these minerals are essential to the high technology sector (Hein et al., 2013a)

The rising demand for rare minerals and the depletion of land-based resources have increased the interest in deep-sea mining. Deep-sea mining is a rising industrial field that covers the mining of deposits from the seabed. Multiple companies like Allseas have now exploration licenses to test their designed collecting machinery (Allseas, 2022). Commercial licenses are not yet given due to a shortage of knowledge about the effects of mining on existing flora and fauna. In the deep ocean, different deposits can be found such as cobalt-rich crusts (CRCs), seafloor massive (polymetallic) sulfides (SMS), and manganese (polymetallic) nodules (Miller et al., 2018). A map showing where these deposits can be found is presented in Figure 1. The nodules can be found in large amounts in the Pacific and Indian oceans, especially in the Clarion Clipperton zone (CCZ) (Hein et al., 2013a).

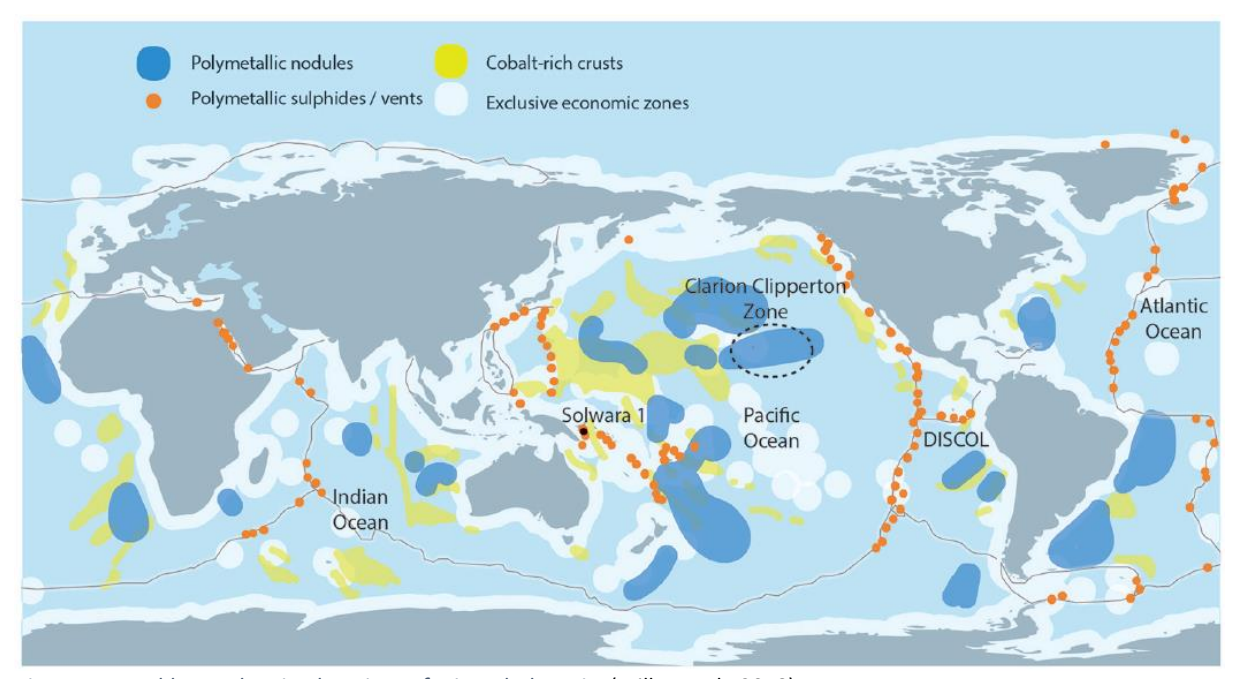


Figure 1 A world map showing locations of minerals deposits (Miller et al., 2018)

#### **Clarion Clipperton Zone**

The Clarion Clipperton Zone (CCZ) in the Pacific Ocean has been the most extensively explored area for deep-sea mineral (DSM) prospects and is estimated to contain 34 billion tons of polymetallic nodules over 9 million km². The weight of polymetallic nodules per square meter of the Clarion-Clipperton Zone (CCZ) seabed can vary depending on several factors, such as the size, density, and abundance of the nodules. However, on average, the weight of nodules per square meter is estimated to be around 5-10 kilograms (Vanreusel et al., 2016). In the 1970s and 1980s, there was a surge in interest in deep-sea mining, particularly for polymetallic nodules in the CCZ. A few trial runs were conducted by contractors, but plans were eventually abandoned due to declining metal prices. The OMA consortium collected about 500 tons of nodules in 1977 and 1978 using a combination of towed collectors and airlifting.

Another consortium, OMI, mined about 800 tons at a water depth of 5,500 m using a remotely operated underwater vehicle (ROV) connected to a pumping system. The other consortia, OMCO and AFTERNOD, were unable to mine any minerals (Schulte, 2013).

#### **Polymetallic nodules**

The polymetallic nodules are rocky lumps rich in commercially interesting minerals such as nickel, copper, manganese, iron oxides, and zinc (see Figure 2). As mentioned before, these nodules were discovered more than a century ago. Nevertheless, meanwhile, land-based resources were discovered. Besides, the lack of legal certainty in the international water and security of tenure has led to minimizing the interest in mining the polymetallic nodules (Beaudoin & Baker, 2013). Recently, the interest in polymetallic nodules came back to life as a consequence of the depletion of land-based resources and the rising demand for minerals alongside the aim toward energy transition (Miller et al., 2018).

Polymetallic nodules are present on the seabed on abyssal plains at 4000 to 6500 m under sea level. They lie on the seabed or are partially/completely buried in it (see Figure 2) Nodules are slowly formed over a long period. The growth rate is around 1 to 10 cm per million years. The majority of these nodules have an average size of 5 to 10 cm and they can be 20 cm in size (Haldar, 2018).



Figure 2 Polymetallic nodules partly/completely buried in the sea bed (**left**) and the cross-section of a polymetallic nodules (**right**) (Miller et al., 2018)

#### Mining operations

During mining, the nodules and sediments are disturbed and collected together, creating a sediment trail behind the hydraulic collectors termed as discharge sediment plume. This plume can be carried by ocean currents, potentially affecting ecosystems under water far from the mining site. Forecasting the spread and impact of the sediment trail is a crucial aspect in assessing the environmental impact of deep-sea mining. Therefore, designing a collector with minimized environmental effects is a key factor to obtain a commercial license (Global Sea Mineral Resources, 2018).

Mining technology of polymetallic nodules consists mainly of three operations, see Figure 4:

• Nodule collector: there are three mechanisms by which the nodules could be collected (see Figure 3): hydraulic, mechanic, and hybrid. Mechanical collectors use moving parts to gather and transport the nodules. They do this by using rotating scoops to dig into the top layer of the seabed and collect the nodules, which are then carried to a conveyor belt. On the other hand, hydraulic collectors do not physically come into contact with the nodules or the sediments. Instead, they create a pressure difference to pick up the nodules, reducing the disturbance to the seabed environment. Hybrid collectors combine both mechanical and hydraulic methods, with the nodules first being dislodged from the seabed using hydraulic pressure and then transported using a mechanical conveyor (Hong et al., 1999).

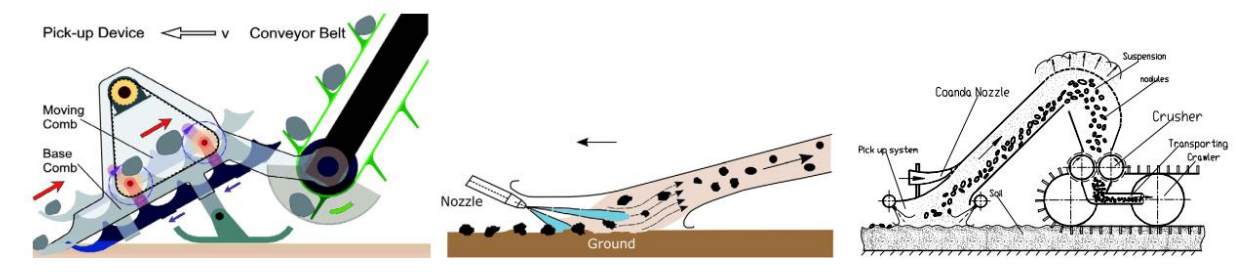


Figure 3 Different mechanisms to collect polymetallic nodules from the seabed; mechanical (left), hydraulic (middle) (ISA, 2001) and hybrid (right) (Yang & Tang, 2003)

The hydraulic method has the preference since the collector causes the least disturbance to the seabed. This is desirable from an environmental point of view since it leads to a minimized interaction with the seabed. This method is also preferred from a commercial point of view since it has a higher pickup efficiency. The collector operates by creating a flow of water over the nodules on the seabed. This flow generates lift and drag forces on the nodules, with the lift force lifting the nodules vertically and the drag force directing the nodules into the collector's collection duct (Alhaddad et al., 2023).

- Separation system: separates the collected nodules from collected sediment. This is done using a
  flow of clean water to separate the nodules from the suspended sediment, reducing the amount
  of sediment that enters the vertical transport system. This is environmentally beneficial as it helps
  to keep the sediment near the seabed. This is also important to reduce costs by minimizing the
  sediment amount transported to the sea surface. Besides, it limits the suspended plume of
  discharged sediment in the mining area (Global Sea Mineral Resources, 2018).
- Vertical transport system: The material is lifted from the collector to the mining vessel through a vertical transport system and pumps. During transportation, the abrasive forces and the action of the riser pumps cause some of the nodules to experience crushing and grinding, resulting in a change in their particle size distribution (PSD) to a finer grain upon reaching the sea surface. The effects of various steps in the transportation process on the quality and fragmentation of the nodules must be assessed to determine their condition when they reach the mining platform on the sea surface. In addition to the impact of transportation through the riser pipes, the nodules will also face a number of centrifugal pumps, estimated to be 12 in number, which will also impact the condition of the nodules (e.g. causing structural disintegration or degradation) (Lang et al., 2019).

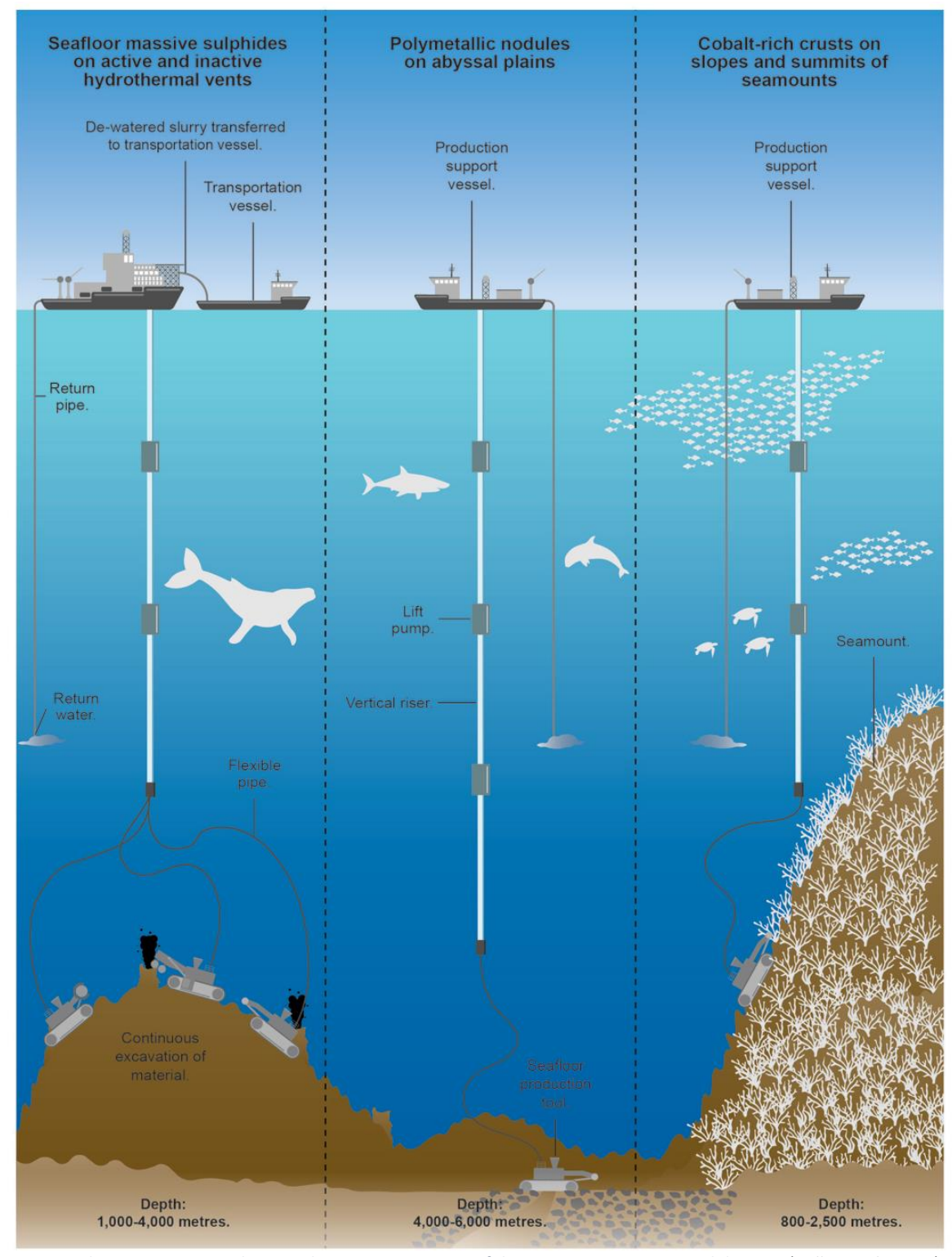


Figure 4 A schematic overview showing the mining processes of the most important mineral deposits (Miller et al., 2018)

#### Coandă-effect-based method

The literature mentions various hydraulic collection methods (ISA, 1999), such as the suck-up-based method, the Coanda-effect-based method, and the double-jet method. The Coandă-effect-based method is believed to result in less sediment disturbance, as the nozzle flow does not directly interact with the seabed. This research focuses on the Coandă-effect-based collector, which is considered the most advanced technology for nodule collection and has been used in recent pilot tests. The collector

utilizes the Coandă effect, a fluid-mechanical phenomenon where a jet flow adheres to an adjacent surface even if it curves. The collector consists of four curved surfaces forming three ducts: the main jet duct, the secondary jet duct, and the collection duct (see Figure 5). As a result of the Coandă effect, the high-velocity water jets flow along the upper curved plate and entrain ambient water towards the collection duct, creating a suction under the collector and dislodging and dragging nodules towards the collection duct (Alhaddad et al., 2023).

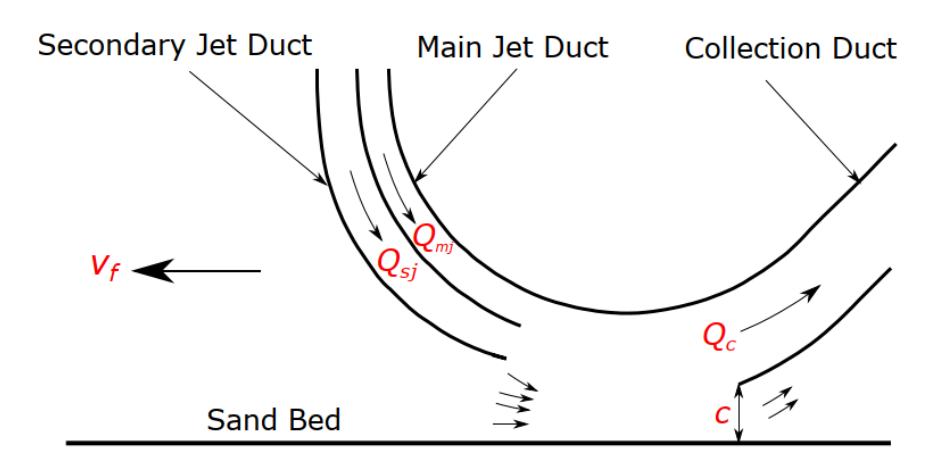


Figure 5 Diagram of the Collector Head: The velocity of the collector is shown as  $v_f$ , and the bottom clearance is denoted by c. The flow rate in the main jet duct, secondary jet duct, and collection duct are represented by  $Q_{mj}$ ,  $Q_{Sj}$ , and  $Q_c$ , respectively. The direction of water entrainment is depicted by small arrows above the bed (Alhaddad et al., 2023).

#### **Cohesive sediment erosion**

Cohesive sediment erosion is a complex process that involves the detachment and transport of fine-grained particles that have a high degree of interparticle bonding, such as clay and silt. The cohesive forces between the particles in the sediment can make it difficult for the water flow to detach and transport them, leading to different erosion mechanisms depending on the hydraulic conditions and sediment properties (Wang, Yang, & & Zhao, 2013).

One of the key theoretical frameworks for cohesive sediment erosion is the concept of shear stress and critical shear stress. Shear stress is the tangential force exerted by flowing water on the sediment bed, and it can be influenced by factors such as water velocity, flow depth, sediment properties, and bed roughness. Critical shear stress, on the other hand, is the minimum shear stress required to initiate sediment erosion and transport. When the shear stress exceeds the critical shear stress, cohesive sediment particles can be detached and transported (Winterwerp & Kesteren, 2004). Different erosion mechanisms can operate depending on the hydraulic conditions and sediment properties. For example, in laminar flow conditions with low shear stress, the cohesive forces between the sediment particles may dominate and lead to erosion through cohesive failure or consolidation. In turbulent flow conditions with high shear stress, erosion can occur through particle-by-particle detachment, abrasion, or fluidization (Mehta & Apte, 2019).

In addition to the hydraulic and sediment factors, other environmental factors can also influence cohesive sediment erosion, such as salinity, pH, and organic matter content. Theoretical and experimental studies have contributed to a better understanding of the complex interplay between these factors and the erosion processes, leading to the development of predictive models and engineering solutions for mitigating the impact of cohesive sediment erosion in different settings (Winterwerp & Kesteren, 2004).

# 1.2. Problem Description

The Coandă-effect-based collector mentioned in (Alhaddad et al., 2023) is not only collecting nodules but also a layer of sediment of 5 to 15 mm (Global Sea Mineral Resources, 2018). The separation system of the collector separates about 90% of the collected sediment (Lang et al., 2019). The separated sediment will be discharged at the rear side of the collector creating a sediment plume. Accurately forecasting the depth of sediment picked up by the collector is crucial for estimating the hydrodynamic behaviour of the sediment plume produced, particularly its run-out distance. To achieve this, the concentration of sediment in the discharge can be estimated based on the amount of eroded sediment, which can be utilized as an input parameter in numerical models.

The consequences of deep-sea mining on biodiversity and its effect on ecosystem function are uncertain. To mitigate the loss of biodiversity, some have proposed to offset it by replacing one type of ecosystem (e.g. coral reefs) with another (e.g. abyssal nodule fields) (Niner et al., 2018). The mentioned study evaluates the challenge of achieving no net loss (NNL) of biodiversity through deepsea mining, using the mitigation hierarchy of avoidance, minimization, and remediation. They concluded that NNL of biodiversity is not achievable at this time. This is because deep-sea environments are highly susceptible to mining impacts, there is limited technology to minimize harm, significant gaps in existing ecological knowledge, and the potential for recovery of deep-sea ecosystems is uncertain. Therefore, the only viable means of reducing biodiversity loss from seabed mining at present are avoidance and minimization of impacts. From an engineering perspective, this could be done by minimizing the sediment discharge plume at the rear side of the collector, so it settles quickly and keeps the disturbance in a limited area. Besides, the spreading of the sediment plume over a not yet collected area will result in a sedimentation layer around the moving collector and thus the nodules get buried in this layer. This deposited sediment will be collected again at a later stage, thus decreasing the collector's pickup efficiency. The ratio nodule/sediment will be higher. Therefore, from an economic perspective, the sedimentation plume needs to be minimized.

There are still many unknowns (e.g., run-out distance and influence on flora and fauna) about the impact of a Coandă-effect-based collector on sediment erosion. Therefore, it has been a subject of concern for researchers. Alhaddad & Helmons (2023) conducted small-scale experiments with non-cohesive sediment to gain a better understanding of the collector's interaction with the sediment bed. Results showed that the collector's forward velocity and jet velocity affect the depth of sediment erosion. The bottom clearance of the collector head to the sediment bed and the angle at which the water jets strike also play a role in sediment erosion.

The study of Alhaddad & Helmons (2023) aimed to determine the sand bed erosion depth of a Coanda-effect-based hydraulic collector in polymetallic nodule mining through small-scale experiments (see Figure 6). The results showed the importance of optimizing the collector's forward velocity, as it is inversely related to sediment erosion depth. Increasing jet velocity and reducing bottom clearance both result in deeper erosion. The study also found that oblique water jets destabilize the sediment bed, leading to sediment pickup. The erosion depth is logarithmically proportional to the flow force impinging on the bed, meaning minimizing erosion requires minimizing this force. Additionally, the study found that the entrainment of ambient water contributes to sediment plumes behind the collector. These findings improve the predictability of sediment erosion caused by Coandă-effect-based collectors, allowing for better optimization of collector design to minimize sediment plumes.

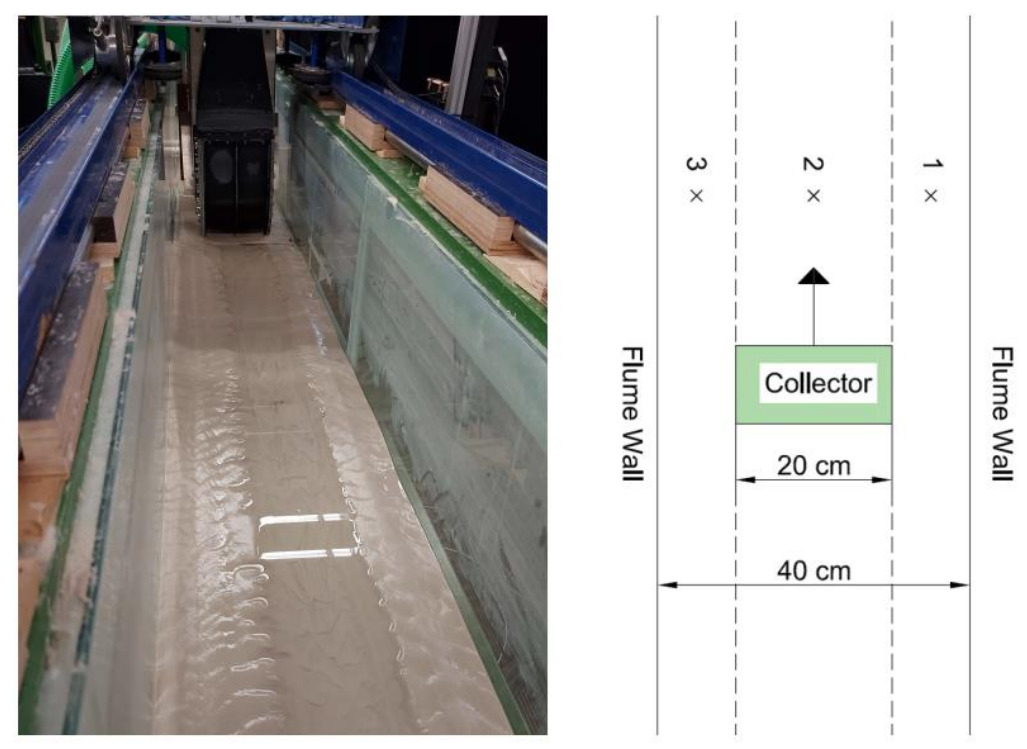


Figure 6 Trench in sand bed due to erosion (left) and schematic view of the flume (right) (Alhaddad & Helmons, 2023).

#### 1.3. Research Objective

Forecasting the depth of the sediment layer picked up by the collector is a crucial aspect of evaluating the hydrodynamic characteristics of the sediment plume that it generates, especially its run-out distance. The run-out distance refers to how far the plume travels from the point of discharge and is influenced by several factors, including the concentration of sediment in the plume. This concentration is dependent on the quantity of sediment passing through the collector and therefore plays a critical role in determining the extent of the sediment plume using numerical modelling methods. The focus of this study is to unravel the primary mechanism responsible for eroding the bed of cohesive sediment during collector operation through small-scale experiments. This will enable mitigating the environmental impact of a Coanda-effect-based hydraulic collector. By understanding the parameters that have the greatest impact on bed erosion (forward velocity of the collector ( $v_f$ ), jet velocities ( $Q_{mj}$  and  $Q_{sj}$ ), and bottom clearance (c)), the experiments will be designed to address the following research questions:

# 1. What is the influence of the collector's forward velocity, jet velocities, and bottom clearance on the water entrainment into the collection duct?

Higher jet velocities are expected to result in increased water entrainment. Smaller clearances are likely to lead to lower flow rates of entrained water since there is less space available for entrainment (Alhaddad et al., 2023). Conversely, higher forward velocities are anticipated to be associated with higher water entrainment, since the velocity of the water under the collector is anticipated to be higher.

# 2. What is the influence of the collector's forward velocity, jet velocities, and bottom clearance on the erosion of cohesive sediments?

Predictions suggest that cohesive sediments are more likely to erode when the collector's forward velocity is lower, as this results in a longer engagement time with the bed. Additionally, higher jet velocities are expected to cause greater erosion due to the increased impingement force. A smaller bottom clearance may also contribute to higher erosion depth.

#### 3. What is the main mechanism by which clay is eroded?

It is expected that jetting erosion will be the main mechanism by which the cohesive sediment is collected. The research of Alhaddad & Helmons (2023) showed that the sediment bed is primarily disturbed through jetting, whereby water jets impinge at an oblique angle on the bed's surface, resulting in the topmost layer of the bed collapsing. Although, the conclusion was based on noncohesive sediment (sand). This research will verify if cohesive sediment shows similar results.

#### 4. How will the presence of the secondary jet duct affect cohesive sediment erosion?

The presence of the secondary jet duct will influence the water entrainment into the collection duct. Water entrainment refers to the process by which water is carried along with a fluid or material flow, such as a current or a stream of air (Rogers & Gawarkiewicz, 2018). It is predicted that the secondary collection duct will reduce the water entrainment, thus erosion of sediment bed will be reduced.

# 5. What is the influence of the collector's forward velocity, jet velocities, and bottom clearance on the velocity of the spillage plume behind the collector?

A higher clearance is expected to result in a higher velocity of the spillage plume, as more water can be spilled due to the increased space available. Conversely, higher forward velocity is anticipated to be associated with lower velocity of the spillage plume, as the higher forward velocity is expected to lead to reduced erosion. Additionally, higher jet velocities are expected to result in higher velocities of the spillage plume, since the erosion is expected to be higher.

The erosion of cohesive sediment beds presents unique challenges compared to non-cohesive sediment beds. This differentiates this research from the study of Alhaddad & Helmons (2023). Besides, this research will study the turbidity currents caused by the spillage behind the collector. Also, it will look into the water entrainment through the collection duct.

The findings from this study will contribute to the understanding of cohesive sediment erosion and discharge sediment plumes and will be valuable in improving the design and operation of polymetallic nodule collectors. By identifying the mechanism of bed erosion, the aim gets feasible to work towards making these operations more efficient while minimizing their impact on the marine environment.

#### 1.4. Research Methodology

As mentioned before, hydraulic collectors have been the most extensively studied technology for mining polymetallic nodules, primarily because it minimizes contact between the collector and the ocean floor. To design a hydraulic collector that disturbs sediment as little as possible, it is crucial to gain a detailed understanding of the interaction between the collector and the sediment bed. To do so, numerical models and experimental studies can be done. Theoretical models may oversimplify complex processes, and the accuracy of the results is highly dependent on the quality of the input data and assumptions made in the model. Therefore, experimental studies are needed to validate numerical models. Experimental studies can provide valuable insights into the physical processes that govern cohesive sediment erosion. For these reasons, a series of small-scale experiments will be conducted to test different operational conditions, aiming to obtain the first quantitative data on sediment erosion caused by a hydraulic collector moving over a cohesive bed.

As mentioned before, the experimental setup used in this study will be similar to the one used by Alhaddad & Helmons (2023), as depicted in Figure 7. The aim is to contrast the behaviour of cohesive and non-cohesive sediment and to obtain more data on the subject. In this research, clay will be used, thus the filter will not work sufficiently. Instead, a separate tank will be used as a sedimentation compartment.

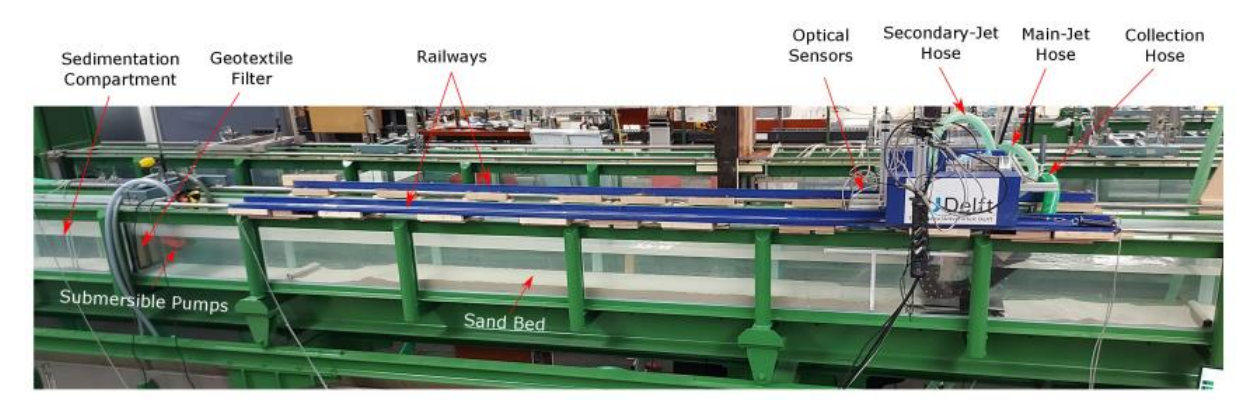


Figure 7 The experimental setup used in Alhaddad & Helmons (2023).

#### The needed material/instrumentation is listed below

- Flume
- Scaled-down collector head
- Mobile carriage
- Collection hose + pump: the pump will be used to transport the collected sediment and water to sedimentation tank.
- Main-Jet hose + pump
- Secondary-Jet hose + pump
- Optical sensors (lasers)
- Sedimentation tank (300 L)
- clay
- Two electromagnetic flowmeters (for flow in jet hoses)
- Acoustic flowmeter (for flow in collection hose)

For a detailed research methodology, please refer to Chapter 5. It contains comprehensive information about the methods and procedures used in the study, including experimental setups, data collection, measurements, and data analysis techniques. This chapter provides a thorough understanding of the research approach and how the various parameters were studied to investigate the influence of different factors on the observed phenomena.

#### 1.5. Structure of The Final Report

The final report of this study is structured as follows.

1.	Introduction	Introduction and research scope
2.	Cohesive Sediment	Literature study
3.	Jet and plumes	
4.	Coandă-Effect-Based Collector	
5.	Experimental research	Testing
6.	Results	
7.	Conclusions	Findings
8.	Discussion and recommendations	

# 2. Cohesive Sediment

Sediments found in coastal water bodies are a crucial component of both the suspended load and sediment bed. These sediments can be classified as either cohesive or non-cohesive. Cohesive sediments are primarily composed of clay-sized ( $<2~\mu m$ ) and silt-sized ( $<75~\mu m$ ) particles, mixed with organic matter and sometimes small amounts of very fine sand(Mehta et al., 1989). Non-cohesive sediments, on the other hand, consist mainly of sand and gravel-sized materials ( $<75~\mu m$ ). The main characteristic that sets cohesive sediments apart from non-cohesive sediments is their cohesive nature, meaning that attractive forces predominate over repulsive forces, allowing particles in close proximity to bind together and form aggregates, or flocs. This is due to the presence of clay and colloidal particles with significant surface physico-chemical forces. Generally, a clay fraction greater than 10% is sufficient for the sediment to exhibit cohesive properties. It should be noted that the shear strength of cohesive sediments is lower compared to non-cohesive sediments (Mehta et al., 1989; van Rijn, 1993). In this chapter theoretical background about cohesive sediment will be provided.

## 2.1. Clay of The Clarion Clipperton Zone (CCZ)

The clay covering the ocean floor is a fundamental constituent of the Clarion Clipperton Zone (CCZ), consisting of small particles that have been carried by ocean currents for millions of years. The clay layer is essential in the development and enlargement of polymetallic nodules and also serves as a home for diverse deep-sea organisms (Hein et al., 2013b).

Shear strength measurements were obtained from a boxcore sample retrieved from the Clarion-Clipperton Zone (CCZ). The shear strength values start at 0 kPa at the surface and gradually increase with depth, see Figure 8. At a depth of 5 cm, the shear strength is approximately 4 kPa.

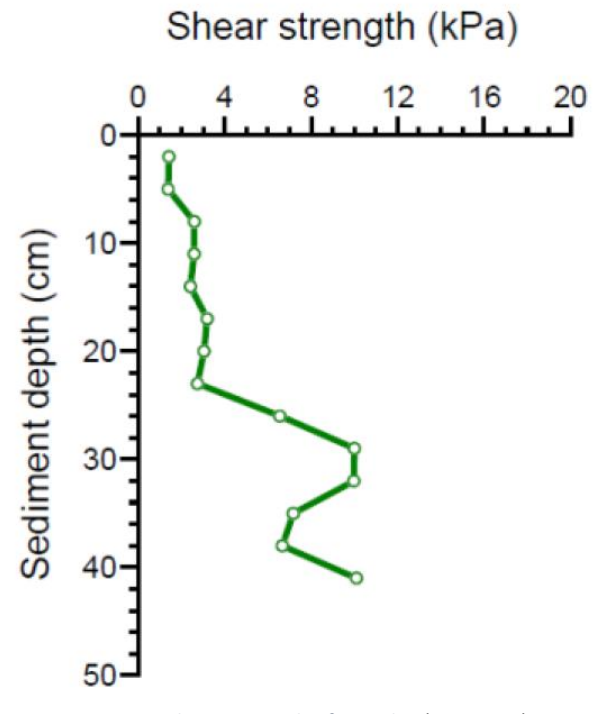


Figure 8 Shear strength of CCZ clay (ISA, 2019).

Table 1 presents the characteristics of CCZ sediment (Boschen-Rose et al., 2020). It is important to acknowledge that there is a distinction between the shear strength of remoulded and undisturbed clay. During experiments, the shear strength of clay can vary based on the duration of its consolidation.

Table 1 Characteristics of CCZ sediment (Boschen-Rose et al., 2020).

Characteristic	CCZ, GSR area
Sediment type	Siliceous ooze
Small scale surface topography	Nodules half-embedded in sediment
D10, D50, D90	2 μm, 9 μm, 66 μm
Wet bulk density	1.25-1.45 g cm <sup>-3</sup>
Porosity	71-85 vol %
Undrained shear	0-6.0 kPa at 0-10 cm
strength	2.5-7.0 kPa at 10-25 cm

#### 2.2. Erosion

Erosion of the sediment bed is a key process that regulates sediment dynamics. As such, it has garnered significant interest and been the subject of extensive study. Understanding the mechanisms behind erosion and the factors that influence it is essential for predicting sediment transport and deposition, as well as managing aquatic environments in a sustainable manner.

To assess the erodibility of bed sediment, two key parameters are typically measured: erosion threshold and erosion rate. The erosion threshold represents the critical hydrodynamic condition required to initiate sediment erosion, while the erosion rate refers to the amount of sediment eroded per unit time once the threshold has been exceeded. The erosion rate is often dependent on the erosion threshold, as the two parameters are closely related (Forsberg et al., 2018).

By quantifying erosion threshold and erosion rate, researchers can gain insight into the mechanisms behind sediment transport and deposition, as well as predict the impacts of hydrodynamic conditions on aquatic ecosystems. Therefore, accurately measuring these parameters is critical for effective sediment management and the maintenance of healthy aquatic environments. The study of Alhaddad & Helmons (2023) at TU Delft involved a series of small-scale experiments to investigate bed-sediment erosion. The experiments explored the impact of critical operational conditions on bed-sediment erosion. Notably, the collector's forward velocity was found to have an inverse relationship with the erosion depth, emphasizing the need for optimization. Conversely, higher jet velocities were observed to result in larger erosion depths. Additionally, larger bottom clearances were associated with smaller erosion depths. The study revealed that the sediment bed primarily experienced disturbance due to water jetting, with water jets impinging obliquely on the bed's surface, leading to the collapse of the uppermost layer. While the study does not provide a comprehensive theoretical description of inclined water jet-induced erosion, it offers practical guidance for minimizing sediment pick-up by the collector. The analysis indicated that the erosion depth is logarithmically proportional to the flow's force on the sediment bed, suggesting that reducing the flow impinging force can minimize erosion depth. Moreover, the study identified that entrainment of ambient water contributes to the formation of a sediment plume just behind the collector head. These findings shed light on critical factors influencing bed-sediment erosion and lay the groundwork for designing a hydraulic collector with minimal environmental impact.

#### 2.3. Aggregation

Aggregation is the process by which flocs are formed from primary sediment particles, due to destabilization and collision, see Figure 9. Destabilization occurs when the double layer around each sediment particle is compressed by divalent ions, leading to van der Waals attractive forces that facilitate aggregation. Collision occurs through three primary mechanisms: Brownian motion, internal shear, and differential settling (Krone, 1963; van Rijn, 1993).

- Brownian motion occurs when fluid particles bombard sediment particles due to thermal gradients, resulting in weakly bonded aggregates in stationary or quasi-stationary waters.
- Internal shear dominates in dynamic aquatic systems, producing more dense and durable aggregates.
- Differential settling occurs during near-slack periods when concentrations are high, leading to weak and low-density aggregates.

Aggregation transfers mass through the particle size spectrum to form larger aggregates with higher porosity, irregularity, fragility, and settling rate (Krone, 1963; van Rijn, 1993). Aggregation is influenced by factors such as sodium adsorption ratio, pH, salinity, sediment size, shape, gradation, density, turbulence, temperature, and the efficiency of particle collision (Forsberg et al., 2018; Krone, 1963; Mehta et al., 1989).

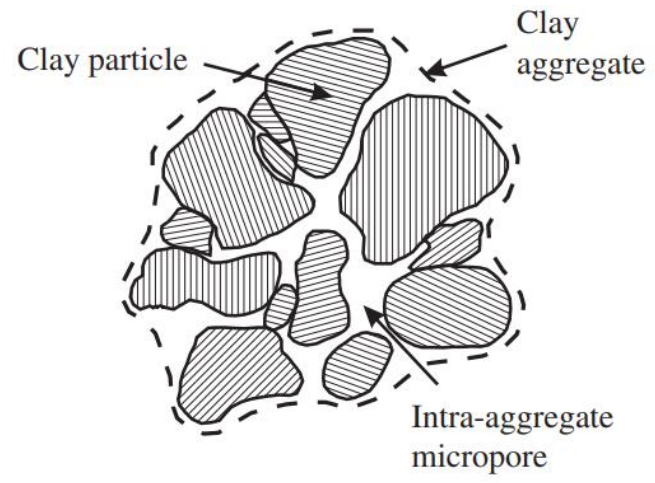


Figure 9 Sketch illustrating the structure of a clay aggregate, composed of multiple clay particles, and the formation of porosity within the aggregate (Christidis, 2011).

The process of flocculation is intensified when there is a small particle size combined with a large concentration, as it leads to a small relative distance between the particles. According to experimental research by Krone (1963), flocculation reaches an equilibrium situation at a salinity of about 5 to 10 promille, which is much smaller than that of sea water (35 promille) (Krone, 1963; Mehta et al., 1989; van Rijn, 1993).

Additionally, high temperature enhances the flocculation process, as the repulsive energy of the double layer decreases in magnitude, leading to decreased repulsion. Organic materials present in and on the flocs significantly intensify the flocculation process due to the binding properties of the organic materials. The binding forces become stronger due to the presence of organic material, and the flocs become larger (van Rijn, 1993).

Large shearing forces in the fluid can break up the flocs, causing them to break into smaller flocs or particles. Large shearing forces exist close to the bottom where the velocity gradients are largest, as well as in small-scale eddies throughout the fluid. Due to turbulent forces, there is a continuous process of flocculation and break-up resulting in a dynamic equilibrium of the flocs (size, density, and strength) (Berlamont et al., 1993; van Rijn, 1993; Winterwerp & Kranenburg, 2002).

In still water (no turbulence), the flocs may grow to larger sizes due to differential settling collisions. However, as the flocs get larger, they fall faster until the fluid shear on the flocs becomes greater than the floc strength resulting in break-up. Underwater photographs show the presence of macroflocs with sizes ranging from 10 to 100 um, and single mineral particles smaller than about 10 mm. As the flocs grow larger, the floc size increases but the density of the flocs (consisting of sediment, fluid, and organic materials) becomes smaller. Excess floc density as a function of floc diameter is shown in Figure 10 based on experimental research. Individual clay particles have an excess density of about 1600 kg/m³ ( $\rho_s$ = 2600 kg/m³,  $\rho$  = 1000 kg/m³). Large flocs of about 1000 um may have a density in the range of 1 to 10 kg/m³ in excess of the fluid density, as most of the floc consists of (pore) fluid (Berlamont et al., 1993; van Rijn, 1993; Winterwerp & Kesteren, 2004).

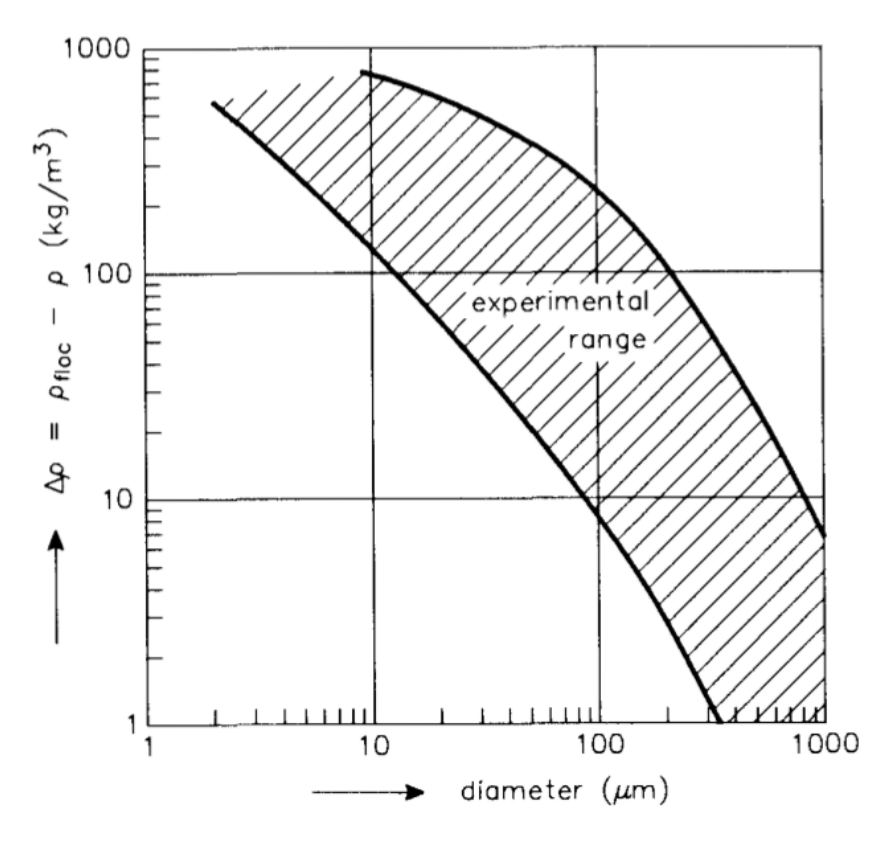


Figure 10 Floc density minus fluid density (Differential density) plotted against the diameter of the floc (van Rijn, 1993).

#### 2.4. Settling Velocity

The settling velocity is an important parameter for sediment particles in suspension, as it governs their transport processes. However, when analysing sediment found in the bed, the settling velocity cannot be directly related to the grain size of the particles, due to the effects of flocculation which can alter the shape, size, and density of particle aggregates. These effects may also vary in space and time due to various factors such as stress history, sediment concentration, organic compounds, and chemical environment such as salinity. Therefore, it is recommended to measure settling velocity in-situ whenever possible (Berlamont et al., 1993).

The settling velocity of cohesive sediments is influenced by various factors including the aggregation process, the concentration of suspended sediments, and the ionic concentration of the suspending medium. At low concentrations of sediments in the water column  $(0,1-0,3 \text{ kg/m}^3)$ , the settling velocity remains constant irrespective of the concentration. However, with increasing concentration  $(1-10 \text{ kg/m}^3)$ , the settling velocity increases due to the formation of stronger, denser, and larger flocs. At

high concentrations (>10 kg/m³), flocs break up again leading to a rapid decrease in settling velocity due to mutual hindrance. The sediment below forms an almost continuous matrix, resulting in hindered settling. This process is characterized by a high-density suspension known as fluid mud. The settling velocity of cohesive sediments in estuarine and coastal waters has been reported to range from  $10^{-7}$  to  $10^{-3}$  m/s (Berlamont et al., 1993; Mehta et al., 1989; Schwartz. Maurice L., 2005).

The near-bed turbulence determines whether settling aggregates bond with particles on the bed or are re-suspended into the water column. The probability that particles reaching the bed will stick to it is defined as the "probability of deposition," which is influenced by the stochastic nature of the near-bed turbulence. The critical shear stress for deposition is determined by the sediment type and can be measured through laboratory flume studies. If the bed shear stress exceeds the critical shear stress for deposition, then deposition will cease, assuming the sediment has uniform properties (Mehta et al., 1989). The deposition rate depends on the aggregate settling velocity, near-bed concentration, and probability of deposition (Schwartz. Maurice L., 2005).

The settling velocity of the clay particles used for this research is expected to be extremely low, and it is anticipated that it will take several hours before the water becomes clear enough for accurate measurements. To address this issue, potential solutions such as using a flocculant or refreshing the water in the flume will be considered and discussed in later stages of the study.

#### 2.5. Consolidation and Erosion Resistance

After sediment aggregates settle on the bed, they lose their flocculated structure and move closer together. Particle-to-particle contact leads to consolidation of the sediment under its own weight. As the pore-water pressure is released, the effective stress of the soil increases. With increasing depth of sediment, the bed's void ratio decreases, and its density and shear strength increase. Understanding the consolidation of cohesive sediment beds is critical for assessing their susceptibility to erosion and estimating the amount of eroded material. The shear strength of consolidated sediments can be estimated from empirical relationships between shear strength and dry density. Experimental data show that the shear strength of sediments increases with clay content, organic matter, salinity, sodium adsorption ratio, and cation exchange capacity. On the other hand, shear strength decreases with an increase in temperature, pH, and sand concentration in the sediment bed (Mehta et al., 1989; Schwartz. Maurice L., 2005; van Rijn, 1993).

To ensure the consistency of shear strength in the clay bed during the testing period, the clay bed will be remoulded and levelled before each experiment. This approach will help maintain a constant shear strength throughout all experiments, ensuring the production of reliable and consistent data.

# 3. Jets and plumes

The assessment of the polymetallic nodule collector's behaviour is significantly influenced by the understanding of jet and plume phenomena. In this chapter, a review of these two phenomena will be presented.

#### 3.1. Jetting

Main soil failure mechanisms induced by a moving jet include two primary forces exerted on the soil (Nobel, 2013):

Stagnation Pressure (Normal Load): The jet flow creates a normal load in the main direction of its
flow due to the mass flow of the jet. This pressure acts perpendicularly to the seabed surface. The
stagnation pressure could be calculated using the following equation:

$$p_{\text{stag}} = \frac{1}{2} \rho_w u_s^2 \tag{1}$$

Where  $\rho_{\scriptscriptstyle W}$  is the water density and  $u_{\scriptscriptstyle S}$  is the vertical velocity of the flow.

 Shear Stress: The high flow velocity and water viscosity generate a shear force parallel to the flow direction. In non-cohesive soils, these shear stresses (τ<sub>b</sub>) can detach individual grains from the seabed.

For non-cohesive soils, the jet's shear stresses lead to individual grain detachment from the seabed. To dislodge a grain, the void space behind it must be filled with water, see Figure 11. The erosion process's velocity primarily depends on the soil's permeability and the jet's flow velocity. A lower water permeability results in a slower erosion process. This process is known as surface erosion and occurs under drained conditions (Rhee, 2010).

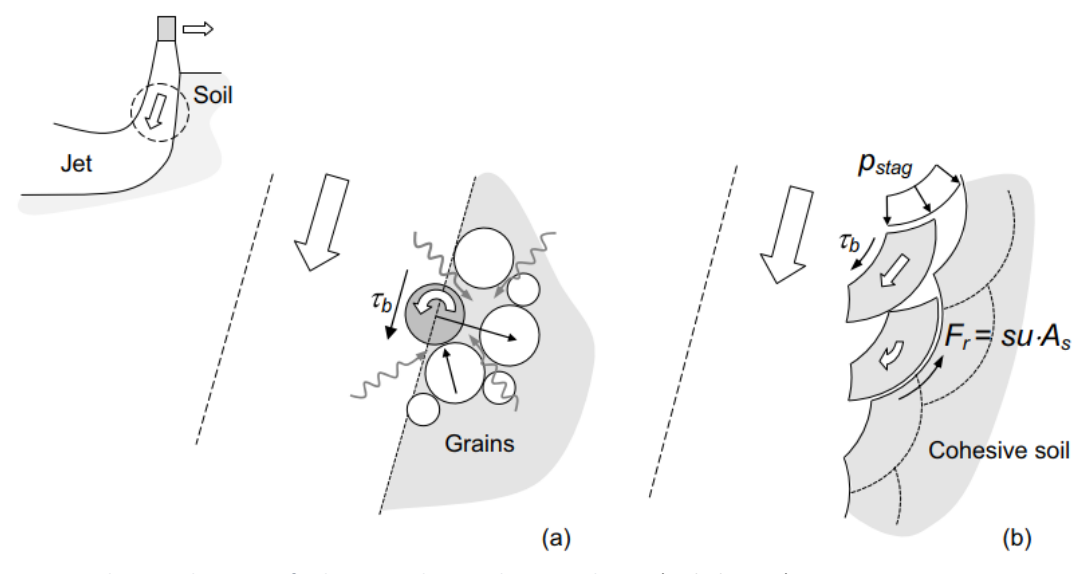


Figure 11 Failure mechanisms of cohesive and non-cohesive sediment (Nobel, 2013).

In cohesive soils, surface erosion induced by a moving turbulent jet is relatively uncommon due to the low water permeability compared to the rapid timescale of the jetting process. Instead, under various loading conditions, different shear surfaces develop within the soil. When the load from the jet ( $p_{stag}$ ) surpasses the soil resistance along these surfaces, soil failure occurs. For instance, in the case of a moving vertical jet, these shear surfaces are primarily formed by the stagnation pressure ( $p_{stag}$ ) exerted by the jet (Figure 11).

The normalized cavity depth is represented in Figure 12 as a function of the ratio between the jet pressure and undrained shear strength. It is noteworthy that the relation is visible despite the presence of scatter.

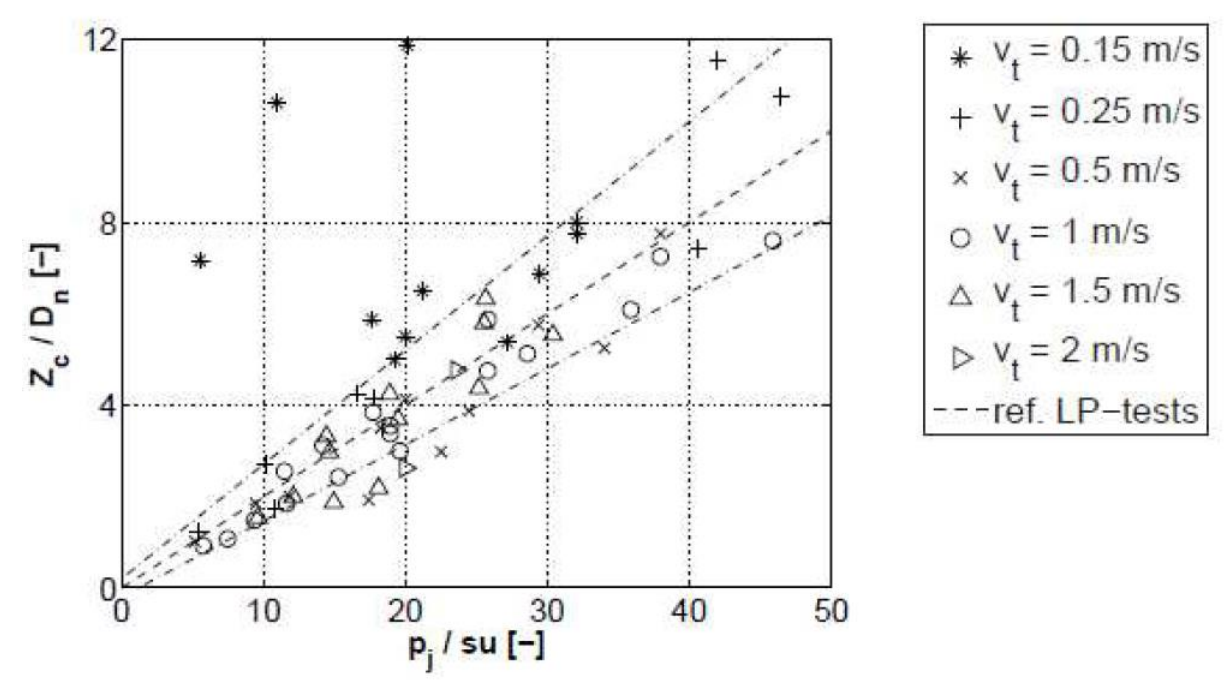


Figure 12 Relation between normalized cavity depth (Erosion depth  $(Z_c)/Nozzle$  diameter  $(D_n)$ ) and the ratio between the jet pressure  $(p_i)$  and the undrained shear strength  $(s_u)$  (Nobel, 2013).

#### 3.2. Plumes and Turbidity Currents

Bed disturbances primarily arise from the motion of a Polymetallic Nodule Mining Tool (PNMT) and the pick-up process, which can be hydraulic, mechanical, or hybrid in nature. Careful optimization of discharge parameters is crucial when discharging sediment-water mixtures to prevent unnecessary expansion of the affected area due to plume dispersion. The horizontal discharge of the sediment-water mixture is divided according to Elerian et al. (2021) into four main parts of interest (see Figure 13):

- 1. Discharge Source: This section encompasses the initial conditions, including momentum, concentration of suspended sediments, and distance from the sea bed (z). The physical parameters are contingent upon the design of the PNMT, such as the methods of collection and separation.
- 2. Jet or Plume Regime: In this region, the flow can either be a jet or plume, depending on the discharge parameters. As the buoyancy force becomes dominant, the flow transitions into a plume.
- 3. Impingement Region: Positioned on the sea bed, this region experiences a change in the direction of the negative buoyant plume due to direct interaction with the seabed. Within this area, sediment deposition and potential sea bed erosion are anticipated to occur.
- 4. Turbidity Current: Beyond the impingement region, a turbidity current is formed.

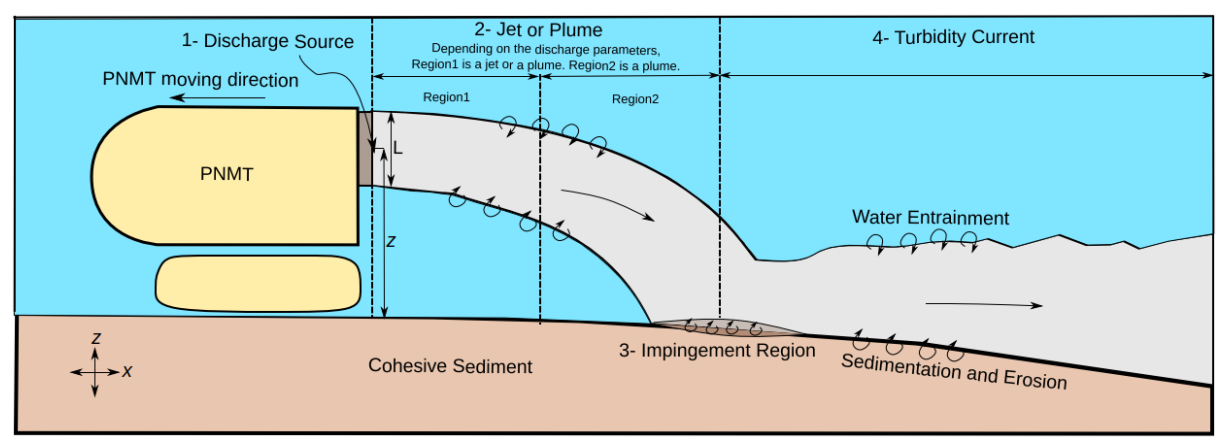


Figure 13 A conceptual sketch illustrates the evolution of the sediment-water mixture discharged from a polymetallic nodule (Elerian et al., 2021)

According to Fernando (2013), the classification of sediment plumes often relates to length and time scales. As such, terms like "nearfield" and "farfield" regions are defined as follows (refer to Figure 14):

- Nearfield Region: This region is situated close to the discharge apparatus and is primarily influenced by the discharge conditions. The flows within this region typically have a length scale of up to a few hundred meters and a time scale ranging from seconds to minutes.
- Farfield Region: Defined as the region where the plume trajectory is predominantly influenced by environmental parameters such as currents and seabed topology. The flows in this region exhibit large time and length scales, typically in the range of days and kilometers, respectively.

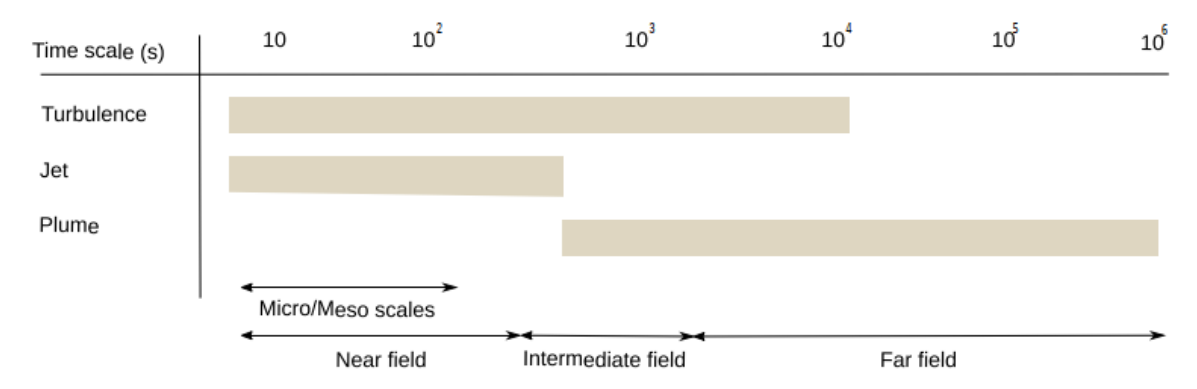


Figure 14 A summary of the key time scales associated with Deep-Sea Mining (DSM) activities (Fernando, 2013).

# 4. Coandă-Effect-Based Collector

A hydraulic collector is a system that employs sediment-water mixtures to gather nodules and transport them to a separator for settling. Among various hydraulic collection methods, the Coandă-effect-based approach exhibits high pick-up efficiency and low flow field disturbance (Yue et al., 2021). The design of the small-scale collector head heavily relies on the Coandă effect to ensure effective nodule collection (Alhaddad & Helmons, 2023). The Coandă effect, an intriguing phenomenon in fluid mechanics, was first discovered by the Romanian scientist Henri Coandă. It describes the tendency of a jet flow to adhere to an adjacent surface, maintaining adhesion even when the surface curves.

Figure 15 presents a schematic of the Coandă-effect-based collector's basic design, comprising three concentric surfaces forming two ducts: the jet duct and the collection duct. The high-velocity water jet in the jet duct follows the curvature of the upper plate due to the Coandă effect. This results in the entrainment of surrounding water towards the upper plate, creating suction that can dislodge nodules from the seabed and carry them towards the collection duct.

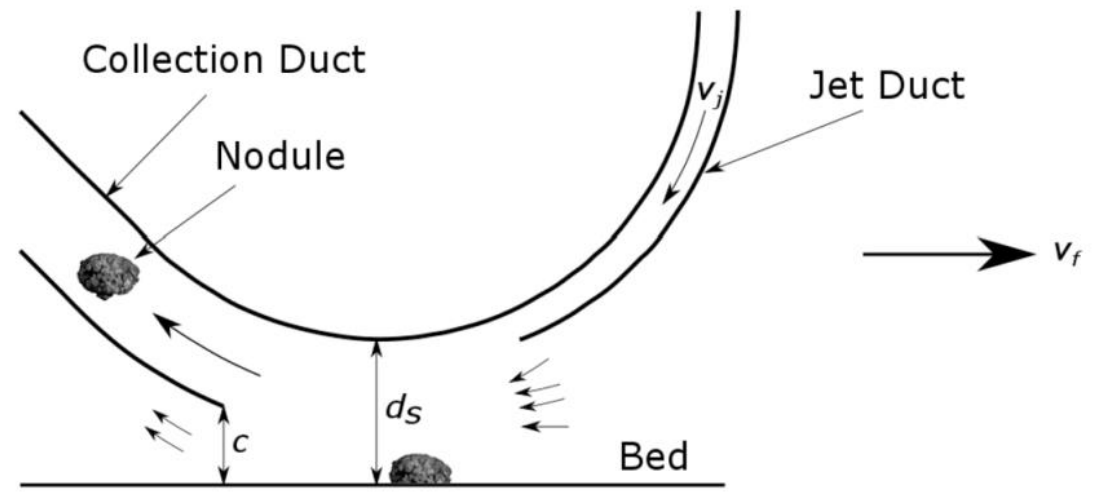


Figure 15 The collector head is schematically represented, where vj represents the jet velocity, vf denotes the forward velocity of the collector, and c signifies the clearance. The smallest arrows indicate the direction of water entrainment (Alhaddad et al., 2023).

To address the research questions, it is essential to delve into the behaviour of the Coandă-Effect-Based Collector concerning water entrainment and spillage.

#### 4.1. Water entrainment

Water entrainment refers to the process by which a fluid, usually water, is drawn or dragged into a moving flow or stream. It occurs when one fluid flows alongside or over another, creating a region of low pressure or a vacuum that causes the second fluid to be pulled into the flow. In the context of fluid dynamics, water entrainment often involves the entrainment of ambient water or surrounding fluid into a higher-velocity fluid stream.

For example, in the case of the Coandă-Effect-Based Collector mentioned earlier, water entrainment occurs when the high-velocity water jet in the jet duct adheres to the adjacent surface of the upper plate, leading to surrounding water being entrained towards the collection duct. The study conducted by Alhaddad et al. (2023) indicates that there is a relationship between the clearance under the collector head and the flow rate of the entrained water. Specifically, it was observed that as the clearance decreases, the flow rate of the entrained water also decreases. This finding is logical and makes sense, as a larger clearance provides more space or room for water to be entrained into the flow.

In the Coandă-Effect-Based Collector system, the clearance under the collector head plays a crucial role in determining the water entrainment process. A smaller clearance restricts the available space for the water to be drawn into the flow, resulting in a reduced flow rate of the entrained water. On the other hand, a larger clearance allows more water to be entrained, leading to a higher flow rate.

Their research also highlight the critical significance of the available time for nodules to respond to the pressure gradient beneath the collector. It is observed that if the available time is insufficient, even with an adequate pressure gradient, the nodules will not be picked up effectively. Amongst the influencing factors, the clearance under the rear cowl of the collection duct emerges as a major determinant in the collection process. Notably, a smaller bottom clearance leads to higher pick-up efficiency, emphasizing its influential role in the overall collection mechanism.

#### 4.2. Spillage

However, as a side effect of the collection process, spillage can occur behind the collector head. The water jets not only entrain ambient water into the collection duct but also inject water behind the collector head. This spilling water flows backward, in the opposite direction of the collector movement, carrying suspended sediments along with it. Consequently, this turbidity flow generates disturbances in the clay bed, leading to erosion and deposition of sediments in different areas.

The behaviour of the spillage plume has not been studied extensively in previous research due to its coexistence with other plumes. The presence of multiple plumes, such as the discharge plume generated during the filtration process of nodules and the plume resulting from the movement of the collector, makes it challenging to isolate and analyse the characteristics of the spillage plume. However, the experimental setup of this research facilitate a focused study on the spillage plume. The suspended sediments and particles carried by the spillage plume may have implications for marine habitats, benthic organisms, and water quality (Global Sea Mineral Resources, 2018). By gaining insights into the characteristics of the spillage plume, this research contributes to a better understanding of its potential environmental effects during polymetallic nodule mining operations.

#### 4.3. Erosion of Sand

Current understanding of sediment erosion caused by moving water jets remains limited. To the best of knowledge, there is no prior documentation of laboratory experiments investigating the erosion resulting from a moving, submerged, inclined water jet. However, in previous research, laboratory experiments were conducted on sand erosion induced by a moving, submerged, inclined jet directed towards a sand bed (Alhaddad & Helmons, 2023). These experiments were analysed in pursuit of a correlation between erosion depth and a flow-related parameter. Consequently, a significant logarithmic correlation was unveiled between erosion depth and the impinging force exerted by the flow onto the sediment bed, as depicted in Figure 16. Specifically, a greater impinging force leads to a greater erosion depth. Thus, the main mechanism by which the sand is eroded is jetting.

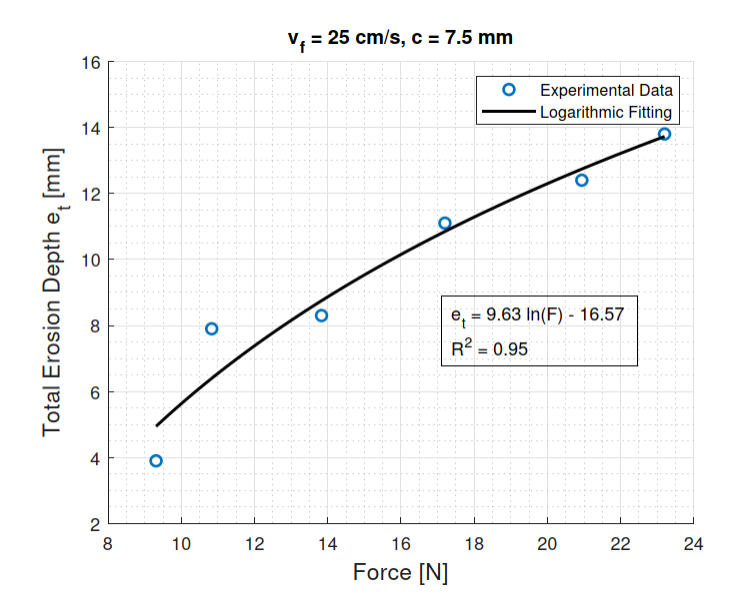


Figure 16 The laboratory experiments conducted in this study reveal a logarithmic relationship between the force exerted by the impinging flow and the total erosion depth ( $e_t$ ) (Alhaddad & Helmons, 2023).

# 4.4. Scaling

The small scale collector used in this research and the research of Alhaddad & Helmons (2023) is scaled down by a factor of 4 in the 2-D plane depicted in Figure 5, with the third dimension (width) remaining constant at 20 cm. The jet velocities and the forward velocity of the collector head are scaled down using Froud scaling:

$$Fr = \frac{V}{\sqrt{g \cdot L}} \tag{2}$$

In equation (2) V represents velocity, g denotes the acceleration due to gravity, and L signifies the characteristic length or linear dimension of the system.

Knowing that g and Fr are constant the following relation could be driven:

$$V_{small} = \sqrt{\frac{1}{4}} \cdot V_{full} = 0.5 \cdot V_{full} \tag{3}$$

# 5. Experimental Research

This chapter provides an overview of the experimental setup, instrumentation, test procedure, and characterization of the used clay, respectively.

#### 5.1. Experimental Setup

The experimental setup is designed to enable the testing and evaluation of the collector head's impact on the clay bed. The experimental setup consists of multiple components to conduct the study, including the collector head, a mobile carriage, three PVC hoses, water pumps, and a water flume. To enable the collector head to move, it will be mounted on a mobile carriage that could move along bespoke railways that is 5 meters in length at the top of the water flume. The carriage could move with a constant and controllable forward velocity. In this setup, the carriage could travel a net distance of 3.2 meters from the beginning to the end of the railways, the compartment through which the collector head moves is susceptible to contamination with clay. To prevent the clay from entering the system's water, a strategic solution is implemented. Two separation walls are employed at the beginning and end of this compartment, effectively closing it off from the rest of the system. By employing these separation walls, any potential introduction of clay particles into the system is mitigated. This separated testing compartment could be emptied using two Submersible pumps. A wooden tray is put inside the testing compartment to facilitate placing the clay on the bed. Figure 17 presents an actual view of the experimental setup with labelled equipment. Pictures of the experimental setup could be found in Appendix A.

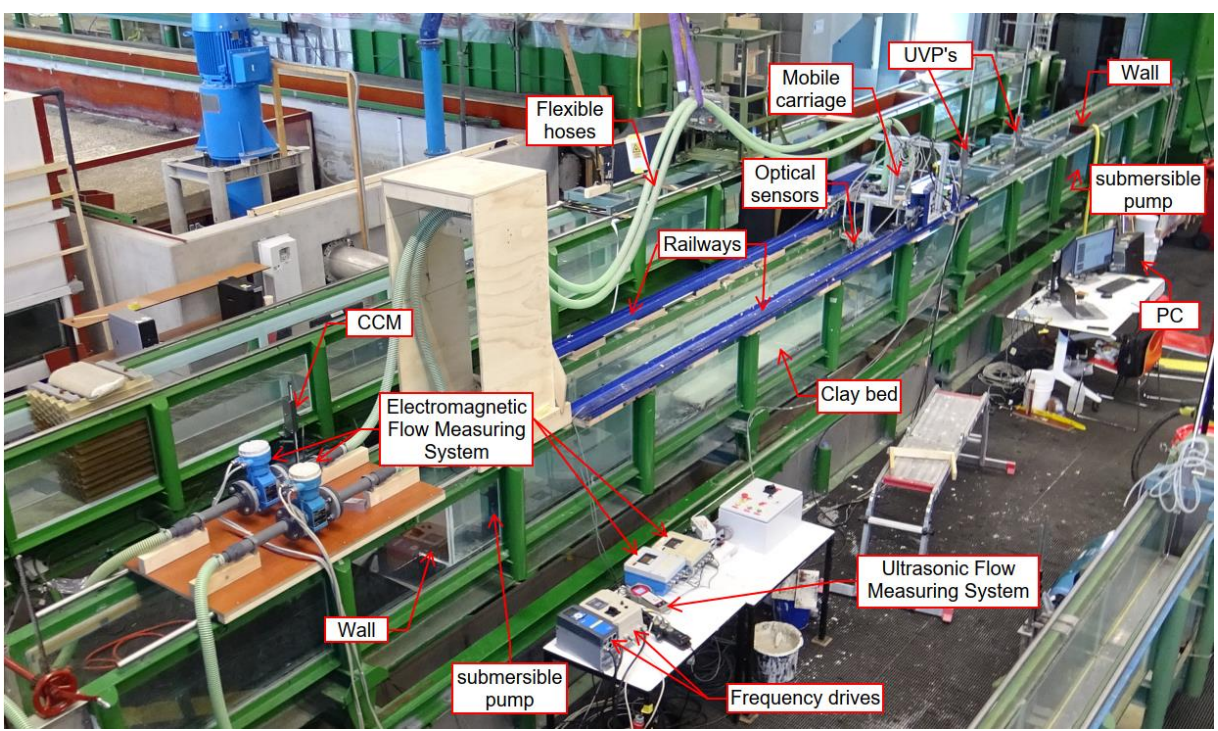


Figure 17 Side view of the experimental setup showing most of the equipment used in the experiments.

The size of the collector head is determined by the scale of the water flume used in the experiment. As a result, the collector head presented in Alhaddad et al. (2023) is reduced in size by a factor of 4 in the 2-D plane illustrated in Figure 5, while the third dimension (width) is maintained at 20 cm. The collector head was fabricated to conduct the experiments of Alhaddad & Helmons (2023) using high-density polyethylene (HDPE) in various parts, which were assembled by fastening them together with bolts and nuts, and sealed with gaskets. The collector head is equipped with three ducts, consisting of two jet ducts (main and secondary) and one collection duct. The jet ducts are connected to individual

water pumps through hoses with an inner diameter of 40 mm, while the collection duct is linked to a separate water pump via a hose with a 63 mm inner diameter, see Figure 18. To facilitate control over the flow rates in all three ducts, variable-frequency drives (VFDs) are employed. These VFDs play a crucial role in regulating the required jet velocity, providing the ability to adjust and fine-tune the experimental conditions as necessary.

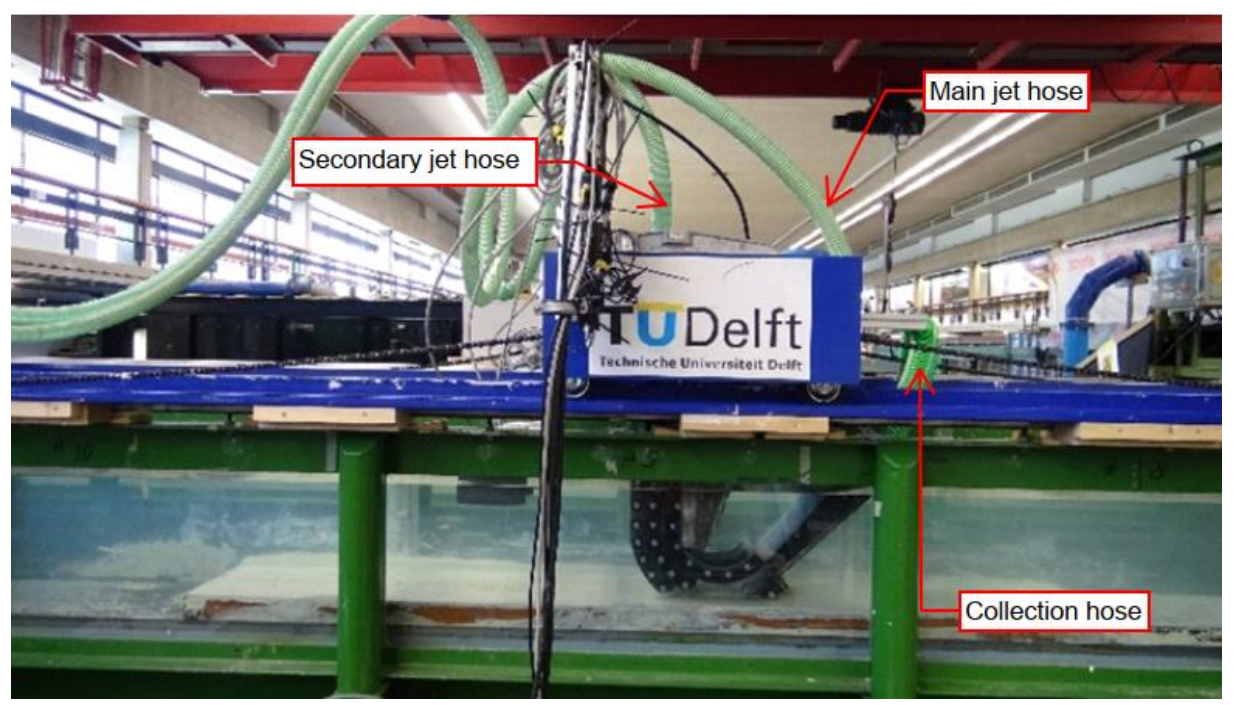


Figure 18 Side view of the experimental setup showing the hoses connected to the collector head.

The discharged water, rich in clay, is directed into separate tanks. In these tanks, the concentration of clay is measured using a conductivity-type concentration meter (CCM). After measuring the clay concentration, the water is discarded appropriately. This process allows for effective management of the clay-laden water, preventing clay from entering the system's water of the water lab.

Before conducting the experiments, an Electromagnetic Current Meter (EMS) was installed in the collection duct to measure the flow velocity of the discharged water under various operational conditions. The known geometry of the collection duct allowed the calculation of the flow rate. This enabled the study of water entrainment phenomena. Furthermore, when the water discharge in the collection duct is known, the pump connected to the collection duct can be synchronized to maintain a consistent discharge rate and prevent any suction from occurring.

#### 5.2. Instrumentation

For this research, multiple sensors were incorporated to measure key parameters such as changes in clay bed bathymetry, flow rates in the ducts, clay concentration in the discharge, and turbidity current front velocity and vertical velocity profile resulting from the collector head spillage. These sensors played a crucial role in providing comprehensive data, enabling a detailed analysis of the experimental phenomena and their implications. These sensors are described below.

#### Wheel encoder

A wheel encoder was utilized to link the laser measurements to their respective positions, see Figure 19. The wheel encoder accurately tracked the movement of the lasers along the horizontal axis as they scanned the clay bed. This synchronization allowed for precise correlation between the measured data and specific spatial coordinates.

#### **Optical sensors (Lasers)**

For the experiments, three optoNCDT 1302 optical sensors were used to measure changes in bathymetry. Specifically, their primary function was to quantify the erosion of the clay bed resulting from the

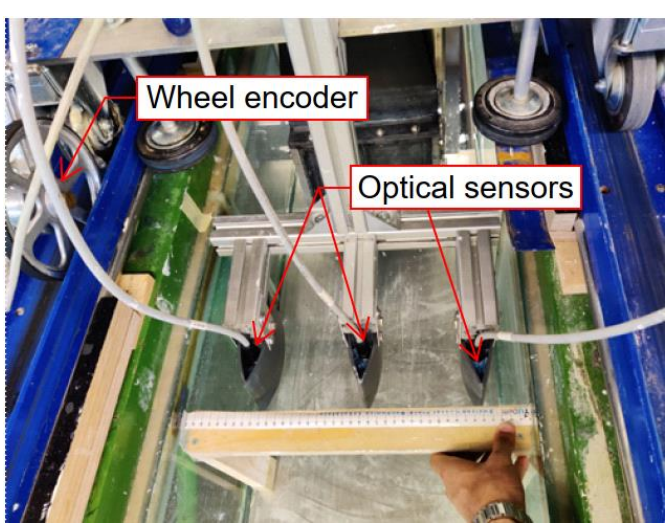


Figure 19 Picture showing the positioning of the optical sensors.

experimental conditions. The closed housing ensured that water did not come into contact with the lasers, preserving their accuracy and functionality throughout the measurements see Figure 19. Moreover, by enabling horizontal movement, the lasers facilitated multiple scans of the clay bed, capturing comprehensive data from various positions. The wooden frame with a measuring lint provided precise positioning, ensuring that the lasers accurately measured and recorded the extent of clay erosion at specific locations. This implementation of optical sensors played a vital role in the comprehensive analysis of clay bed dynamics and erosion patterns, yielding valuable insights into the experimental outcomes. For the results of the lasers, see 6.2.

#### **Electromagnetic Current Meter (EMS)**

The EMS is utilized in the experimental setup to measure the velocity of water currents at specific locations. The EMS was mounted into the collection duct to measure the velocity of the discharged water, see Figure 20. By knowing the velocity, the flow rate of the water can be determined. Normally, water flows out of the collection duct on its own, and no pump is required for this process. However, in the current system, the collection hose introduces significant friction, impeding the natural flow of water. To counteract this frictional effect, a pump is implemented to compensate and ensure the outflow of water. The velocity of the water



Figure 20 EMS mounted into the collection duct.

exiting the collection duct is measured under various operating conditions and the flow rate out of the collection duct is determined. The optimization of the collection pump is pursued to ensure a constant discharge and to only compensate for the friction of the hose.

Additionally, knowing the flow rate out of the collection duct will facilitate the investigation of water entrainment. Water entrainment refers to the movement of ambient water caused by the water jets discharged from the jetting ducts. It is expected that the flow rate out of the collection duct will be higher than the flow rate in the main and secondary jet duct combined.

#### **Ultrasonic Velocity Profile (UVP)**

In the scientific investigation, a single UVP-Duo instrument was employed, equipped with two transducers. These transducers emit bursts of ultrasonic signals at a frequency of 4 MHz. However, it is important to note that the system cannot acquire velocity profiles simultaneously from both transducers; instead, it can only obtain them sequentially, one after the other. The primary objective of these transducers is to measure the vertical velocity profile of the turbidity current.

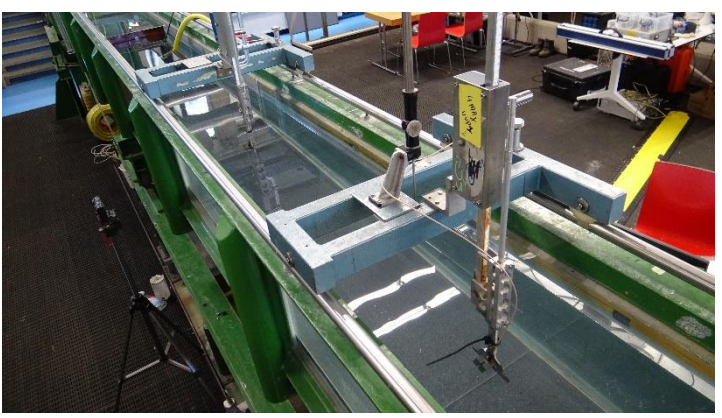


Figure 21 The two transducers are fastened behind the collector head.

By leveraging the data gathered from the velocity profiles, it becomes possible to derive important parameters characterizing the turbidity current. Among these are the associated characterizing height h (m), which represents the thickness of the turbidity current, and the layer-averaged velocity U (m/s), which reflects the average velocity of the current within its depth. These parameters could be determined using these relations (Mehta et al., 1989):

$$Uh = \int_0^{z_\infty} u \, \mathrm{d}z \tag{4}$$

$$U^2h = \int_0^{z_\infty} u^2 \mathrm{d}z \tag{5}$$

#### Conductivity-Type Concentration Meter (CCM)

The conductivity-type concentration meter (CCM) system is an instrument designed to measure the concentration of sediment-water suspensions at a specific point. Its functioning is based on detecting changes in conductivity caused by varying amounts of suspended sediment within the measuring volume. This type of instrument has proven to be particularly reliable for high sediment concentrations. The conductivity of the clay-water mixture directly relates to its density. The CCM is capable of measuring sediment concentrations up to 50% by volume (Deltares, 2016). To calculate the volumetric sediment concentration ( $C_v$ ), the following relation is utilized:

$$C_{v} = F_{\text{cal}} \left( 1 - \frac{V_0}{V_m} \right) \tag{6}$$

where  $V_0$  represents the reference voltage for clear water,  $V_m$  denotes the measured voltage, and  $F_{cal}$  is the calibration factor. The calibration factor,  $F_{cal}$ , is determined by comparing voltages obtained from clear water and various clay-water mixtures that utilize the same sand type used in the experiments, see Figure 22.





Figure 22 Calibration of the CCM (Left) and the position of the CCM during the experiments.

The calibration factor,  $F_{cal}$ , is determined through 20 variations of the clay volume in the water. The resulting value for  $F_{cal}$  is found to be -0.4847. See Figure 23 for the calibration curve.

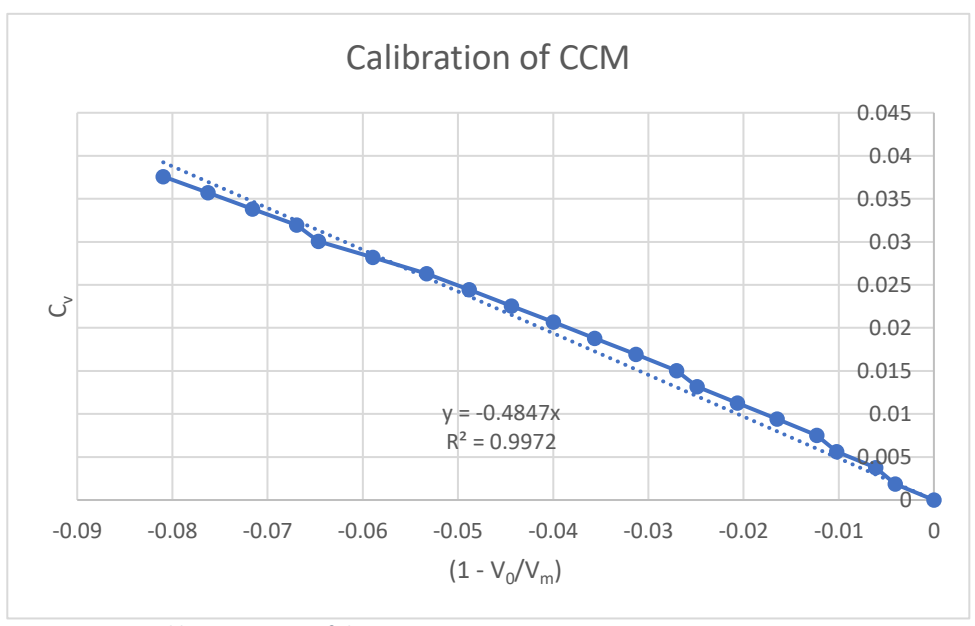


Figure 23 Calibration curve of the CCM.

# **Electromagnetic Flow Measuring System**

The Electromagnetic Flow Measuring System is a sophisticated instrument employed to accurately measure the flow rate of conductive fluids, such as water, in various applications.

In the experimental setup, two Electromagnetic Flow Measuring System plays a crucial role in precisely measuring the flow rate in both the main and secondary jet ducts, see Figure 17. Using variable-frequency drives, the flow rate can be adjusted to achieve the desired level for the experiment.

#### **Ultrasonic Flow Measuring System**

The Ultrasonic Flow Measuring System is an instrument utilized to measure fluid flow rates in various applications. It operates based on the principle of ultrasonic wave propagation through the fluid. By transmitting ultrasonic signals through the fluid and measuring the time it takes for the signals to travel upstream and downstream, the system calculates the flow velocity and subsequently determines the discharge rate.



Figure 24 Attachment of the transducers to the PVC pipe.

In the context of the experiment, the Ultrasonic Flow Measuring System is fastened on a PVC pipe to precisely measure the discharge of the collection pump. This help controlling the aimed flow rate through the collection duct.

#### Digital camera's

In the experiment, two digital cameras were employed to film two significant aspects of the study. The first camera recorded the movement of the collector head as it moves over the clay bed, see Figure 25. The second camera was used to capture the turbidity current generated by the spillage behind the collector head, see Figure 26. The use of digital cameras provided a visual and detailed record of the experimental processes. This enables analysing and interpreting the data accurately.



Figure 25 Picture showing the collector head moving over the clay bed (Test #5).



Figure 26 Picture showing the turbidity current developed behind the collector head (Test #5).

## 5.3. Test Procedure and Data Acquisition

The tests were conducted by replicating the same steps and maintaining consistent conditions throughout. This approach facilitates the comparison of experimental results, ensuring reliable and meaningful observations. The sequence of steps for each test is as follows:

- Empty the testing compartment from water using the two submersible pumps.
- Fill the prepared clay in the wooden tray till the needed depth of 5 cm.
- Level the clay bed with a wooden plate.
- Add water until reaching a water level of 36 cm, leaving a 7 cm clearance between the water surface and the top of the flume.
- Measure the initial bathymetry using optical sensors by driving the mobile carriage forward and then backward to the starting point. Do this twice making six scans by using three lasers.
- Turn on the water pumps. VFDs (variable-frequency drives) will be used to obtain the target flow rate in each duct.
- Drive the mobile carriage forward at the required velocity and stop at the end of the rails using sensors mounted at each end point.
- Empty the flume using the submersible pumps to get rid of the turbulent water.
- Clean the testing compartments from clay chunks using wet vacuum cleaner. Leave the eroded clay bed untouched.
- Fill the flume carefully with clean water, so the clay bed will not get disturbed. Now the water is clear enough to enable the optical sensors to measure the bed.
- Drive the carriage along the flume again to measure the final bathymetry. Do this five times making in total fifteen scans.
- The erosion will be analysed by measuring the change in bathymetry. A cross-sectional profile could be determined using the average value of the fifteen scans.

Four different values for each parameter will be tested as presented in Table 2, providing ample variations to comprehensively study the influence of these different parameters. By exploring a range of values for each parameter, researchers can thoroughly assess how each one impacts the experimental outcomes.

Table 2 Matrix of the aimed tests

Test #	Q <sub>mj</sub> [L/s]	V <sub>mj</sub> [m/s]	Q <sub>sj</sub> [L/s]	V <sub>sj</sub> [m/s]	Q <sub>c</sub> [L/s]	c [mm]	V <sub>f</sub> [m/s]
1	4.4	4.4	6.1	0.976	10.5	3.0	0.5
2	4.4	4.4	6.1	0.976	10.5	3.0	0.375
3	4.4	4.4	6.1	0.976	10.5	3.0	0.25
5	4.4	4.4	6.1	0.976	10.5	3.0	0.125
4	4.4	4.4	6.1	0.976	10.5	0.0	0.125
6	4.4	4.4	6.1	0.976	10.5	5.0	0.125
7	4.4	4.4	6.1	0.976	10.5	8.0	0.125
8	4.4	4.4	0.0	0.0	4.4	3.0	0.125
9	4.4	4.4	3.0	0.48	7.4	3.0	0.125
10	4.4	4.4	4.7	0.752	9.1	3.0	0.125
5	4.4	4.4	6.1	0.976	10.5	3.0	0.125
11	3.0	3.0	6.1	0.976	9.1	3.0	0.125
12	2.0	2.0	6.1	0.976	8.1	3.0	0.125
13	0.0	0.0	6.1	0.976	6.1	3.0	0.125

The velocities of the main and secondary jets are determined based on the flow rate and dimensions of their respective ducts. The main duct has a height of 5 mm and a width matching that of the collector head (200 mm). On the other hand, the secondary jet duct measures 31,25 mm in height and 200 mm in width, the same as the collector head.

A wide range of experiments is needed to provide validation measurements for numerical models. Besides, the results from these experiments will provide valuable insights into the behaviour of cohesive sediment and help advance the understanding of bed erosion caused by Coandă-effect-based polymetallic nodule collector.

Four additional tests were conducted to gain a deeper understanding of various aspects, see Table 3. These tests aimed to examine:

- 1. The influence of the presence of the secondary jet duct, which was crucial in addressing the fourth research question.
- 2. The impact of both the main and secondary jets, exploring their individual and combined effects on the experimental outcomes.
- 3. The reproducibility of the experiments, ensuring the reliability and consistency of the results.
- 4. The influence of the consolidation of the clay bed, studying how the compactness of the sediment affects the behaviour of the system.

This comprehensive approach allows to gain valuable insights into various factors that affect the experimental system, contributing to a more thorough understanding of the complex interactions between the variables and their implications on the study's objectives.

Test #	Q <sub>mj</sub> [L/s]	V <sub>mj</sub> [m/s]	Q <sub>sj</sub> [L/s]	V <sub>sj</sub> [m/s]	Q <sub>c</sub> [L/s]	c [mm]	V <sub>f</sub> [m/s]					
Test 18 help	Test 18 helps study the influence of the presence of the secondary jet duct.											
8	4.4	4.4	0.0	0.0	4.4	3.0	0.125					
18	4.4	4.4	No duct	-	4.4	3.0	0.125					
Test 19 help	os study the	impact of bot	h the main a	nd secondary	jets.							
19	3.0	3.0	4.4	0.704	7.4	3.0	0.125					
9	4.4	4.4	3.0	0.48	7.4	3.0	0.125					
Test 5 was	repeated to	test the repro	ducibility of	the experime	nts.							
5	4.4	4.4	6.1	0.976	10.5	3.0	0.125					
5 rep.	4.4	4.4	6.1	0.976	10.5	3.0	0.125					
Test 10 was	Test 10 was repeated after allowing the clay bed to consolidate for three days.											
10	4.4	4.4	4.7	0.752	9.1	3.0	0.125					
10 cons.	4.4	4.4	4.7	0.752	9.1	3.0	0.125					

For each experiment the following data was collected:

- Bathymetry change using optical sensors. Fifteen scans are made at different locations to allow determining an averaged cross-sectional profile of the eroded clay bed.
- Concentration of the clay in the discharged water using CCM.
- Vertical velocity profile of the turbidity current using UVP's.
- Two recorded video's of the collector head moving over the clay bed and of the turbidity current developing behind the collector head.

#### **Data analysis**

As the collector moves forward over the clay bed, a layer of clay is eroded, and a portion of it is captured and directed towards the collection duct. Simultaneously, the remaining eroded clay becomes suspended in the water column behind the collector head, resulting in the generation of a turbidity flow, see Figure 27. It is noteworthy that not all the eroded clay ends up in the collection duct due to the action of the water jets. These water jets not only entrain ambient water into the collection duct but also inject water behind the collector head, termed as the 'spilling water', Figure 5. The spilling water flows backward, counter to the collector's movement, with sufficient velocity to keep clay particles in suspension. Consequently, these suspended clay particles gradually settle down onto the clay bed, forming a deposition layer of a few millimeters within 1-4 hours after the completion of each experimental run. This is why the flume is emptied after each experiment, since it takes too long for the clay particle to settle.

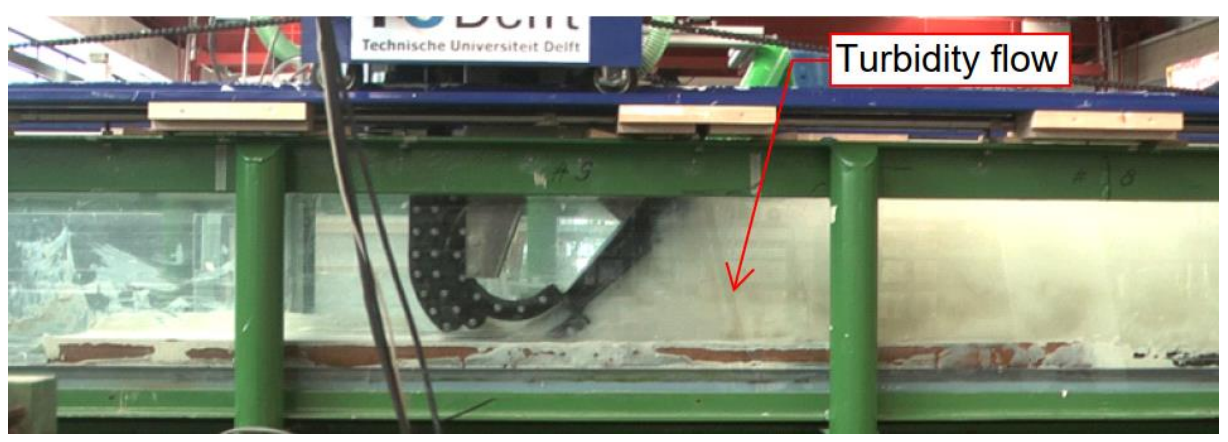


Figure 27 An experimental run in progress showing the turbidity flow generated behind the collector.

Prior to conducting the experiment and after leveling the clay bed, six scans of the clay bed were taken at specific distances from the left side, namely 5 cm, 10 cm, 18 cm, 20 cm, 30 cm, and 35 cm. These initial scans provided a baseline representation of the clay bed's topography before any disturbance from the experiment. As an example, Figure 28 (left) presents the scans taken before experiment 10 took place.

Following the completion of the experiments, a total of 15 scans were obtained at various distances from the left side, namely 5 cm, 10 cm, 12 cm, 14 cm, 16 cm, 18 cm, 19 cm, 20 cm, 22 cm, 24 cm, 26 cm, 28 cm, 30 cm, 33 cm, and 35 cm. The capability of the lasers to move horizontally, as depicted in Figure 19, allowed for the acquisition of these multiple scans, which captured the altered topography of the clay bed after the experiment. As an example, Figure 28 (right) presents the scans taken after experiment 10 took place.

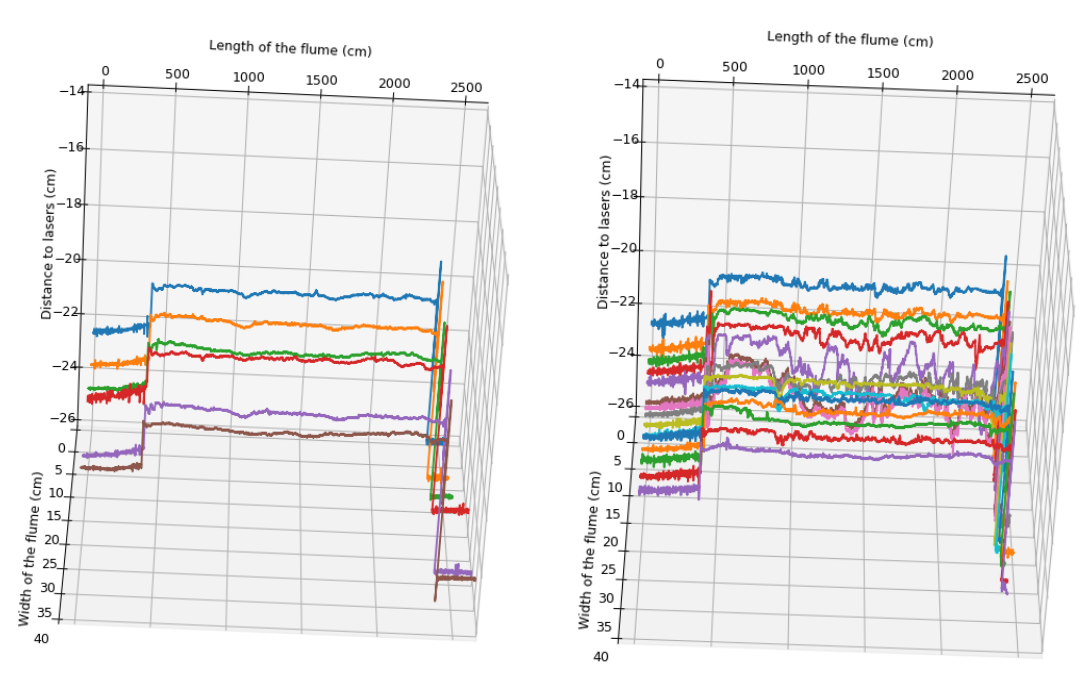


Figure 28 The six scans measured before experiment 10 (left) and the fifteen scans measured after experiment 10 (right).

The collector head encounters abrupt changes in bottom clearance at both the beginning and end of the wooden tray housing the clay bed, as depicted in Figure 29. These transitions in clearance are visually represented as peaks in the graphs, as illustrated in Figure 28 for example. The presence of these abrupt changes makes the results acquired near them unreliable. To ensure the reliability of the results, it has been decided, based on optical observations from multiple experiments, to discard the data obtained from the first 50 cm and the last 20 cm of the clay bed, as shown in Figure 29. This precautionary approach helps to ensure the integrity of the data and enhances the validity of the conclusions drawn from the study.

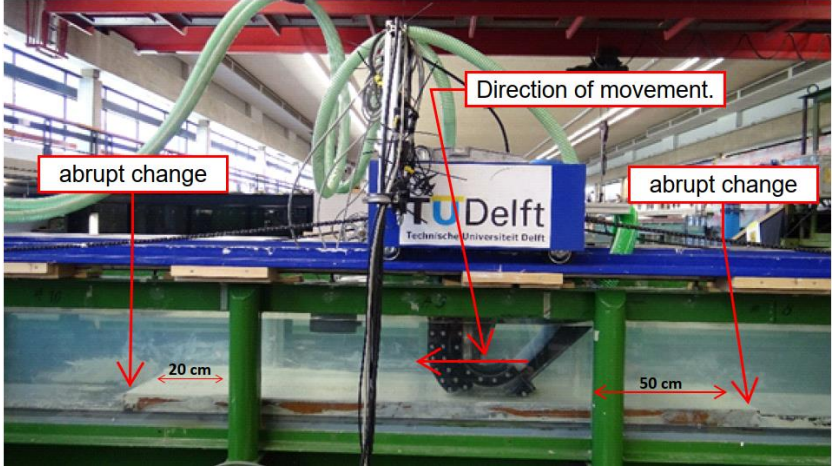


Figure 29 The experimental setup showing the abrupt changes at the beginning and at the end of the tested clay bed.

To illustrate how the results are incorporated, Experiment 10 will be used as an example. Figure 30, Figure 31 and Figure 32 presents full line scans of points at 5 cm, 20 cm, and 35 cm of Experiment 10 before and after the experiment. Disturbances in the clay bed are evident in Figure 30, with observable areas of erosion and deposition. Figure 31 shows a scan taken in the middle of the flume, revealing the eroded clay bed. Notably, the first half meter exhibits a distinct pattern of erosion, and as a precaution,

this region is discarded from further analysis. Besides, Figure 32 displays the scan at 35 cm from the left side, where the line profiles before and after the experiment are nearly identical. This indicates minimal changes in this particular region of the clay bed, reinforcing the significance of considering specific areas when evaluating the overall effects of the experiment.

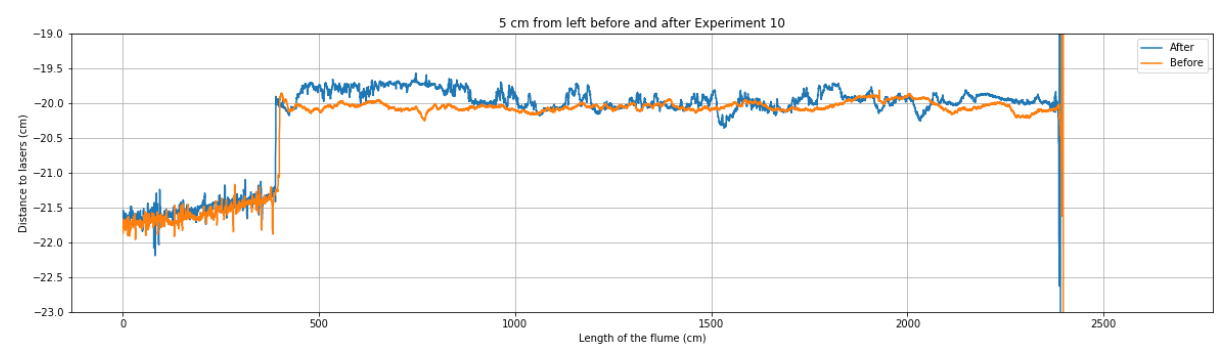


Figure 30 Scans before and after Experiment 10 at 5 cm from the left side of the flume.

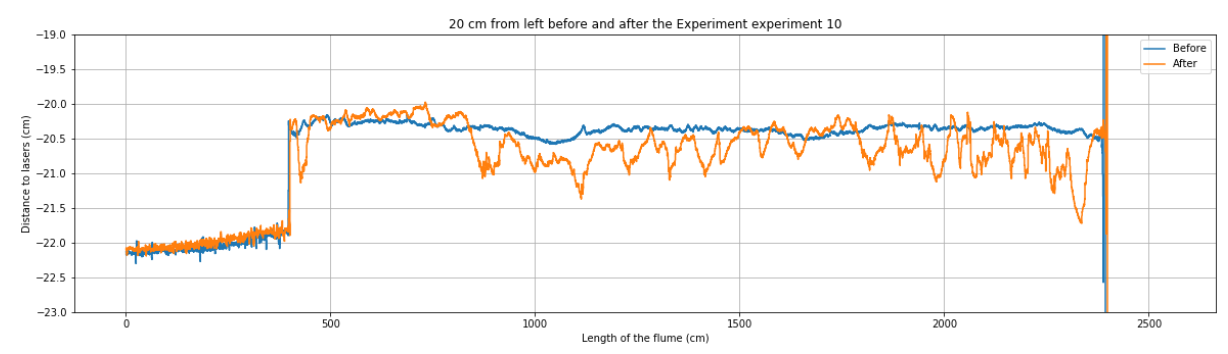


Figure 31 Scans before and after Experiment 10 in the middle of the flume.

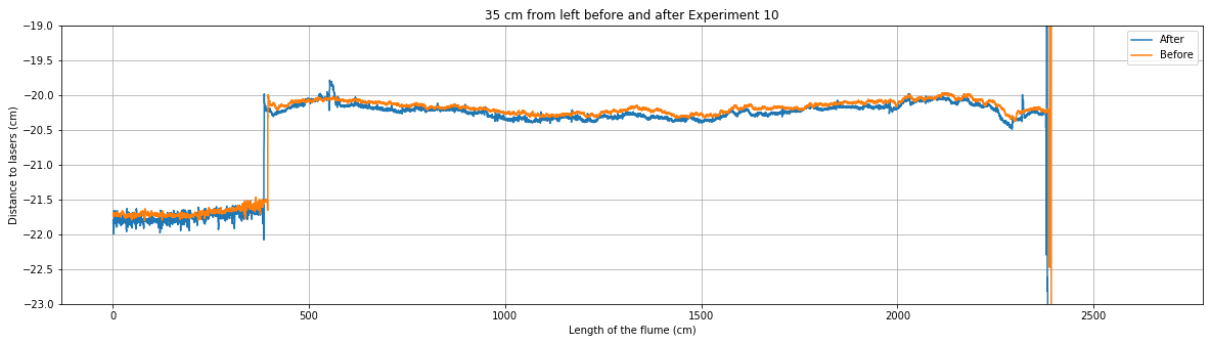


Figure 32 Scans before and after Experiment 10 at 35 cm from the left side of the flume.

The clay erosion of the bed is predominantly characterized by inhomogeneity, evident in both the length and width directions, as depicted in Figure 33. This inhomogeneity poses challenges in obtaining a complete and comprehensive image of the eroded clay bed solely through individual line scans. To overcome this limitation, a decision has been made to capture 15 line scans across the clay bed.

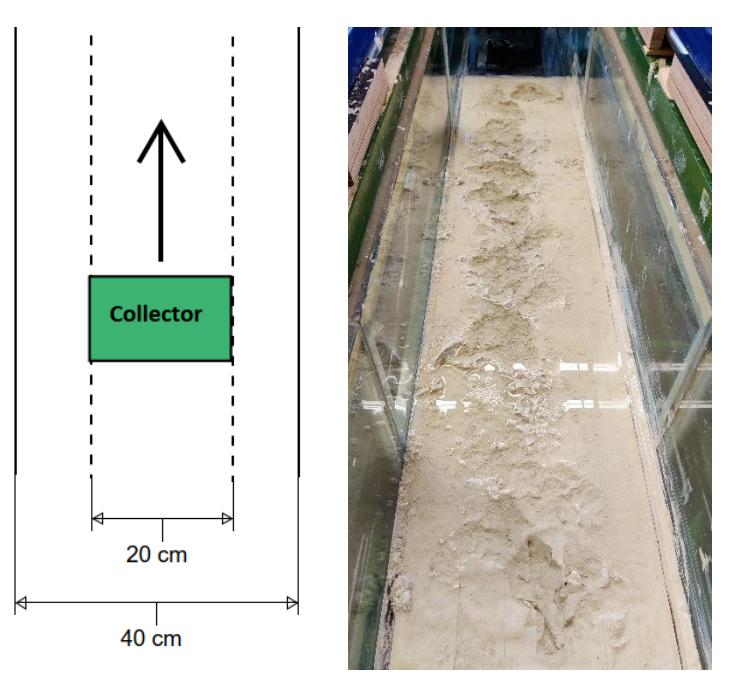


Figure 33 Shallow trench created at the sand bed as a result of clay erosion of experiment 12 (right). Top view of the water flume depicting the position of the collector.

Each of these 15 line scans will be utilized to calculate an average value. These average values will be subsequently employed to construct a cross-sectional profile of the clay bed, see Figure 34. This cross-sectional profile will provide crucial information, enabling the determination of both the maximum clay depth and the eroded clay area. The cross-sectional analysis will contribute valuable insights into the mechanisms underlying the clay bed erosion, contributing to the overall findings and implications of the study.

In the pursuit of a comprehensive analysis, the described steps will be applied to all experiments conducted to acquire cross-sectional profiles as the one depicted in Figure 34. The vertical lines correspond with the area covered by the collector head. The horizontal line at y = 0 represents the clay bed before the experiments. Measured points below this line means that erosion found place and measured points above this line means that the clay bed is disturbed.

In the forthcoming sections, the crosssectional profiles will be presented with respect to the various influencing parameters individually. This focused presentation will enable a systematic and in-depth analysis of

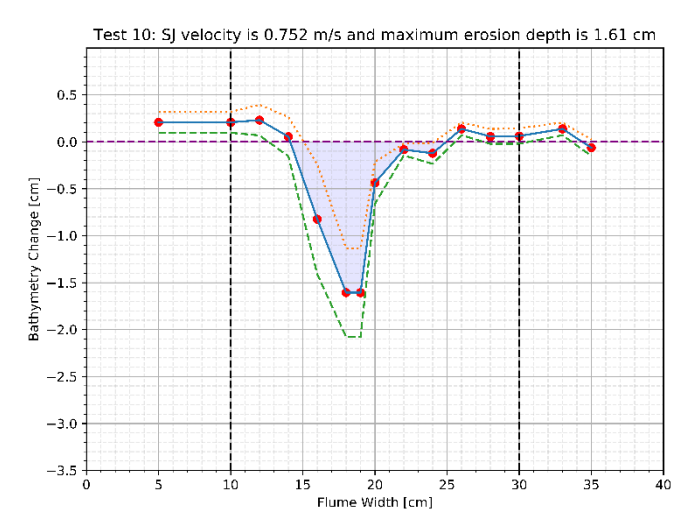


Figure 34 The cross-sectional profile of the clay bed after experiment 10.

the impact of each parameter on the clay bed's erosion behaviour. By isolating and scrutinizing the influence of the concerned parameters, we aim to unveil the specific mechanisms governing the sediment erosion processes within the experimental setup.

## 5.4. Clay Characterization

To conduct the experiments successfully, it is essential to create cohesive sediment, and therefore, a carefully prepared clay is required. The synthesized clay should resemble the properties of deep-sea clay, particularly focusing on matching the shear strength characteristics. Additionally, the clay must exhibit erosion under the available operating conditions, including the jet velocities. Moreover, it is crucial for the clay to be easy to mix, ensuring a homogeneous and consistent mixture for reliable experimentation. Furthermore, ease of cleaning is preferred to avoid excessive stickiness, which could interfere with the experimental setup. By meeting these criteria, the prepared clay will serve as a suitable medium for studying sediment transport dynamics, contributing to a more accurate representation of real-case scenarios and providing valuable insights into sediment behaviour under controlled conditions. In this chapter the composition of the prepared clay will be discussed. Besides, the clay properties will be presented. These properties are obtained from rheological tests done at Deltares.

## 5.4.1. Composition of Clay

In the preparation of the clay mixture, the study of Shakeel et al. (2021) served as a reference. Bentonite suspensions are known for their thixotropic behaviour, displaying high viscosity and yield stresses, even at low volume fractions of solids. This behaviour is attributed to the swelling nature of Na-montmorillonite present in bentonite. When water molecules penetrate the interlayers of clay platelets, they cause the hydration of sodium ions, resulting in the swelling and delamination of clay platelets. This delamination leads to an increase in particle concentration, a decrease in clay platelet size, and an increase in particle's specific surface area. The high particle concentration and surface area lead to enhanced particle-particle interactions, contributing to the suspension's high yield stress values.

In contrast, kaolinite (or kaolin) suspensions exhibit non-Newtonian behaviour, with a yield stress at high solid content (around 30-40 wt%). The non-swelling nature of kaolinite prevents delamination, resulting in a lower surface area compared to montmorillonite particles, which limits particle-particle interactions.

The distinct rheological properties of these two clays can be utilized by mixing them in specific ratios to tune the rheological properties of the clay mixture for specific applications. By carefully adjusting the clay composition, researchers can tailor the behaviour of the clay mixture to suit particular experimental requirements, enabling the study of sediment transport dynamics under controlled conditions. Figure 35 presents the yield stress for different kaolinite/bentonite ratio for different total solid content (Shakeel et al., 2021).

In the experimentation process, multiple clay mixtures were prepared, varying the ratios of kaolinite and bentonite as well as the total solid content. The fall cone test was utilized as a means

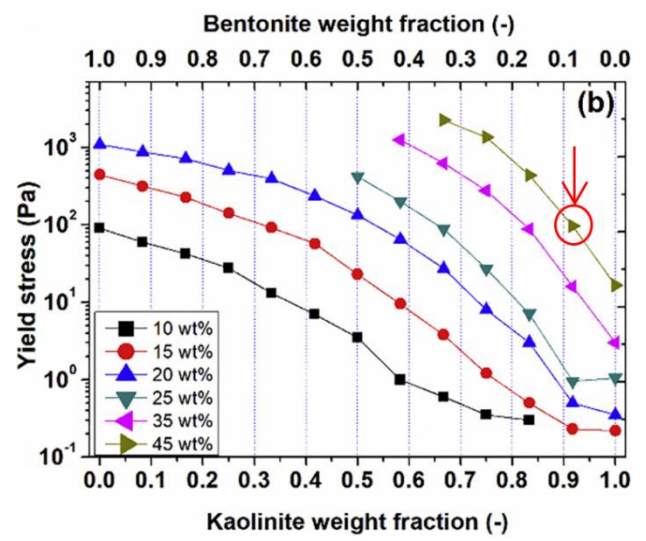


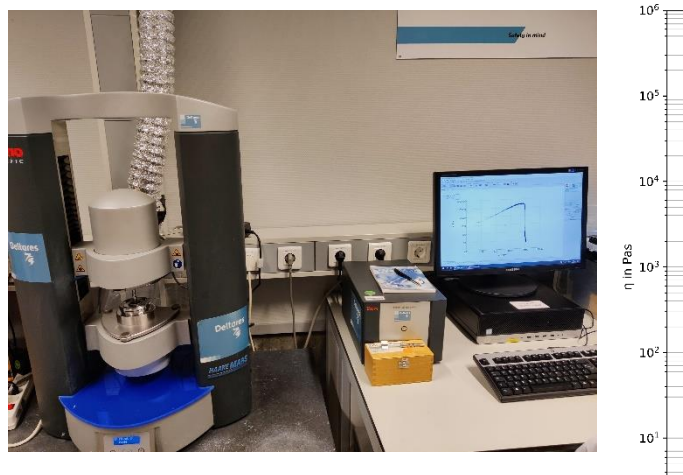
Figure 35 Yield stress as a function of kaolinite/bentonite ratio for different total solid content (Shakeel et al., 2021).

to get a sense of the strength of the prepared clay mixtures. Additionally, the ease of mixing and the stickiness of the clay were taken into consideration during the selection process.

After careful evaluation, the chosen clay mixture was composed of 8% bentonite and 92% kaolinite, with a total solid content of 45%, see Figure 35. This specific blend offered the desired rheological properties and behaviour for the experimental objectives. As shown in the graph, this mixture gives a shear strength of 0,1 kPa. The clay will be tested at Deltares to verify this value. The chosen composition of the clay mixture played a critical role in providing valuable insights into the behaviour of clay erosion and sediment-laden currents.

### 5.4.2. Shear strength

To verify the shear strength of the prepared clay, a shear strength test was conducted at Deltares. Figure 36 displays the testing setup and illustrates the viscosity decline of the clay sample. The results of the test confirmed that the shear strength of the clay was nearly 0,1 kPa, validating the intended properties of the clay mixture. The successful verification of the shear strength through the conducted test ensures the reliability and accuracy of the preparation method, confirming that the clay is well mixed and suitable for the objective of this research.



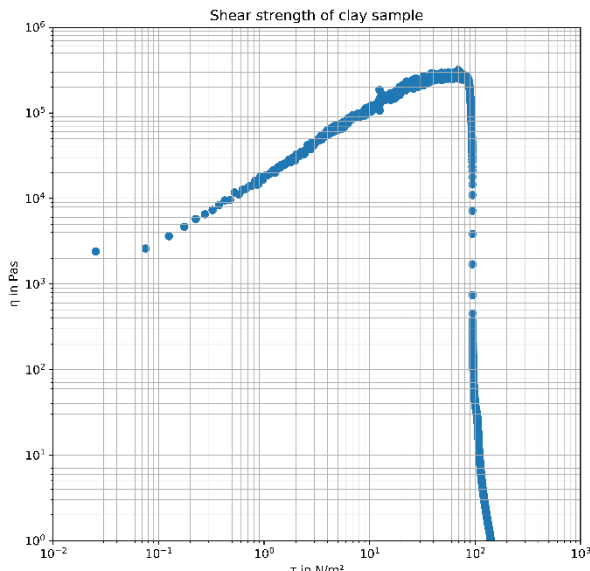


Figure 36 Shear strength testing setup at Deltares (left) and apparent viscosity as a function of stress for suspensions for the tested clay sample (right).

#### 5.4.3. Particle size distribution

The particle size distribution analysis conducted at Deltares provided the values for D10, D50, D60, and D90, which are 2.1, 5.9, 7, and 14.7, respectively. To calculate the coefficient of uniformity (CU), we divide the particle size at 60% passing (D60) by the particle size at 10% passing (D10):

Coefficient of Uniformity (CU) = D60 / D10 =  $7 / 2.1 \approx 3.33$ 

With a coefficient of uniformity (CU) of approximately 3.33, the clay is considered to be uniformly graded. The relatively close values of D60 and D10 indicate a more consistent particle size distribution, suggesting that the clay has a more uniform arrangement of particle sizes.

Figure 38 and Figure 37 presents the particle size distribution, the cumulative particle size distribution and the testing setup of the clay.

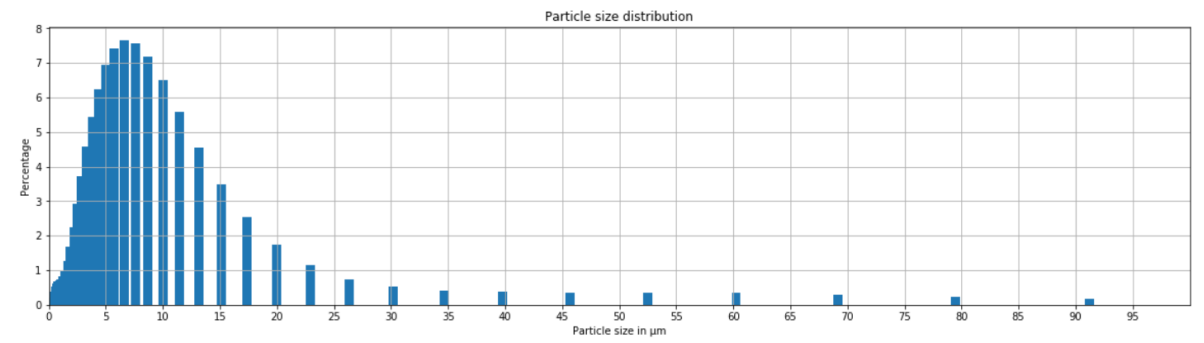


Figure 38 Particle size distribution of the prepared clay.

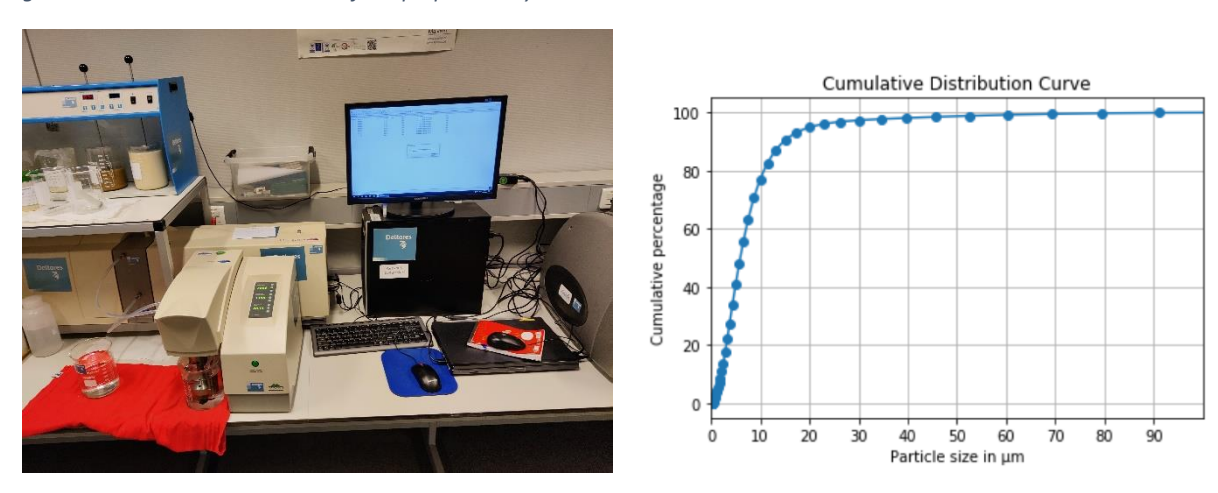


Figure 37 Testing setup at Deltares (left) and the cumulative particle size distribution of the clay (right).

## 5.4.4. Bulk Density of clay

The bulk density of the clay was measured using a  $100 \, \text{mL}$  container with a hole at the top to remove excess clay and ensure the container is completely filled, see . The density was calculated as follows:

Weight of container: 69,41 g
Total weight: 204,60 g
Net weight of clay: 135,19 g
Volume: 100 mL

Bulk density =  $135,19 / 100 = 1,3519 \text{ g/mL} = 1352 \text{ kg/m}^3$ .



Figure 39 The container filled with clay on the scale.

#### 5.4.5. Solid content

The solid content of the clay was determined by conducting an oven-drying test. The clay sample was weighed before and after being dried in the oven to remove all the water content. The difference in weight before and after drying allowed the calculation of the solid content, which was found to be approximately 0.43. This value closely matches the solid content used during the clay preparation process.

Weight before: 35,74 gWeight after: 15,45 gSolid content = 15,45/35,74 = 0,43.

## 6. Results

After completing the experiments as described in the previous chapter, a substantial amount of data has been collected. In the following sections, the data will be presented and analysed in the order of the research questions.

Firstly, in section 6.1, the results of the Electromagnetic Current Meter (EMS) regarding water entrainment will be presented. Section 6.2 will focus on the erosion of the clay bed and the influence of different parameters. Subsequently, section 6.3 will delve into studying the main mechanism behind the erosion observed. Moving on to section 6.4, the analysis will explore the influence of the presence of the secondary jet duct. Lastly, section 6.5 will analyse the turbidity currents of the spillage plume behind the collector head. This systematic approach to presenting and analysing the data aims to comprehensively address the research questions and provide valuable insights into the complex interactions and phenomena observed during the experiments.

#### 6.1. Water Entrainment

Water entrainment is a significant phenomenon to comprehend in order to conduct more realistic experiments. It plays a crucial role in influencing the movement of ambient water around the collector and, consequently, impacts clay erosion as well. To quantify the water entrainment, an EMS is mounted on the collection duct once the collection hose has been removed. This EMS device accurately measures the velocity of the discharged flow, as depicted in Figure 40. It is important to mention that the water level was 37 cm, and the outlet extended 3 cm above the water surface.



Figure 40 An experimental run in progress showing the water flowing out the collection duct while the EMS is measuring.

The measurement of the flow rate in the collection duct serves two important purposes in this study. Firstly, it allows to investigate the effect of different parameters (forward velocity, clearance, main and secondary jet velocity) on water entrainment. By monitoring the flow rate, it can be understood how these parameters influence the amount of ambient water drawn into the collection duct, which in turn affects the overall dynamics of the system, including clay erosion.

Secondly, the measurement of the flow rate also helps in optimizing the use of the pump connected to the collection duct. The pump is employed to compensate for the friction introduced by the collection hose, which is not present in real-world scenarios. By understanding the flow patterns and characteristics of the water entrainment, the pump's operation can be fine-tuned to simulate the measured flow more accurately without interference or disruption. This optimization ensures that the experiments mimic real-world conditions as closely as possible, leading to more reliable and meaningful results. Overall, the flow rate measurement in the collection duct is a crucial tool for enhancing the understanding and accuracy of the experimental setup in studying water entrainment and its impact on the system dynamics.

To achieve this, the velocity of the discharged water is measured in a series of experiments, as documented in Table 11. The water level was maintained at the same level during all experiments. It is important to note that the experiments listed in the table are conducted with the collector in a stationary position. To further investigate the influence of forward velocity, the same experiments are replicated using two different forward velocities: 12,5 cm/s and 25 cm/s. As a result, the total number of experiments conducted is 21 (as listed in Appendix B1) multiplied by 3 (for each of the two forward velocities and the stationary position), resulting in a total of 63 experiments.

The EMS measures a voltage that can be utilized to calculate the horizontal vector of the discharged water velocity through calibration formulas provided with the EMS. However, it is important to note that the collection duct is inclined at a 45-degree angle with respect to the horizontal axis. As a result, the velocity vector is determined using appropriate trigonometric calculations based on the measured horizontal velocity vector. Subsequently, the flow rate can be calculated by utilizing the inner diameter of the collection duct, which is 48 mm.

Additionally, to ensure the accuracy and reliability of the calculated flow rate, it is verified using a simple and independent method. A bucket and timer are employed to measure the actual flow rate of random experiments manually. The water discharged from the collection duct is collected in the bucket for a specific time duration, and the volume of water collected is measured. By dividing the volume of water by the time, the flow rate is calculated independently. This random verification process is conducted to cross-check and validate the flow rate obtained through the EMS measurements and calculations.

Figure 41, Figure 42, and Figure 43 depict the influence of different parameters on water entrainment. Surprisingly, the obtained results show no water entrainment, resulting in the lower flow rate in the collection duct compared to the main and secondary jets' flow rates. This outcome contradicts the initial hypothesis for this research question and does not align with the findings reported in (Alhaddad et al., 2023). The lack of water entrainment in the experiments could potentially be attributed to the confined setup utilized in the experiments. The collector head's limited free space within the flume, with only 10 cm on the left and right side, and the partial submergence of the collector head might have influenced the water entrainment dynamics, leading to these unexpected results.

It appears that no actual values for water entrainment were obtained from the results due to the absence of any measurable water entrainment in the experiments. However, the results did provide valuable insights into the influence of the different parameters on the flow rate in the collection duct. The experimental data allowed for the assessment of how variations in parameters such as forward velocity, clearance, main and secondary jet flow rate affected the flow rate in the collection duct. It is worth highlighting that the water level plays a pivotal role in studying water entrainment. In this specific scenario, the outlet extended 3 cm beyond the water surface, and the setup was constrained by this height limitation. Later, in order to investigate the impact of the secondary jet duct on water entrainment, adjustments were made to reduce the collector head's height. Consequently, water entrainment occurred in this modified setup, as detailed in Chapter 6.4.1. This underscores the significance of the water level in these experiments.

Figure 41 illustrates the relationship between the main jet flow rate and the flow rate in the collection duct. As anticipated, an increase in the main jet flow rate corresponds to a higher flow rate in the collection duct. Additionally, the figure indicates that a larger bottom clearance results in a lower flow rate in the collection duct. Moreover, higher forward velocity contributes to a higher flow rate in the collection duct.

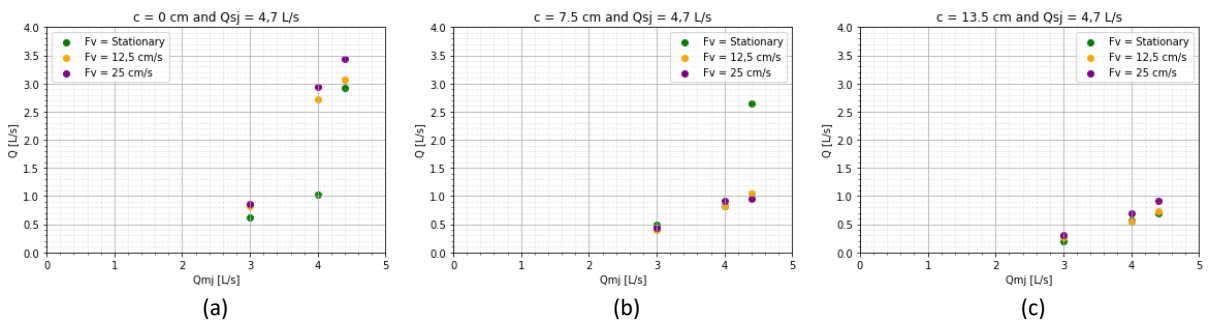


Figure 41 The influence of the main jet flow rate on water entrainment while maintaining the secondary jet flow rate and using three different forward velocities and three clearance values (0 mm (a), 7,5 mm (b), and 13,5 mm (c)).

Figure 42 depicts the correlation between the secondary jet flow rate and the flow rate in the collection duct. As expected, an increase in the secondary jet flow rate corresponds to a higher flow rate in the collection duct. The figure further verifies that a larger bottom clearance leads to a lower flow rate in the collection duct. Additionally, higher forward velocity results in a higher flow rate in the collection duct.

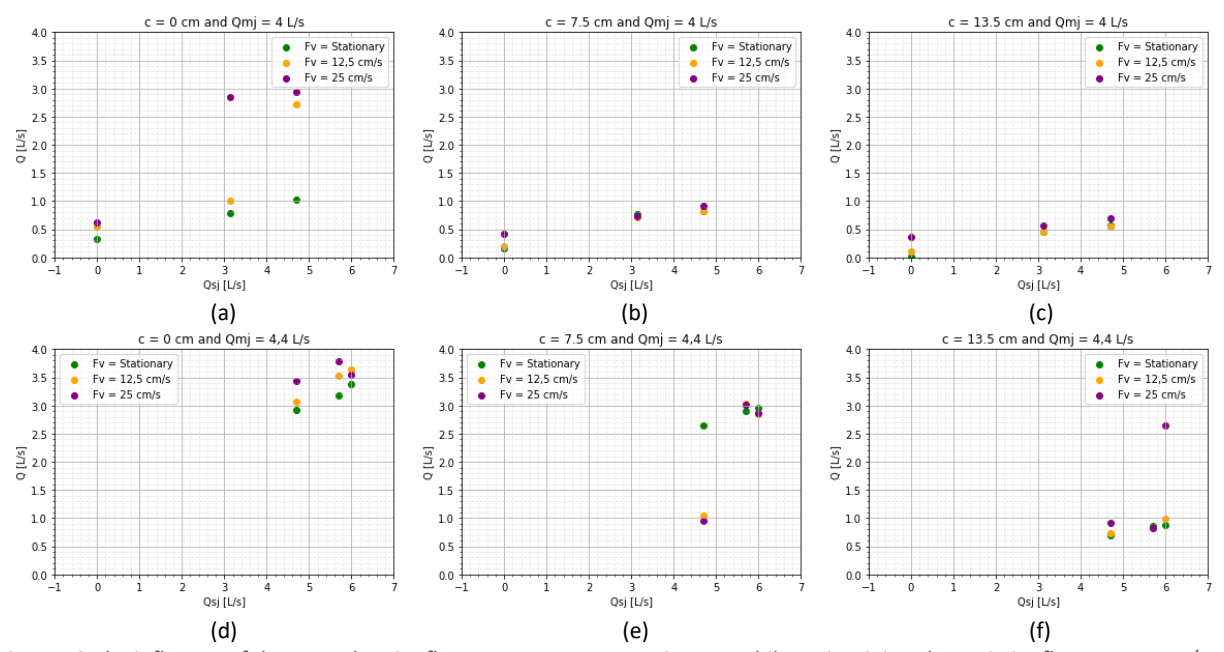


Figure 42 The influence of the secondary jet flow rate on water entrainment while maintaining the main jet flow rate at 4 L/s (a, b and c) and at 4,4 L/s (d, e and f) and using three different forward velocities and three clearance values.

Figure 43 presents the relationship between the total flow rate of both the main jet and the secondary flow rate with the flow rate in the collection duct. Consistent with expectations, an increase in the total flow rate corresponds to a higher flow rate in the collection duct. The figure also confirms that a larger bottom clearance is associated with a lower flow rate in the collection duct. Moreover, higher forward velocity leads to a higher flow rate in the collection duct.

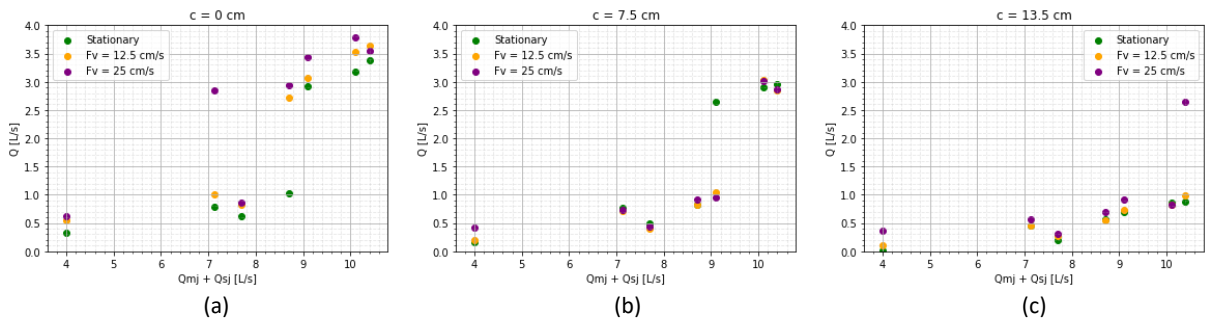


Figure 43 The influence of the total flow rate of both main and secondary jet flow rates using three different forward velocities and three clearance values (0 mm (a), 7,5 mm (b), and 13,5 mm (c)).

In contrast to the study conducted by Alhaddad et al. (2023), the present research reveals a different trend in the behaviour of water entrainment. Specifically, it is observed that a larger bottom clearance results in a lower flow rate in the collection duct. This finding may be attributed to the presence of conflicting factors influencing this process. A larger clearance leads to a decrease in the pressure gradient, which could contribute to the observed lower flow rate. Additionally, the confined system used in this research might limit the movement of the ambient water, potentially leading to different results compared to Alhaddad's study. These discrepancies emphasize the complexity of the collection mechanism and the need for a comprehensive understanding of the influencing factors.

## 6.2. Clay Erosion

### 6.2.1. General Description of Clay Erosion

After conducting the experiments and analyzing the data obtained from the Electromagnetic Current Meter (EMS), it was observed that no water entrainment occurred within the limited experimental setup. Moreover, the flow rate in the collection duct was found to be notably low. In response to these findings, a decision was made to maintain the flow rate through the collection duct at a value equal to the sum of both the main and secondary jet flow rates. This adjustment aims to create hydraulic conditions close to those of a Coandă-effect-based collector. This is done to enhance the reliability of the results obtained from the experiments and gain insights into the underlying mechanisms governing the interaction between the collector head and the clay bed.

The initial phase of experimentation involves conducting the first thirteen experiments, as specified in Table 2. These experiments aim to investigate the influence of four key parameters: the forward velocity of the collector, the clearance beneath the collector head, and the velocities of both the main and secondary jets. By systematically varying and controlling these parameters, valuable insights into their impact on the clay erosion will can be obtained.

#### 6.2.2. Forward Velocity

In this scientific study, the influence of the forward velocity of the collector's head is examined through four tests. The velocity is varied, while all other parameters remain constant, as presented in Appendix C2 in Table 13. The flow rates in both the main jet duct and secondary jet duct are maintained at 4.4 L/s and 6.1 L/s, respectively, while the clearance remains fixed at 3 mm. By systematically adjusting the forward velocity while holding these parameters steady, the direct impact of forward velocity on clay erosion can be analysed. This controlled approach ensures that any observed variations can be specifically attributed to changes in forward velocity, providing valuable insights into the system's dynamics.

Figure 30 displays the cross-sectional profiles of the clay bed following the completion of the four experiments detailed in Appendix C2 in Table 13. The original level of the clay bed is shown for reference. Additionally, the standard deviation of the averaged cross-section is presented. The region

between the two black vertical lines corresponds to the area covered by the collector head during the experiments. This figure allows for a visual comparison of the clay bed's shape and variations resulting from the different experimental conditions. The figure also shows the maximal erosion depth of each experiment.

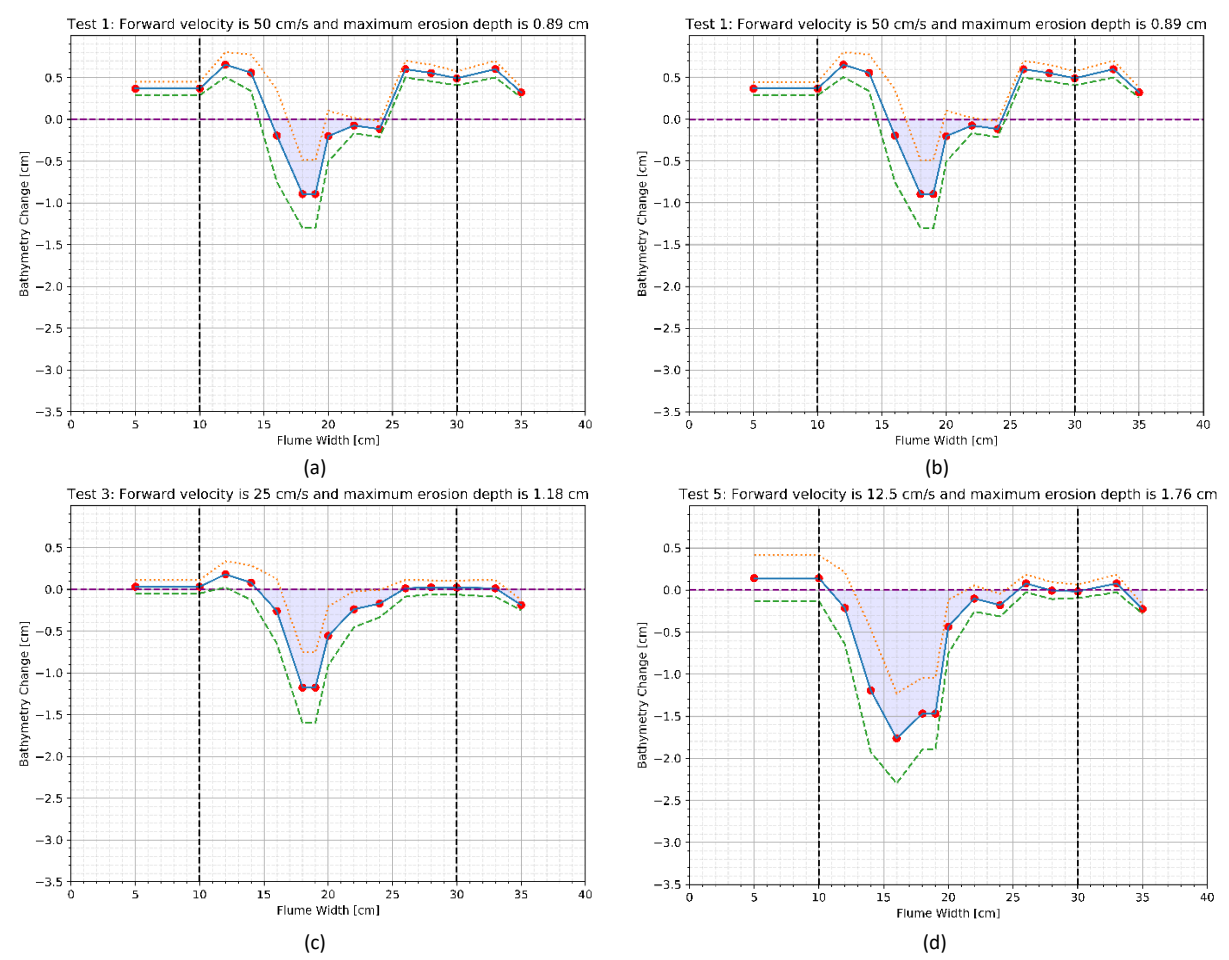


Figure 44 Cross-sectional profiles of the clay bed after tests 1 (a), 2 (b), 3 (c) and 5 (d) regarding the influence of the collector's forward velocity.

The forward velocity of the collector,  $v_f$ , significantly influences the erosion process. Notably, the experimental findings clearly illustrate that a lower  $v_f$  results in a greater erosion depth (refer to Figure 45). This correlation is unsurprising since a lower  $v_f$  implies that the clay bed remains exposed to the water jets for a longer duration, consequently leading to a more substantial erosion and thicker sediment layer being removed.

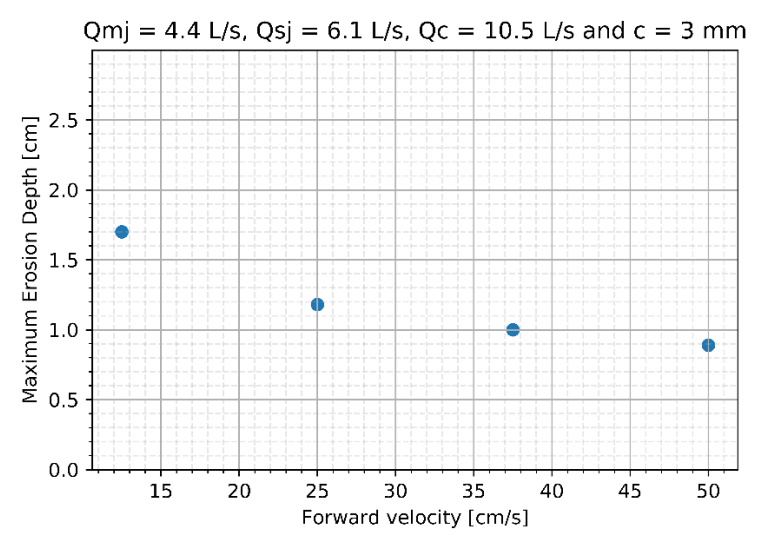


Figure 45 Influence of collector's forward velocity on the erosion depth.

#### 6.2.3. Bottom Clearance

The effect of bottom clearance on clay erosion is investigated through four tests. While maintaining all other parameters constant, as presented in Appendix C2 in Table 14, the bottom clearance is systematically varied, while the forward velocity is held constant at 12,5 cm/s. The flow rates in the main jet duct and secondary jet duct are fixed at 4.4 L/s and 6.1 L/s, respectively. By systematically adjusting the bottom clearance while holding these parameters steady, the direct impact of clearance on clay erosion can be thoroughly analysed. This controlled experimental approach allows for a focused examination of the relationship between bottom clearance and clay erosion.

Figure 46 illustrates the cross-sectional profiles of the clay bed after conducting the four tests specified in Appendix C2 in Table 14. It is noteworthy to mention that experiment 4 exhibited the highest erosion depth among all the tests. Notably, in this experiment, the bottom clearance was set to 0 mm, resulting in the most significant erosion observed in the clay bed.

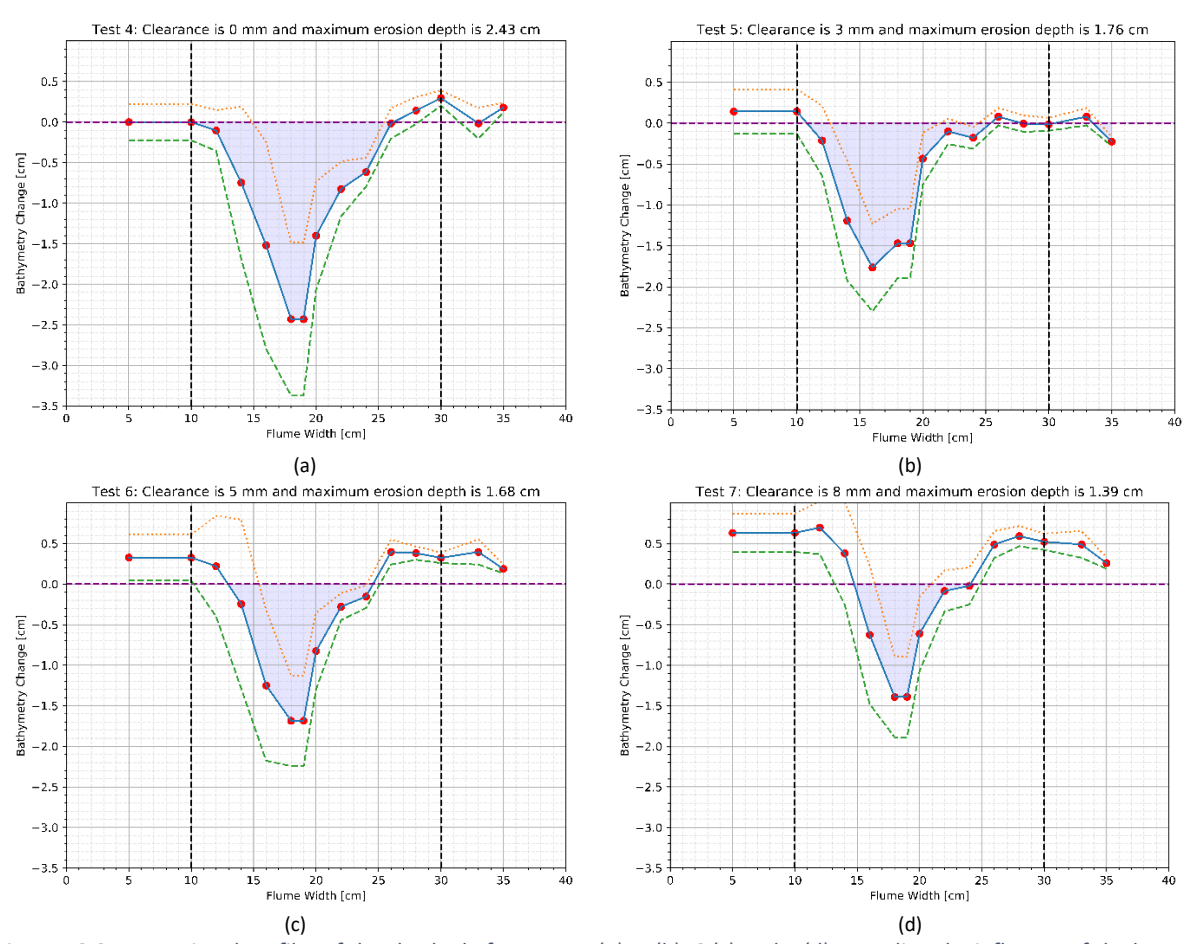


Figure 46 Cross-sectional profiles of the clay bed after tests 4 (a), 5 (b), 6 (c) and 7 (d) regarding the influence of the bottom clearance under the collector head.

The experimental results demonstrate that a smaller bottom clearance results in a larger erosion depth, see Figure 47. This correlation is also expected and is attributed to the fact that a larger clay layer is exposed to the water jets when the underside of the collector is closer to the clay bed.

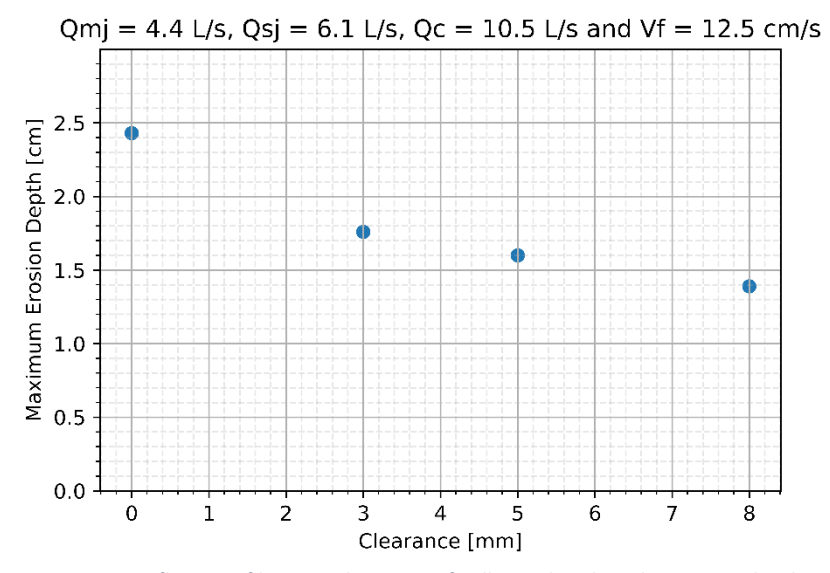


Figure 47 Influence of bottom clearance of collector head on the erosion depth.

#### 6.2.4. Main and Secondary Jet Velocities

### **Main Jet Velocity**

The effect of main jet velocity on clay erosion is studied through four tests. While keeping all other parameters constant, as shown in Appendix C2 in Table 15, the main jet velocity is systematically varied, while the bottom clearance remains fixed at 3 mm, and the forward velocity is held constant at 12.5 cm/s. The flow rate in secondary jet duct are maintained at 6.1 L/s. Analysis of the direct impact of main jet velocity on clay erosion can be achieved by systematically adjusting the main jet flow rate while keeping these parameters steady. This controlled experimental approach enables a focused examination of the relationship between main jet velocity and clay erosion.

Figure 48 illustrates the cross-sectional profiles of the clay bed after conducting the four tests specified in Appendix C2 in Table 15.

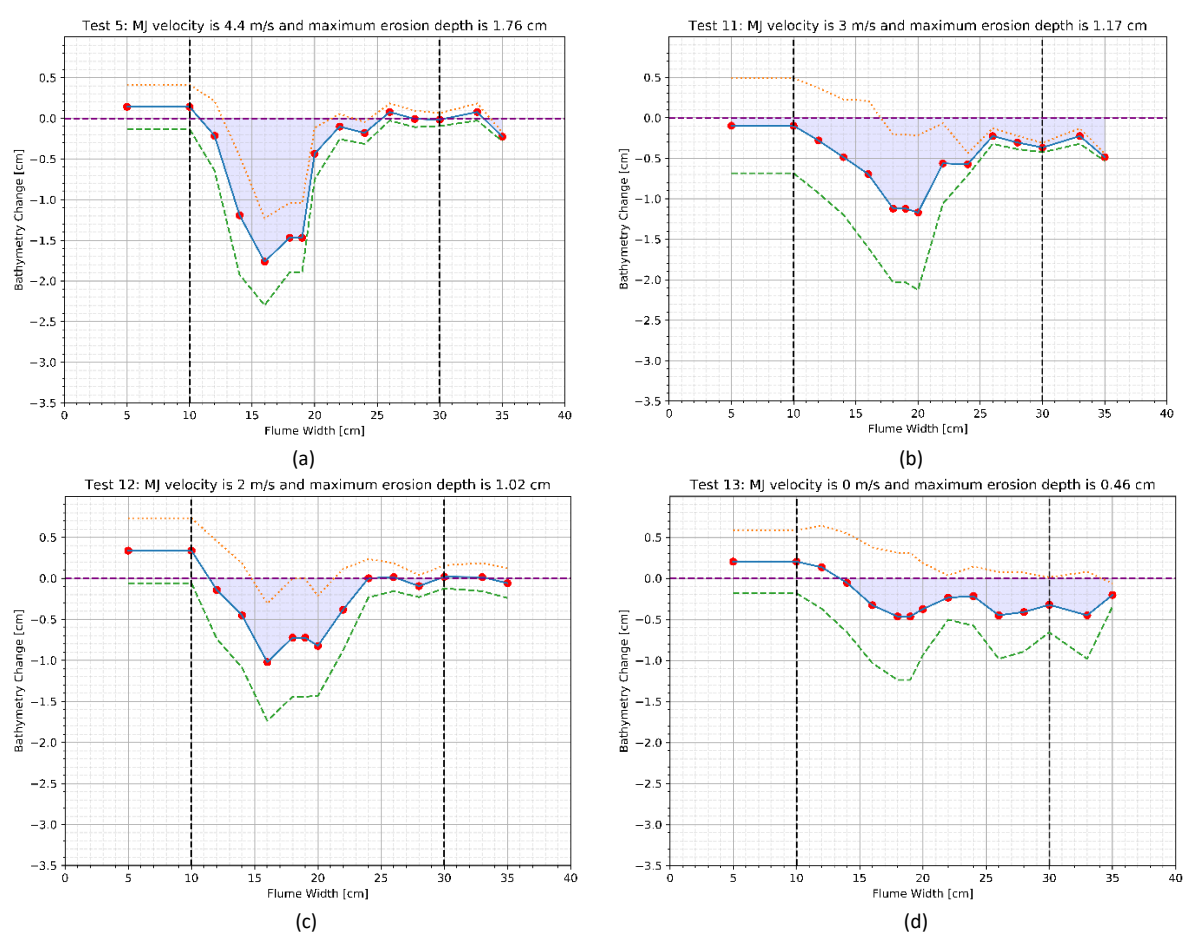


Figure 48 Cross-sectional profiles of the clay bed after tests 5 (a), 11 (b), 12 (c) and 13 (d) regarding the influence of the main jet velocity.

It is important to highlight that the flow rate in the secondary jet duct is relatively higher compared to the flow rate in the main jet duct, even though the velocity is lower (Appendix C2 in Table 15). This difference in jet velocity is attributed to the much larger height of the secondary jet duct (31.25 mm) compared to the main jet duct (5 mm). Consequently, when the flow rate of the main jet is reduced, the velocity of the water under the collector head experiences a significant decrease. As a result, lower water velocity leads to a reduction in the impingement force, resulting in shallow but wider erosion patterns. Additionally, it is observed that the standard deviation of the erosion data is higher, indicating that the clay eroded in non-uniform chunks rather than homogeneously.

#### **Secondary Jet Velocity**

The effect of secondary jet velocity on clay erosion is investigated through four tests, while all other parameters are kept constant, as indicated in Appendix C2 in Table 16. The main jet velocity is systematically varied, while the bottom clearance remains fixed at 3 mm, and the forward velocity is held constant at 12.5 cm/s. Additionally, the flow rate in the main jet duct is maintained at 4.1 L/s. By systematically adjusting the secondary jet flow rate while holding these parameters steady, the direct impact of secondary jet velocity on clay erosion can be analysed. This controlled experimental approach allows for a focused examination of the relationship between main jet velocity and clay erosion.

Figure 49 displays the cross-sectional profiles of the clay bed following the completion of the four tests specified in Appendix C2 in Table 16.

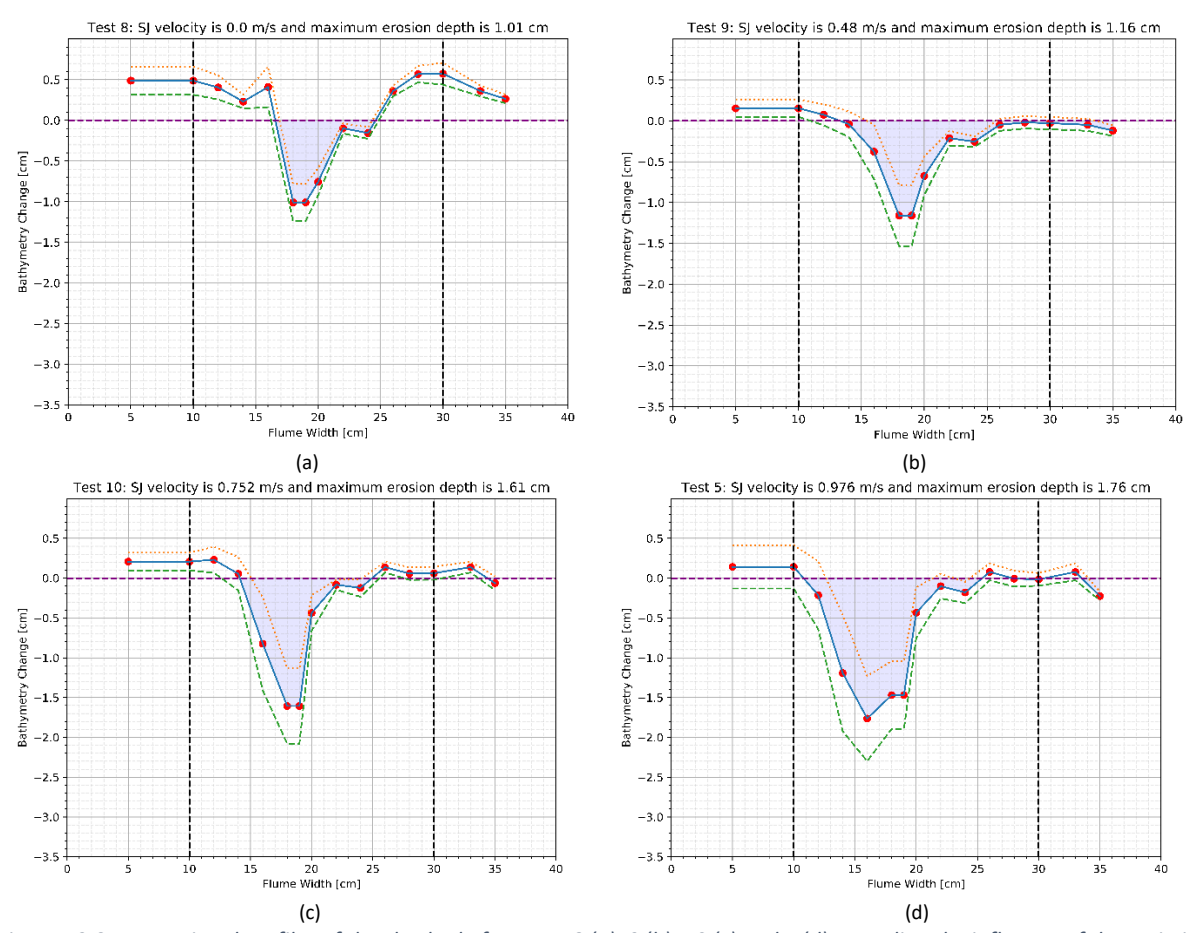


Figure 49 Cross-sectional profiles of the clay bed after tests 8 (a), 9 (b), 10 (c) and 5 (d) regarding the influence of the main jet velocity.

Indeed, an important observation is that when there is little to no flow rate in the secondary jet, the erosion becomes more concentrated in the middle and is less deep. This phenomenon suggests that the absence or reduction of the secondary jet flow rate alters the distribution and intensity of erosion in the clay bed. The concentration of erosion in the middle indicates a localized effect, likely influenced by the main jet's impingement. The decrease in erosion depth when decreasing the flow rate of the secondary jet can be attributed to the significant reduction in the total flow rates of both jets. As the flow rate in the secondary jet decreases, the combined effect of the main and secondary jets is weakened, resulting in a lower total impingement force on the clay bed.

The erosion depths were measured for experimental runs with different flow rates through the main jet,  $Q_{mi}$  (see Figure 50 (a)). It is evident that a higher  $Q_{mi}$ , and thus a higher jet velocity, leads to a larger

erosion depth in the clay bed. The same trend is observed for the effect of flow rates through the secondary jet,  $Q_{sj}$  (see Figure 50 (b)). The reason behind the observed correlations between the flow rates in the jets and sediment erosion will be analysed in Section 0.

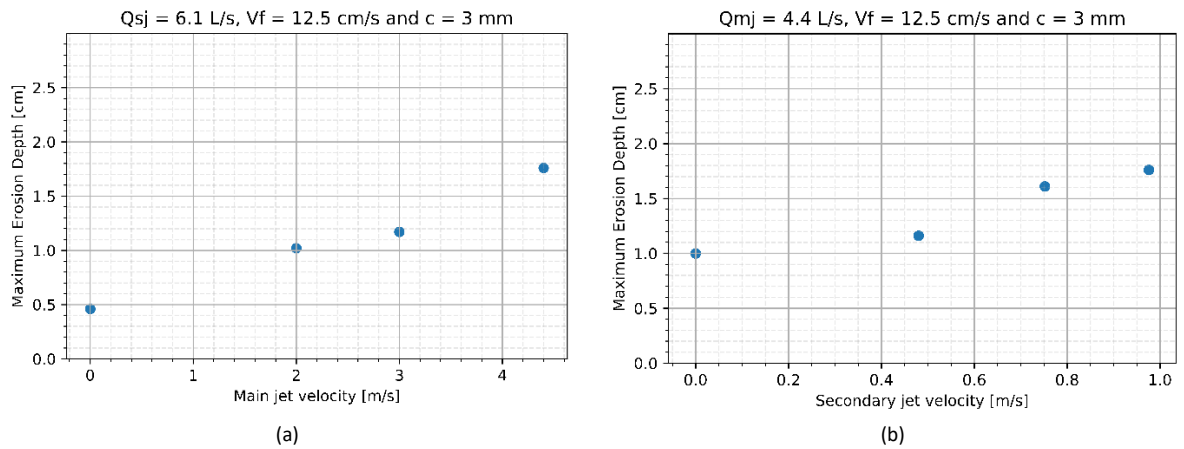


Figure 50 The influence of the main jet velocity (a) and the secondary jet velocity (b) on the erosion depth.

## 6.2.5. Time Effects on Clay Erosion

In this research, prior to each experiment, the clay bed is meticulously remoulded and levelled. This procedure is crucial to ensure consistent and reliable results while facilitating meaningful comparisons among the different experiments. Understanding how the clay bed would respond under more natural conditions with time for consolidation is also an essential aspect of the study. As depicted in Appendix C2 in Table 17, a specific experiment, namely experiment 10, is repeated after allowing the clay bed to consolidate undisturbed for three days over a long weekend. This additional step aims to observe and analyse the potential effects of consolidation on the clay bed's erosion.

Figure 51 illustrates the cross-sectional profiles of the clay bed after conducting the two tests specified in Appendix C2 in Table 17. It is noteworthy to mention that after the clay bed was allowed to consolidate for three days, the erosion depth noticeably decreased. Specifically, the erosion depth decreased by 18 mm. This observation suggests an increase in the shear strength of the clay bed, indicating that it now requires a higher impingement force to achieve the same erosion depth as before consolidation. The process of consolidation appears to have contributed to the clay bed's increased resistance to erosion.

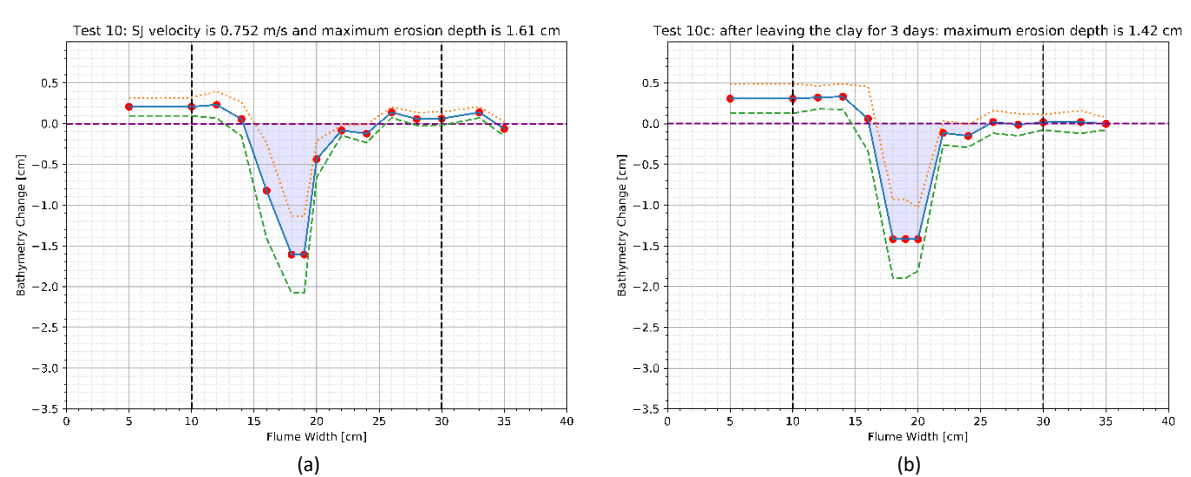


Figure 51 Cross-sectional profiles of the clay bed after tests 10 (a) and 10c (b) regarding the influence of the consolidation of the clay bed.

### 6.2.6. Reproducibility of Experiments

To ensure the robustness and credibility of the experimental results, it is imperative to ascertain their reproducibility under consistent operational conditions. Thus, experiment 5 was deliberately repeated (see Appendix C2 in Table 18) to evaluate the extent to which similar results could be obtained. The replication of Experiment 5 allows for an examination of the consistency and reliability of the observed outcomes, enabling to validate the reliability of their findings.

Figure 52 displays the cross-sectional profiles of the clay bed following the completion of the two tests specified in Appendix C2 in Table 18. The observation of similar cross-sectional profiles in the two experiments provides strong validation for the obtained results and enhances the overall reliability of the findings. The consistency in the clay bed's cross section indicates that the experimental conditions were well-controlled and reproducible, leading to consistent erosion patterns. This level of agreement between the experiments strengthens the confidence in the accuracy and precision of the data, supporting the reliability of the study's outcomes. Such validation is essential in scientific research to ensure the robustness of the conclusions and to foster a higher level of confidence in the research findings.

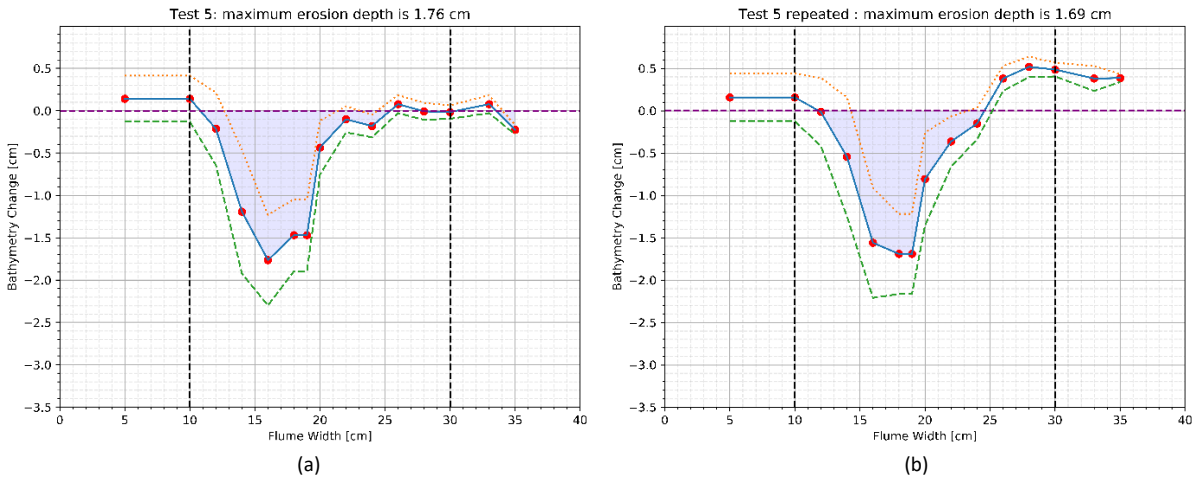


Figure 52 Cross-sectional profiles of the clay bed after tests 5 (a) and 5 repeated (b) regarding the reproducibility of the experiments.

The disturbance of the clay bed, as indicated by the measured points above the original clay bed, is assumed to occur randomly. The replication of this experiment has served to validate this assumption.

## 6.3. Analysis of Clay Erosion

In this section, the potential correlation between erosion depth and both impingement force and dynamic pressure is analysed. Additionally, observations regarding erosion patterns is presented and the scaling back to the full-scale model is discussed.

#### 6.3.1. Impingement Force

First, a possible correlation between the impingement force and the erosion depth will be studied. This is also done by Alhaddad & Helmons (2023) for sand. Subsequently, potential correlations between clay and sand erosion will be discussed.

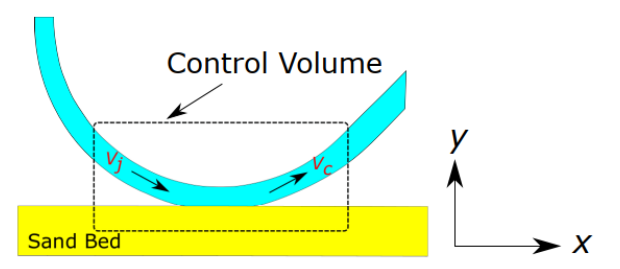


Figure 53 Water impingement of the collector head.

For the collector, the resultant force denoted as F, exerted by the water jets on the bed is calculated. This calculation is based on the control volume illustrated in the right panel of Figure 53, where the component forces  $F_x$  and  $F_y$  in the x and y directions are determined, respectively. Notably, the velocity of water spilling behind the collector head was not quantified in our tests. Therefore, the analysis of the total impinging force assumes the absence of water entrainment during the collector's operation. It's important to highlight that the contribution of water entrainment to the total striking force is negligible when compared to the water jets and does not affect the conclusions drawn in this study. The component forces and resultant force are as follows (Alhaddad & Helmons, 2023):

$$F_{x} = \dot{m} \left( v_{j} \cos \theta_{1} - v_{c} \cos \theta_{2} \right), \tag{7}$$

$$F_{y} = \dot{m} \left( -v_{j} \sin \theta_{1} - v_{c} \sin \theta_{2} \right), \tag{8}$$

$$F = \sqrt{F_x^2 + F_y^2},\tag{9}$$

In the given context, where  $v_j$  represents the velocity of the combined water jet from the two jet ducts,  $\theta_1$  (40°) stands for the angle between  $v_j$  and the X-axis,  $v_c$  denotes the flow velocity within the collection duct,  $\theta_2$  (45°) indicates the angle between  $v_c$  and the X-axis, and  $\dot{m}$  represents the mass per unit time entering or leaving the control volume. This mass per unit time can be computed as follows:

$$\dot{m} = \rho Q_i = \rho Q_c. \tag{10}$$

Impingement force calculations were performed for the experiments conducted at a forward velocity of 12.5 cm/s and a bottom clearance of 3 mm as depicted in Table 4. A possible logarithmic correlation between the maximum erosion depth and the impingement force is presented in Figure 54. The fitting (R²) is 0.3654 meaning that this correlation is does not explain much of the variation in the dependent variable. n other words, the model does not fit the data well. This finding contradicts the results obtained for sand erosion, see Figure 16.

Table 4 Impingement force calculations for the experiments conducted at a forward velocity of 12.5 cm/s and a bottom clearance of 3 mm.

Test #	<i>ṁ</i> [kg /s]	v <sub>i</sub> [m/s]	v <sub>c</sub> [m/s]	F <sub>x</sub> [N]	F <sub>y</sub> [N]	F [N]	Erosion depth [mm]
5	10.50	1.45	1.40	1.25	-20.17	20.21	17.60
8	4.40	0.61	0.59	0.22	-3.54	3.55	10.00
9	7.40	1.02	0.99	0.62	-10.02	10.04	11.60
10	9.10	1.26	1.21	0.94	-15.15	15.18	16.10
11	9.10	1.26	1.21	0.94	-15.15	15.18	11.70
12	8.10	1.12	1.08	0.75	-12.00	12.03	10.20
13	6.10	0.84	0.81	0.42	-6.81	6.82	4.60
19	7.40	1.02	0.99	0.62	-10.02	10.04	5.60

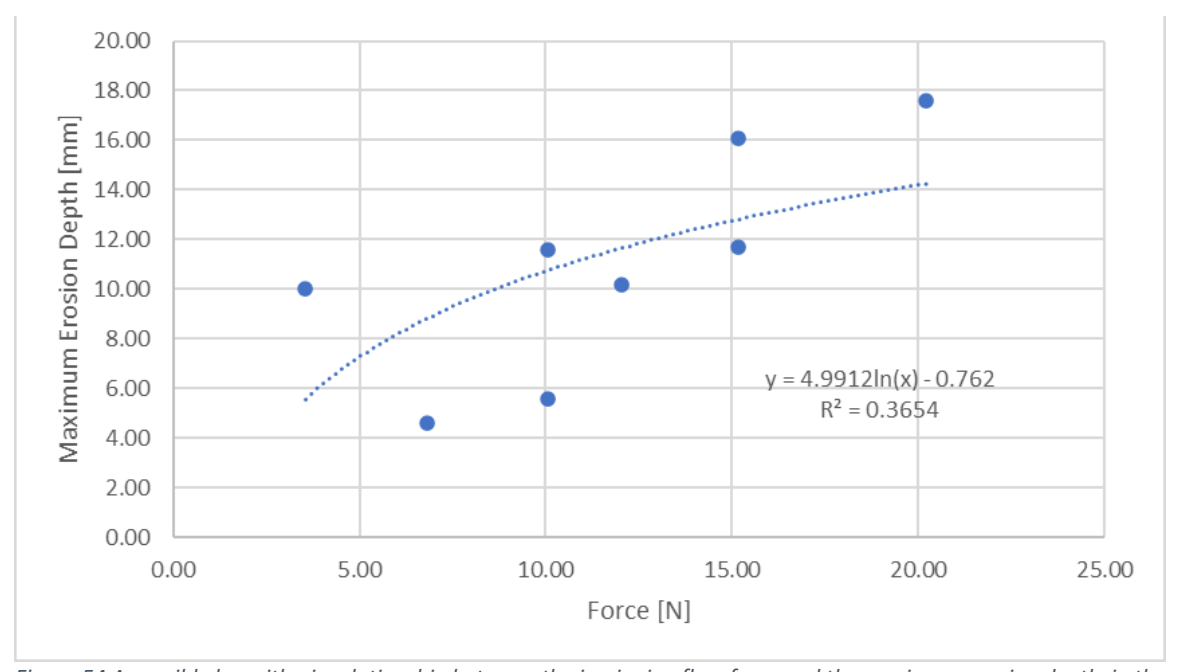


Figure 54 A possible logarithmic relationship between the impinging flow force and the maximum erosion depth in the laboratory experiments conducted as part of this study where the forward velocity is 12.5 cm/s and the clearance is 3 mm.

## 6.3.2. Dynamic Pressure

To investigate the possible relationship between erosion depth and dynamic pressure, the velocity vector was calculated for both the main and secondary jet velocities. Subsequently, the dynamic pressure for this study was separately calculated for the main and secondary jets. To estimate the total pressure, these two values were summed up as an approximation denoted as  $p_j$ . The dimensionless factors  $p_j/s_u$  and  $Z_c/D_n$  were then calculated, where  $s_u$  represents the undrained shear strength of the clay. The value 0,1 was used, as it was obtained from the rheological tests conducted at Deltares. Here,  $Z_c$  denotes the erosion depth, and  $D_n$  refers to the duct height (36.25 mm). These calculations enable assessment of any potential correlation between erosion depth and dynamic pressure, see Table 5.

Table 5 Calculation of stagnation pressure by experiment with collector's forward velocity of 12,5 cm/s.

Test #	V <sub>mj</sub>	p <sub>1,stag</sub>	V <sub>sj</sub>	p <sub>2,stag</sub>	Total p <sub>j</sub>	p <sub>j</sub> /s <sub>u</sub>	Z <sub>c</sub> /D <sub>n</sub>
	[m/s]	[N/m²]	[m/s]	[N/m²]	[N/m <sup>2</sup> ]	[-]	[-]
4	4.40	9680.00	0.98	476.29	10156.29	101.56	0.67
5	4.40	9680.00	0.98	476.29	10156.29	101.56	0.49
6	4.40	9680.00	0.98	476.29	10156.29	101.56	0.44
7	4.40	9680.00	0.98	476.29	10156.29	101.56	0.38
8	4.40	9680.00	0.00	0.00	9680.00	96.80	0.28
9	4.40	9680.00	0.48	115.20	9795.20	97.95	0.32
10	4.40	9680.00	0.75	282.75	9962.75	99.63	0.44
11	3.00	4500.00	0.98	476.29	4976.29	49.76	0.32
12	2.00	2000.00	0.98	476.29	2476.29	24.76	0.28
13	0.00	0.00	0.98	476.29	476.29	4.76	0.13

Figure 55 illustrates the relationship between the measured cavity depths ( $Z_c$ ) and the height of the two ducts combined ( $D_n$ ), normalized as a function of the jet ratio ( $p_j/s_u$ ). The plot also includes a trend line to represent the correlation between these non-dimensional parameters. Despite some scatter present in the data, a clear linear correlation is observed. The non-dimensional erosion depth increases proportionally with the jet ratio. Despite minor inaccuracies and variations in the flow rates of both the main and secondary jet ducts (approximately  $\pm 0.3$  L/s), the correlation between the normalized measured erosion depths and the trend line is notably strong, with an  $R^2$  value of 0,89.

It is important to note that in study of Nobel (2013) (refer to the Figure 56), similar scatter in the data was observed. This indicates that the presence of some variability or dispersion in the results is a common phenomenon in both investigations.

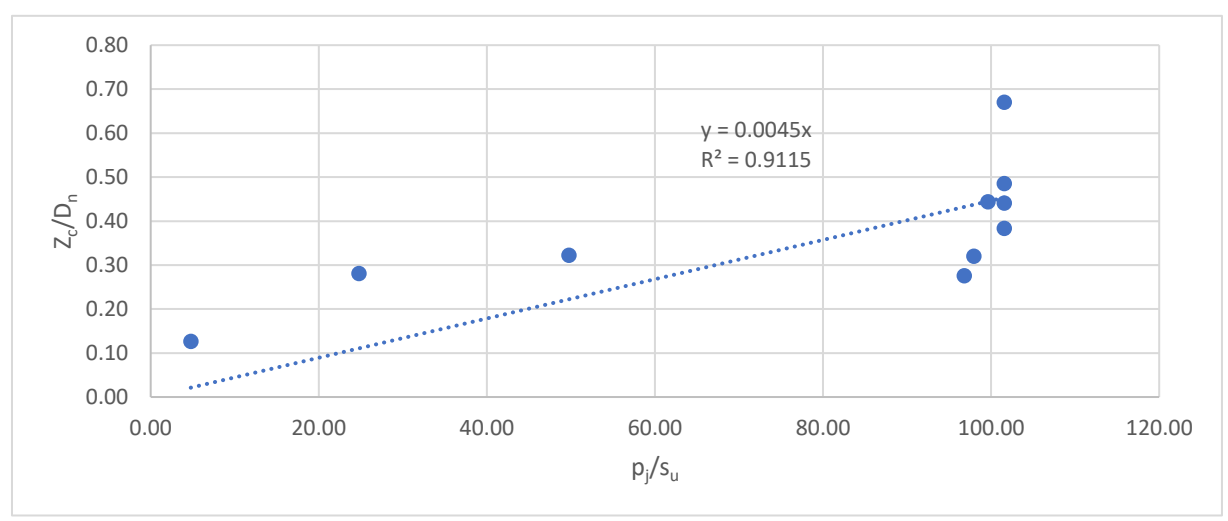


Figure 55 The normalized cavity depth  $(Z_o/D_n)$  is plotted as a function of the jet ratio  $(p_i/s_u)$  for all tests conducted with a forward velocity of the collector head at 12,5 cm/s.

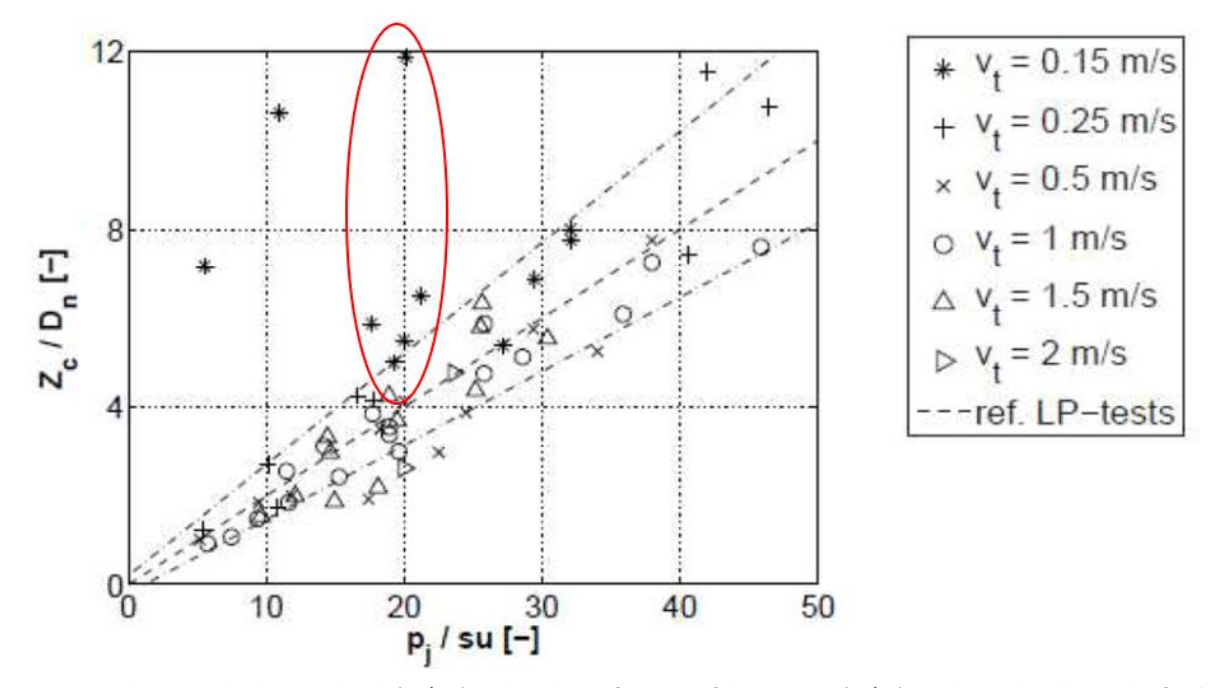


Figure 56 The normalized cavity depth (Zc/Dn) is plotted as a function of the jet ratio (pj/su) as obtained in the study of Nobel (2013) different forward velocities ( $v_t$ ).

#### 6.3.3. Erosion Patterns

The erosion patterns exhibited distinct behaviour corresponding to the variations in the main and secondary jets. The height difference between the main jet duct (5 mm) and the secondary jet duct (31.25 mm) means that the flow velocity in the main jet is higher than the secondary jet at similar flow rates, as shown in the Table 6. When only the main jet was present, deep and well-defined erosion patterns were observed on the clay bed. Conversely, the separate presence of the secondary jet resulted in wider and shallower erosion patterns. Interestingly, erosion was even observed outside the area covered by the collector head.

Table 6 Operational conditions of tests 8 and 13.

Test #	Q <sub>mj</sub> [L/s]	V <sub>mj</sub> [m/s]	$Q_{sj}[L/s]$	V <sub>sj</sub> [m/s]	Q <sub>c</sub> [L/s]	c [mm]	V <sub>f</sub> [m/s]
8	4.4	4.4	0.0	0.0	4.4	3.0	0.125
13	0.0	0.0	6.1	0.976	6.1	3.0	0.125



Figure 57 Erosion patterns of tests 8 (left) and test 13 (right).

In the study of Nobel (2013) such observations were also revealed. In this research two jets can be distinguished:

- The Penetrating jet (Figure 58 (a)): This mechanism is identified by a high jet velocity, a narrow
  deep cavities and a soil wall structure with small straight nearly vertical nerves. The excavated
  soil completely dissolves in the jet and ambient water.
- The Dispersing jet flow (Figure 58 (d)): This mechanism is characterized by a low jet velocity, a
  wide shallow cavities and an irregular soil wall structure. After the tests, dislodged soil lumps
  can be found.

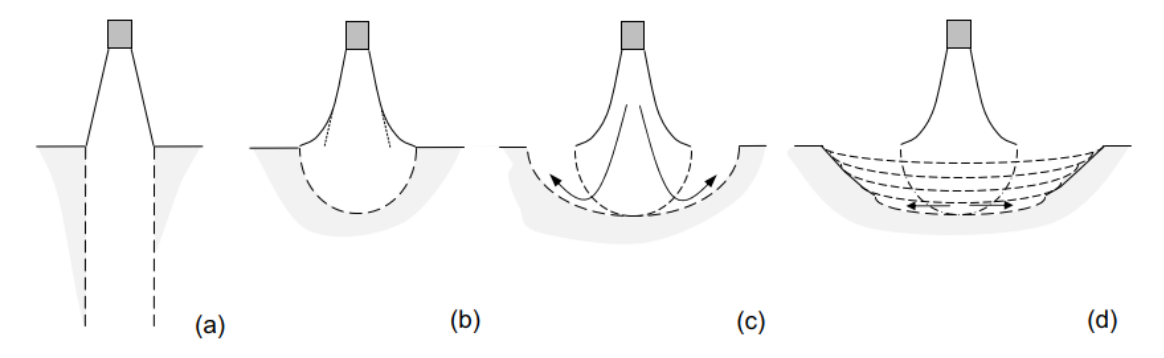


Figure 58 The defined soil failure mechanisms include according to Nobel (2013): (a) Penetrating jet, (b) Deflecting jet, (c) Dispersing jet flow, straight penetration, (d) Dispersing jet flow, gradual penetration.

## 6.3.4. Scaling

Utilizing the measured erosion depths from the conducted experiments, and considering that the collector head is scaled down by a factor of 4 in the 2D dimension, Froude scaling can be applied to predict the maximum erosion depth at the full scale. This prediction can be carried out by calculating the erosion rate of the small-scale model ( $v_{e,small}$ ) as follows:

$$V_{small} = \frac{d_{small}}{t_{small}} \rightarrow t_{small} = \frac{d_{small}}{V_{small}}$$

$$v_{e,small} = \frac{Erosion \ depth_{small}}{t_{small}}$$
(11)

$$v_{e,small} = \frac{Erosion \ depth_{small}}{t_{emall}} \tag{12}$$

Where V<sub>small</sub> is the forward velocity of the collector head, d<sub>small</sub> is the distance over which the tilted water jets touch the clay bed (scaled down version) and t is the time. Using Froud scaling the full scale maximum erosion depth could be anticipated as follows:

$$t_{full} = \frac{4 \cdot d_{small}}{V_{small} / \sqrt{0.25}} = 2 \cdot t_{small}$$
 (13)

$$v_{e,full} = 2 \cdot v_{e,small} \tag{14}$$

$$Erosion \, depth_{full} = v_{e,full} \cdot t_{full} = 4 \cdot v_{e,small} \cdot t_{small} = 4 \cdot Erosion \, depth_{small} \tag{15}$$

Following this procedure, the anticipated maximum erosion depth of the full scale model is calculated and presented in Table 7. The maximum erosion depth is found to be 9.7 cm for an extreme scenario where the forward velocity of the full scale is 25 cm/s, the clearance is 0 mm and the main and the secondary jet velocities are respectively 8.8 m/s and 2.0 m/s. The maximum erosion depth falls within the expected range as reported by Boschen-Rose et al. (2020). This alignment with their findings suggests the validity of the prediction based on Froude scaling and the conducted experiments.

Table 7 Anticipating the full scale maximum erosion depth based on Froud scaling.

Test #	V <sub>f,small</sub> [m/s]	t [s]	Erosion Depth [cm]	v <sub>e,small</sub> [cm/s]	v <sub>e,full</sub> [cm/s]	V <sub>f,full</sub> [m/s]	Expected Erosion Depth [cm]
1	0.5	0.3	0.89	2.97	5.93	1.0	3.6
2	0.375	0.4	1.00	2.50	5.00	0.75	4.0
3	0.25	0.6	1.18	1.97	3.93	0.5	4.7
5	0.125	1.2	1.76	1.47	2.93	0.25	7.0
4	0.125	1.2	2.43	2.03	4.05	0.25	9.7
6	0.125	1.2	1.60	1.33	2.67	0.25	6.4
7	0.125	1.2	1.39	1.16	2.32	0.25	5.6
8	0.125	1.2	1.00	0.83	1.67	0.25	4.0
9	0.125	1.2	1.16	0.97	1.93	0.25	4.6
10	0.125	1.2	1.61	1.34	2.68	0.25	6.4
5	0.125	1.2	1.76	1.47	2.93	0.25	7.0
11	0.125	1.2	1.17	0.98	1.95	0.25	4.7
12	0.125	1.2	1.02	0.85	1.70	0.25	4.1
13	0.125	1.2	0.46	0.38	0.77	0.25	1.8

#### 6.3.5. CCM Results

The results obtained from the Conductivity-Type Concentration Meter (CCM) were deemed unreliable, as it indicated a concentration in the discharge higher than 3%. However, upon back-calculating the eroded area of the clay bed, it was observed that the calculated area significantly exceeded the actual erosion area (refer to Appendix C3). To further validate the measurements, the erosion rate was calculated, and the real clay concentration in the discharged water was estimated, resulting mostly in under 1% concentrations. It was concluded that the CCM does not provide accurate results for such low concentrations. This was also mentioned in Deltares (2016). Additionally, the CCM's sensitivity to temperature posed uncertainties since temperature measurements were not taken during the experiments, making it challenging to ensure a constant temperature throughout the tests.

## 6.4. Secondary Jet Duct

#### 6.4.1. Water Entrainment

It is hypothesized that the presence of the secondary jet duct influences water entrainment and, consequently, clay erosion. This expectation arises from the idea that the duct creates a reserved space in front of the collector head, thereby affecting the behaviour of the ambient water in this region. To verify this hypothesis, a series of experiments are conducted to measure the flow rate in the collection duct using the EMS and the setup provided in section 6.1. Initially, 27 tests are conducted while maintaining the secondary jet velocity at 0, see Appendix B2. Subsequently, the same 27 tests are repeated after the secondary jet duct has been removed, see Figure 59. This experimental design results in a total of 54 tests, which will provide valuable data to determine the influence of the secondary jet duct on water entrainment and clay erosion dynamics.





Figure 59 Front (left) and side view (right) of the collector head after the removal of the secondary jet duct.

Figure 60 depicts the influence of the secondary jet duct on the flow rate in the collection duct, considering various values of bottom clearance and forward velocity. Notably, the flow rate in the collection duct was higher when the secondary jet duct was still fastened in place. This observation contradicts the initial hypothesis, which anticipated a reduction in flow rate in the presence of the secondary jet duct. The unexpected increase in flow rate with the duct in place but without flow rate suggests that other factors may be contributing to the flow dynamics and water entrainment in the experimental setup.

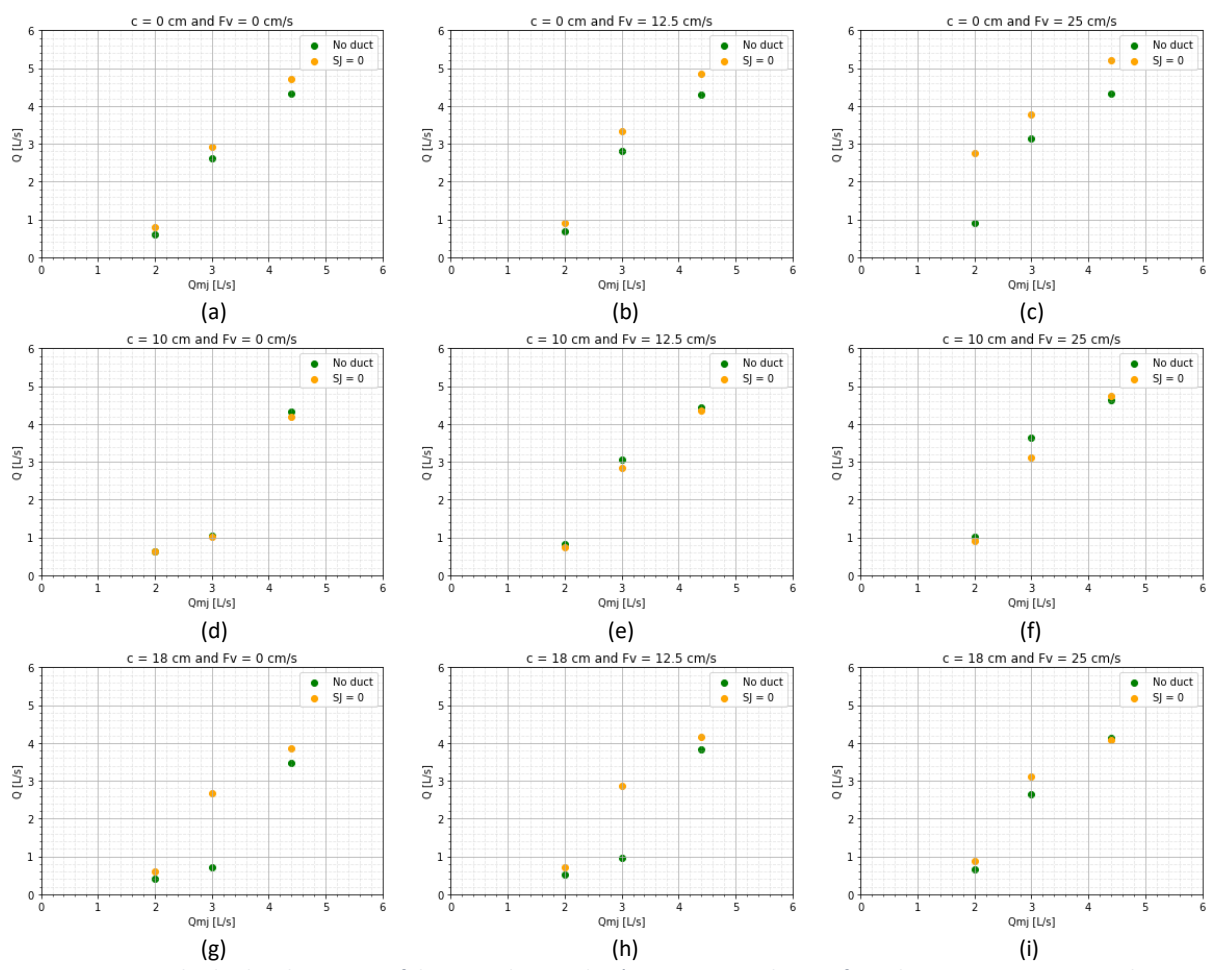


Figure 60 Nine graphs display the impact of the secondary jet duct's presence. Each row of graphs maintains a constant bottom clearance while varying the forward velocity.

An important point to highlight is that in this setup, the collector head was lowered with 4 cm compared to the tests conducted in Section 6.1. The water level was at 37 cm, causing the outlet of the collection duct to be submerged 1 cm below the water surface. As a result of this adjustment, the collector head is now fully submerged underwater. This modification has significantly improved the results concerning water entrainment. Notably, it is observed that the flow rate in the collection duct was measured to be higher than the main jet flow rate, indicating that water entrainment has indeed taken place.

To comprehend the increased water entrainment observed when the secondary jet duct is present with 0 flow rate, Figure 61 depicts the anticipated flow direction of ambient water for both cases, with and without the secondary jet duct. The figure illustrates that the presence of the secondary jet duct enhances the development of a horizontal flow pattern, leading to higher flow velocities under the collector head. Consequently, more water is expected to be directed towards the collection duct due to this intensified horizontal flow. These hypohteses necessitate further investigation to comprehend the intricate interactions and underlying mechanisms affecting flow rate and water entrainment in the presence of the secondary jet duct. To verify and understand these observations, additional data, such as the velocity under the collector head and the pressure gradient, should be gathered.



Figure 61 Expected flow direction with (right) and without the secondary jet duct (left).

### 6.4.2. Clay Erosion

To investigate the influence of the presence of the secondary jet duct on clay erosion, Test 18 was conducted, as shown in Figure 62. This test is identical to test 8, with a secondary jet velocity of 0, but with the secondary jet duct removed, as documented in Table 8. The purpose of test 18 is to compare the erosion patterns and dynamics in the absence of the secondary jet duct with the conditions when the duct is present.

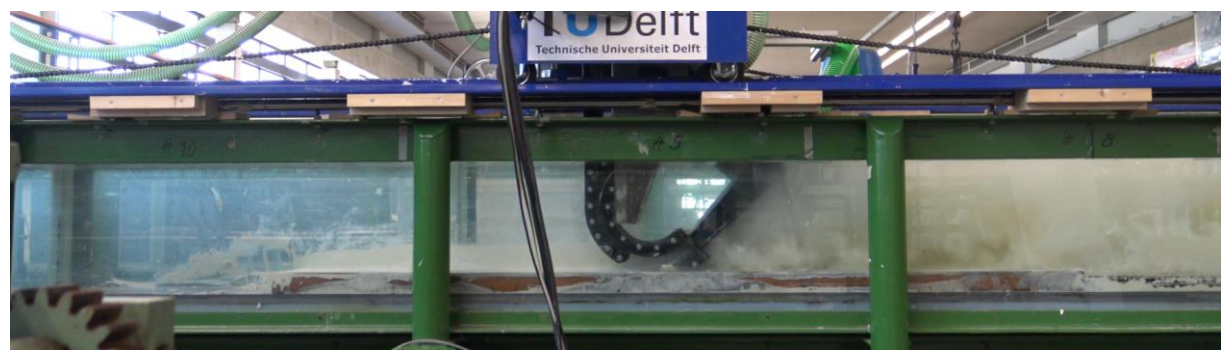


Figure 62 Experiment 18 in progress showing the collector head (without the secondary jet duct) moving over the clay bed.

Table 8 Tests conducted to study the influence of the secondary jet duct.

Test #	Q <sub>mj</sub> [L/s]	V <sub>mj</sub> [m/s]	$Q_{sj}[L/s]$	V <sub>sj</sub> [m/s]	Q <sub>c</sub> [L/s]	c [mm]	V <sub>f</sub> [m/s]
8	4.4	4.4	0.0	0.0	4.4	3.0	0.125
18	4.4	4.4	No duct	-	4.4	3.0	0.125

Figure 63 displays the cross-sectional profiles of Test 8 and Test 18, comparing the cases with and without the secondary jet duct. Notably, Test 18 exhibits significantly more erosion, indicating that the removal of the secondary jet duct leads to an increase in erosion depth. This finding highlights the influential role of the secondary jet duct on clay erosion dynamics in the experimental setup.

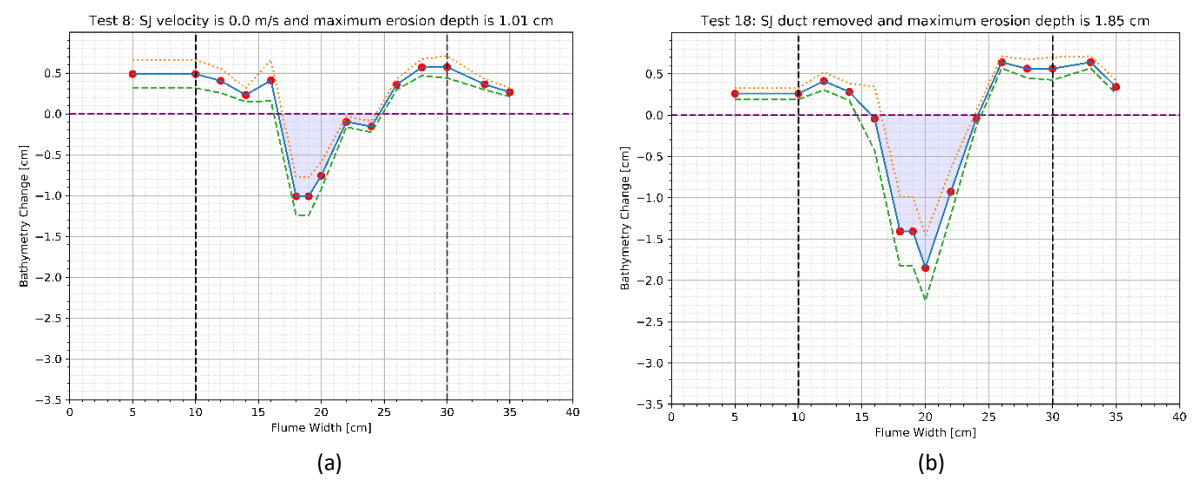


Figure 63 Cross-sectional profiles of Test 8 with the secondary jet velocity held at 0 (a) and Test 18 with the secondary jet duct removed (b), while maintaining all other parameters constant.

The observed decrease in water entrainment and higher erosion when the secondary jet duct was removed can be attributed to the attachment of the flow under the collector head. When the secondary jet duct is present, the flow under the collector head is better attached, leading to more water entrainment and a reduced impingement force on the clay bed. However, in the absence of the secondary jet duct, the flow under the collector head becomes less well-attached, resulting in reduced water entrainment and a higher impingement force on the clay bed. This change in flow dynamics under the collector head directly influences the water entrainment and erosion rates, highlighting the critical role played by the secondary jet duct in influencing these processes in the experimental setup. The study of Alhaddad et al. (2023)also showed that a higher discharge in the collection duct results in a lower erosion depth. This confirms the results obtained from this study.

To assess the attachment of the flow under the collector head, a rope was utilized to indicate the flow direction, as depicted in Figure 64. This experiment maintained the same parameters as test 8. The observation revealed that the rope was not touching the clay bed, indicating a low impingement force and a high water entrainment. The absence of contact between the rope and the clay bed suggests that the flow under the collector head is well-attached, leading to increased water entrainment. This finding supports the notion that the presence of the secondary jet duct contributes to better flow attachment, resulting in higher water entrainment and lower impingement force on the clay bed.



Figure 64 A robe was used to see how the flow is directed under the collector for the conditions of test 8.

## 6.5. Turbidity Currents

The phenomenon of spilling water behind the collector generates a plume that moves in the opposite direction of the collector. To examine this plume's behaviour, videos are recorded for each experimental run to visually assess its characteristics. Additionally, an Ultrasonic Velocity Profiler (UVP) equipped with two transducers operating at 4 MHz is employed to measure the vertical velocity profiles at two specific positions.

Using the video analysis tool 'Tracker,' the front velocity of the turbidity currents is calculated after each experiment, as presented in Table 9. To further examine the behaviour of these turbidity currents, the x-t diagrams, depicting their positions over time, are available in Appendix D1.

Test #	Q <sub>mj</sub> [L/s]	V <sub>mj</sub> [m/s]	Q₅j [L/s]	v <sub>sj</sub> [m/s]	Q <sub>c</sub> [L/s]	c [mm]	V <sub>f</sub> [m/s]	Front velocity [cm/s]
1	4.4	4.4	6.1	0.976	10.5	3	0.5	0.59
2	4.4	4.4	6.1	0.976	10.5	3	0.375	x
3	4.4	4.4	6.1	0.976	10.5	3	0.25	0.59
5	4.4	4.4	6.1	0.976	10.5	3	0.125	1.77
4	4.4	4.4	6.1	0.976	10.5	0	0.125	1.78
6	4.4	4.4	6.1	0.976	10.5	5	0.125	1.67
7	4.4	4.4	6.1	0.976	10.5	8	0.125	1.86
8	4.4	4.4	0	0	4.4	3	0.125	1.63
9	4.4	4.4	3	0.48	7.4	3	0.125	2.45
10	4.4	4.4	4.7	0.752	9.1	3	0.125	1.91
5	4.4	4.4	6.1	0.976	10.5	3	0.125	1.77
11	3	3	6.1	0.976	9.1	3	0.125	x
12	2	2	6.1	0.976	8.1	3	0.125	0.56
13	0	0	6.1	0.976	6.1	3	0.125	0.92
8	4.4	4.4	0	0	0	3	0.125	1.63
18	4.4	4.4	No duct	-		3	0.125	2.69
10	4.4	4.4	4.7	0.752	9.1	3	0.125	1.91
10 con	4.4	4.4	4.7	0.752	9.1	3	0.125	1.36

Using the transducers of the UVP, the vertical velocity profile of the turbidity current is obtained. Figure 65 displays the turbidity current of Test 9, with the transducers measuring the velocity profile of the current's body. Consequently, Figure 66 presents the vertical velocity profiles that were obtained from the measurements. The vertical velocity profiles of the other tests are presented in Appendix D2.

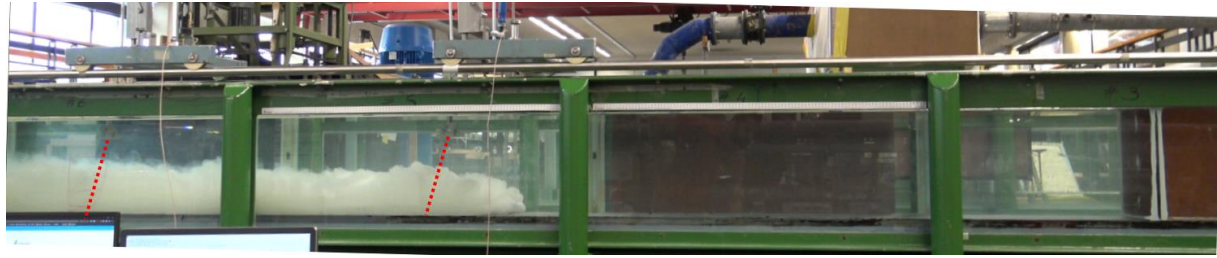


Figure 65 Experiment 9 in progress while the turbidity current reached both transducers.

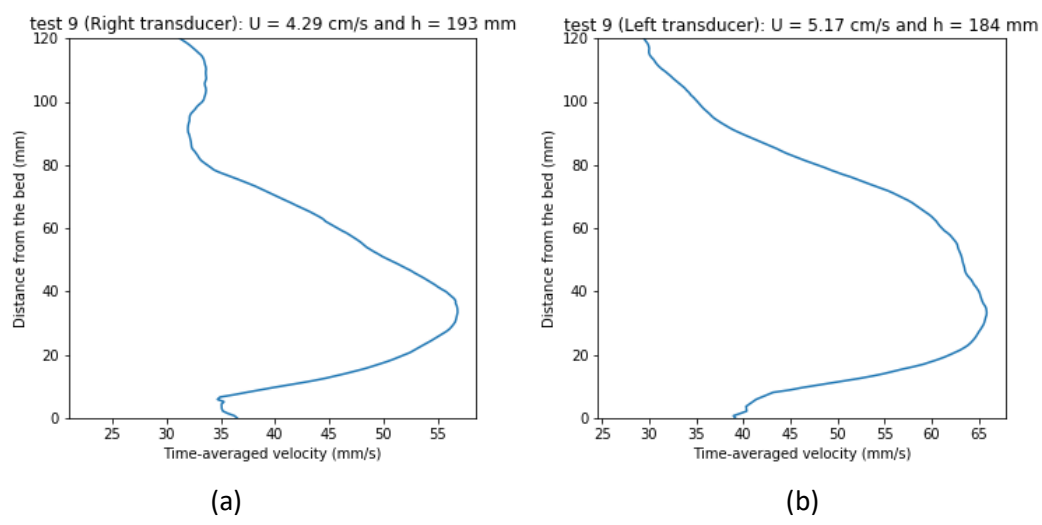


Figure 66 The vertical velocity profiles of turbidity current's body of both the right (a) and left transducers (b).

The data obtained from the velocity and concentration profiles allows for the derivation of crucial parameters characterizing the turbidity current. Among these parameters, the characterizing height (h) in meters represents the thickness of the turbidity current, while the layer-averaged velocity (U) in meters per second reflects the average velocity of the current within its depth. These essential parameters can be determined using the following relations:

$$Uh = \int_0^{z_\infty} u \, \mathrm{d}z \tag{16}$$

$$U^2 h = \int_0^{z_o} u^2 \mathrm{d}z \tag{17}$$

The calculated characterizing height (h) and layer-averaged velocity (U) can be found in Table 10. However, it is important to note that the data is not available for all conducted tests. This limitation is attributed to the UVP malfunctioning during some experiments, requiring the use of another UVP lent from the faculty of 3ME.

The analysis of front velocities and the velocity of the body of the turbidity current reveals minimal variations, indicating the absence of a discernible trend in the behaviour of the spillage plume. Due the lack of significant variations, it is evident that the spillage plume behind the collector remains mostly consistent across different operating parameters. As a result, further investigation into this particular plume may not be necessary, as the change in operating parameters does not appear to have a substantial impact on its behaviour.

Table 10 List of the tests showing the calculated characterizing height h (m) and layer-averaged velocity U (m/s) Using the velocity profile obtained with the UVP.

		Right transducer			Left transducer			
Test #	Front velocity [cm/s]	U [cm/s]	h [mm]	U * h [cm²/s]	U [cm/s]	h [mm]	U * h [cm²/s]	
1	0.59	х	Х	Х	х	Х	Х	
2	x	х	Х	Х	Х	Х	Х	
3	0.59	х	Х	Х	Х	Х	Х	
5	1.77	2.7	120.0	32.0	2.3	132.0	29.7	
4	1.78	2.8	136.0	37.9	2.6	129.0	33.9	
6	1.67	2.8	129.0	35.5	3.0	138.0	40.8	
7	1.86	2.5	130.0	32.9	2.1	126.0	26.1	
8	1.63	2.7	93.0	25.1	2.6	95.0	24.3	
9	2.45	4.3	193.0	82.8	5.2	184.0	95.1	
10	1.91	2.9	148.0	42.5	3.3	151.0	49.4	
5	1.77	2.7	120.0	32.0	2.3	132.0	29.7	
11	x	х	Х	Χ	Х	Х	Х	
12	0.56	х	Х	Х	Х	Х	Х	
13	0.92	х	Х	Х	Х	Х	Х	
8	1.63	2.7	93.0	25.1	2.6	95.0	24.3	
18	2.69	3.3	151.0	49.5	2.6	115.0	29.3	
10	1.91	2.9	148.0	42.5	3.3	151.0	49.4	
10 con	1.36	2.3	179.0	41.5	2.2	91.0	20.3	

# 7. Conclusions

The primary focus of this research was to investigate clay erosion and its relationship with various operating parameters of the collector. By gaining insights into the erosion behaviour, the aim was to minimize clay pickup and maintain low clay concentration in the discharged water at the rear of the collector. This objective is crucial to reduce the size and impact of the discharge plume generated at the rear side of the collector. The study has provided valuable insights into the behaviour of the Coandă-Effect-Based Collector and its impact on cohesive sediment erosion. Addressing several fundamental questions, the research sheds light on the intricate dynamics of water entrainment, erosion patterns, and plume behaviour. These findings hold significant implications for optimizing the collector's design and efficiency while also contributing to a better understanding of the environmental consequences associated with nodules mining activities.

The first question addressed the influence of the collector's forward velocity, jet velocities, and bottom clearance on water entrainment into the collection duct. While actual values for water entrainment were not obtained due to its absence in the experiments, the flow rate in the collection duct was effectively assessed. The results revealed that an increase in the main and/or the secondary jet flow rate corresponded to a higher flow rate in the collection duct, while a larger bottom clearance resulted in a lower flow rate. The present study's investigation of water entrainment behaviour yielded results that differed from previous research. Notably, a larger bottom clearance was found to correspond to a lower flow rate in the collection duct. This observation can be attributed to the interplay of various factors influencing the process. An increase in bottom clearance appears to reduce the pressure gradient, potentially contributing to the observed decrease in flow rate. Furthermore, the controlled experimental setup utilized in this study may introduce unique dynamics, leading to variations in comparison to Alhaddad's findings. These disparities emphasize the intricate nature of the collection mechanism and highlight the importance of gaining a comprehensive understanding of the influencing factors.

The second question explored the influence of the same operating parameters on cohesive sediment erosion, see Figure 67. The research findings indicate an inverse relationship between the collector's forward velocity and the erosion depth of the bed sediment. Slower movement of the collector results in a longer exposure time for the bed sediment to the flow, leading to a greater erosion depth. Conversely, higher forward velocities are associated with shallower erosion depths. Moreover, an increase in the jet velocity contributes to a larger erosion depth. Additionally, when the collector's underside is closer to the sediment bed, a larger portion of the sediment layer is exposed to the water flow, resulting in a more significant erosion depth.

By utilizing the measured erosion depths obtained from the conducted experiments and taking into account the scaling down of the collector head by a factor of 4 in the 2D dimension, we can employ Froude scaling to predict the maximum erosion depth at the full scale. In an extreme scenario, where the forward velocity of the full scale is 25 cm/s, the clearance is 0 mm, and the main and secondary jet velocities are 8.8 m/s and 2.0 m/s, respectively, the maximum erosion depth is calculated to be 9.7 cm. Notably, this maximum erosion depth aligns with expectations and falls within the range reported by Boschen-Rose et al. (2020).

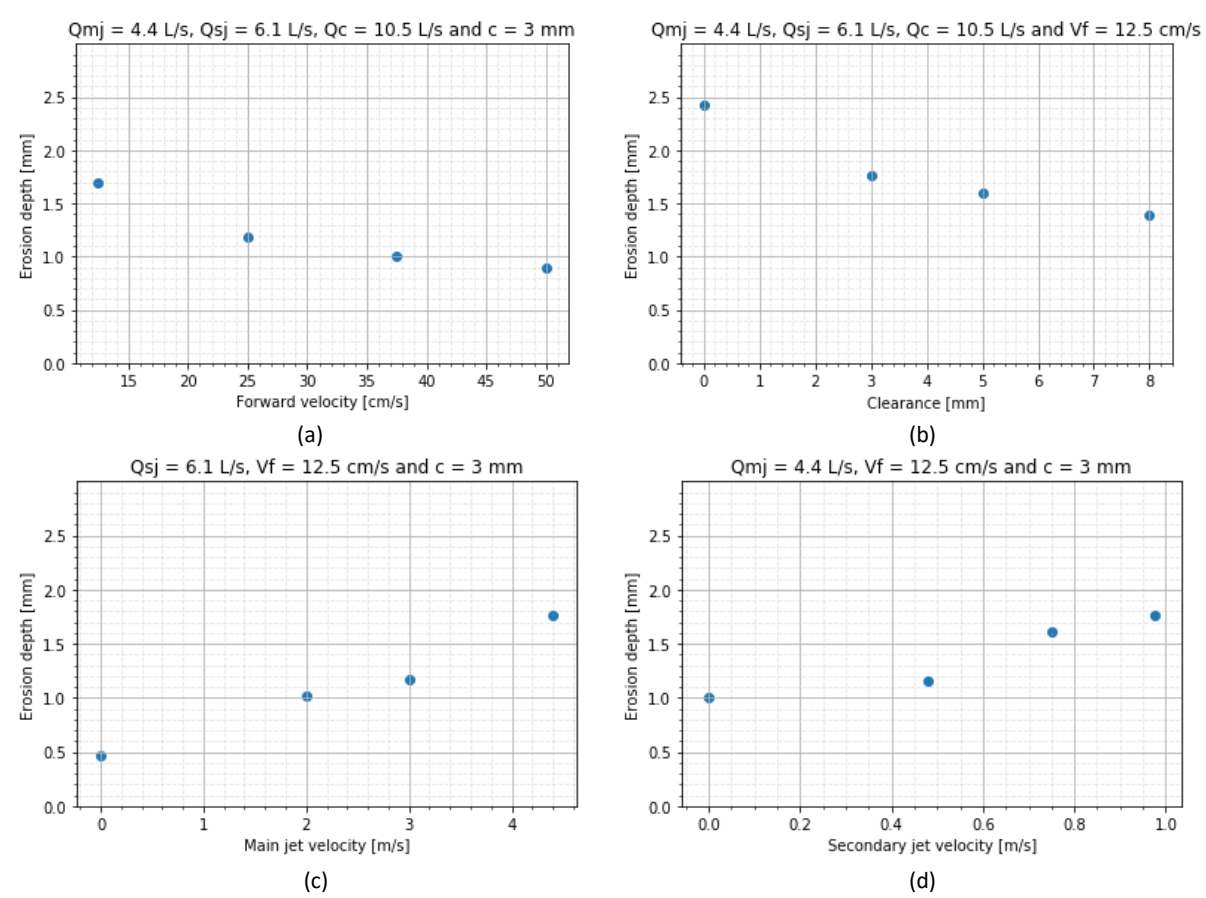


Figure 67 The influence of the collector's forward velocity (a), the bottom clearance (b), the main (c) and the secondary jet velocity (d) on erosion depth of clay.

The main mechanism by which clay is eroded is jetting. The study explored the correlation between erosion depth and both impingement force and dynamic pressure. The findings revealed that a logarithmic function describing the relationship between impingement force and erosion depth did not provide a good fit for the data. Interestingly, this contradicts the results reported by Alhaddad & Helmons (2023) for sand erosion, where a clear logarithmic correlation between erosion depth and impingement force was observed. On the other hand, higher erosion depth is found to be linked to the increase in dynamic pressure, as evidenced by the clear linear correlation observed. The investigation of the relationship between the measured cavity depths ( $Z_c$ ) and the duct height ( $D_n$ ), normalized by the jet ratio ( $p_i/s_u$ ), has revealed a linear correlation. It reveals that the non-dimensional erosion depth increases proportionally with the jet ratio. Despite some scatter in the data, this correlation remains evident.

The presence of the secondary jet duct was the focus of the fourth question, with investigations into its effects on water entrainment and cohesive sediment erosion. Surprisingly, the flow rate in the collection duct was higher with the duct in place, contrary to initial expectations. The observed increase in flow rate suggested the influence of additional factors affecting water entrainment and flow dynamics. The development of a horizontal flow pattern under the collector head with the duct in place likely contributed to the increased flow rate towards the collection duct. This unexpected finding highlights the complexity of flow interactions.

The fifth question cantered on the behaviour of the spillage plume behind the collector. Minimal variations were observed in front velocities and the velocity of the turbidity current, indicating a consistent behaviour of the spillage plume across different operating parameters. This suggests that the change in operating conditions may not significantly impact the behaviour of the spillage plume.

Overall, this research has significantly advanced the understanding of the Coandă-Effect-Based Collector and its influence on cohesive sediment erosion. The findings contribute to the development of more efficient and environmentally friendly sediment mining practices.

### 8. Discussion and Recommendations

In this chapter the key findings and recommendations arising from our research on the Coandă-Effect-Based Collector's behaviour and its impact on cohesive sediment erosion will be explored. The investigation sought to answer fundamental questions related to water entrainment, erosion patterns, and plume behaviour. However, as with any scientific study, there are limitations to consider. The experimental setup and conditions may not perfectly replicate real-world scenarios, and uncertainties may be present in the results due to measurement errors and other external factors. Therefore, future research should continue to explore and refine the understanding of the collector's behaviour under various conditions to achieve more robust and accurate conclusions. Nonetheless, the insights gained from this study are valuable steps towards sustainable and responsible nodules mining practices. For future research it is important to take the following into consideration:

• The use of an experimental setup where the collector head is fully submerged.

A completely submerged collector head indeed presents several advantages that can lead to more accurate and reliable results in sediment collection and erosion studies. By submerging the collector head entirely, it can operate under conditions closer to the natural environment, mimicking the actual flow dynamics and minimizing interference with ambient water movement. One key advantage is the reduction of air-water interactions, which can introduce uncertainties in the experiments. With a fully submerged collector head, air entrainment is eliminated, allowing for a clearer focus on the water-sediment interactions and erosion patterns. This can result in more precise measurements and data collection. Additionally, a fully submerged collector head can minimize turbulence and disturbances caused by the free water surface, creating a more controlled and stable experimental setup. This stability is crucial in accurately studying the effects of different operating parameters on water entrainment and sediment erosion. Furthermore, a completely submerged collector head can better simulate the actual conditions in deep-sea mining scenarios, where the collector operates underwater to extract valuable minerals. By replicating these conditions in the laboratory, the research outcomes become more relevant and applicable to real-world scenarios

• Water entrainment and the effect of the secondary jet duct.

The present study has offered significant insights into the behaviour of water entrainment, particularly in relation to the secondary jet duct. However, a more comprehensive understanding of this process requires further data collection and analysis. The hypothesis formulated based on anticipated flow directions suggests that the secondary jet duct may facilitate the development of a horizontal flow pattern, leading to higher flow velocities under the collector head. This intensified flow could potentially contribute to the observed increase in water entrainment when the secondary jet duct is present with zero flow rate. To validate and comprehend these observations, additional data, including velocity measurements under the collector head and pressure gradient analysis, is necessary. These additional data points will shed light on the intricate interactions and underlying mechanisms influencing flow rate and water entrainment in the presence of the secondary jet duct. By further investigating these aspects, we can enhance the understanding of the collector's behaviour and optimize its performance in cohesive nodule mining processes.

• Reliability of Conductivity-Type Concentration Meter (CCM).

The reliability of the results obtained from the CCM in this study has been questioned due to indications of high concentration in the discharged water. However, further analysis revealed that the calculated eroded area of the clay bed significantly exceeded the actual erosion area, raising doubts about the accuracy of the CCM. To validate the measurements, the erosion rate was calculated, and

real clay concentration in the discharged water was estimated, showing predominantly under 1% concentrations. These findings underscore the limitations of the CCM in detecting low concentrations. Additionally, the CCM's sensitivity to temperature introduces uncertainties, as temperature measurements were not taken during the experiments, hindering the assurance of a constant temperature throughout the tests. Considering these limitations, it is advisable to explore alternative methods or instruments for precisely measuring low clay concentrations in the discharged water to ensure reliable and accurate data in future experiments.

#### Effect of the collection hose.

The collection hose was securely attached to the mobile carriage and positioned on the right side of the flume. The collection hose, when filled, had significant weight, imposing a substantial load on the rear part of the moving mobile carriage. Consequently, this load caused a slight deviation of the collector head towards the left side of the flume during the experiments. This explains why the erosion measurements from all experiments exhibited a slight shift to the right side. An attempt was made to connect the collection hose to a crane situated above the experimental setup. However, this approach resulted in unwanted air voids within the hose, making it impossible for the pump to operate properly.

In conclusion, this research has shed light on important aspects of the Coandă-Effect-Based Collector's behaviour, particularly regarding water entrainment and erosion patterns. However, additional data gathering and refinement of measurement methods are essential to further comprehend the impact of the secondary jet duct and improve the accuracy and reliability of concentration measurements. These recommendations will enhance the understanding of the collector's performance and facilitate more effective design and optimization of the nodule collector.

### References

- Alhaddad, S., & Helmons, R. (2023). Sediment Erosion Generated by a Coandă-Effect-Based Polymetallic-Nodule Collector. *Journal of Marine Science and Engineering*, 11(2), 349. https://doi.org/10.3390/jmse11020349
- Alhaddad, S., Mehta, D., & Helmons, R. (2023). Mining of deep-seabed nodules using a Coandă-effect-based collector. *Results in Engineering*, *17*. https://doi.org/10.1016/j.rineng.2022.100852
- Allseas. (2022, November 14). *Trial run concludes with record haul*. https://allseas.com/news/trial-run-concludes-with-record-haul/
- Beaudoin, Y. C., & Baker, E. (2013). Deep Sea Minerals: Manganese Nodules, a physical, biological, environmental and technical review. Pacific Deep Sea Minerals and Mining View project Global Seafloor Geomorphic Features Map View project.

  https://www.researchgate.net/publication/260596851
- Berlamont, J., Ockenden, M., Toorman, E., & Winterwerp, J. (1993). The characterisation of cohesive sediment properties. In *Coastal Engineering* (Vol. 21).
- Boschen-Rose, R., Stigter, H., Taymans, C., & Mravak, Z. (2020). Blue Nodules Deliverable Report D1.7 Environmental Impact Assessment (EIA) components for test mining up to prototype level (TRL 6).
- Christidis, G. E. (2011). Industrial clays. *European Mineralogical Union Notes in Mineralogy*, *9*(1), 341–414. https://doi.org/10.1180/EMU-notes.9.9
- Deltares. (2016). *Conductivity type concentration meter*. https://www.deltares.nl/app/uploads/2016/04/ CCM-Conductivity-type-concentration-meter.pdf
- Elerian, M., Alhaddad, S., Helmons, R., & van Rhee, C. (2021). Near-Field Analysis of Turbidity Flows Generated by Polymetallic Nodule Mining Tools. *Mining*, 1(3), 251–278. https://doi.org/10.3390/mining1030017
- Fernando, H. J. S. (2013). Handbook of Environmental Fluid Dynamics (Vol. 2). CRC Press.
- Forsberg, P. L., Skinnebach, K. H., Becker, M., Ernstsen, V. B., Kroon, A., & Andersen, T. J. (2018). The influence of aggregation on cohesive sediment erosion and settling. *Continental Shelf Research*, 171, 52–62. https://doi.org/10.1016/j.csr.2018.10.005
- Global Sea Mineral Resources. (2018). Environmental Impact Statement.
- Haldar, S. K. (2018). *Mineral exploration : principles and applications*.
- Hein, J. R., Mizell, K., Koschinsky, A., & Conrad, T. A. (2013a). Deep-ocean mineral deposits as a source of critical metals for high- and green-technology applications: Comparison with land-based resources. In *Ore Geology Reviews* (Vol. 51, pp. 1–14). https://doi.org/10.1016/j.oregeorev.2012.12.001
- Hein, J. R., Mizell, K., Koschinsky, A., & Conrad, T. A. (2013b). Deep-ocean mineral deposits as a source of critical metals for high- and green-technology applications: Comparison with land-based resources. In *Ore Geology Reviews* (Vol. 51, pp. 1–14). https://doi.org/10.1016/j.oregeorev.2012.12.001

- Hong, S., Choi, J.-S., Kim, J.-H., & Yang, C.-K. (1999). Experimental Study On Hydraulic Performance of Hybrid Pick-up Device of Manganese Nodule Collector. International Society of Offshore and Polar Engineers.
- ISA. (1999). PROPOSED TECHNOLOGIES FOR MINING DEEP-SEABED POLYMETALLIC NODULES.
- ISA. (2019). Environmental Impact Assessment for the testing of a pre-protoype manganese nodule collector vehicle in the Eastern German license area (Clarion-Clipperton Zone) in the framework of the European JPI-O MiningImpact 2 research project.
- Krone, R. B. (1963). A STUDY OF RHEOLOGIC PROPERTIES OF ESTUARIAL SEDIMENTS.
- Lang, A. M., Dasselaar, S., Aasly, K., & Larsen, E. (2019). *D3.4 Report describing the process flow overview*.
- Mehta, A. J., Hayter, E. J., Parker, W. R., Krone, R. B., & Teeter, A. M. (1989). *COHESIVE SEDIMENT TRANSPORT. I: PROCESS DESCRIPTION*.
- Miller, K. A., Thompson, K. F., Johnston, P., & Santillo, D. (2018). An overview of seabed mining including the current state of development, environmental impacts, and knowledge gaps. In *Frontiers in Marine Science* (Vol. 4, Issue JAN). Frontiers Media S. A. https://doi.org/10.3389/fmars.2017.00418
- Niner, H. J., Ardron, J. A., Escobar, E. G., Gianni, M., Jaeckel, A., Jones, D. O. B., Levin, L. A., Smith, C. R., Thiele, T., Turner, P. J., Van Dover, C. L., Watling, L., & Gjerde, K. M. (2018). Deep-sea mining with no net loss of biodiversity-an impossible aim. In *Frontiers in Marine Science* (Vol. 5, Issue MAR). Frontiers Media S. A. https://doi.org/10.3389/fmars.2018.00053
- Nobel, A. (2013). On the excavation process of a moving vertical jet in cohesive soil.
- Rhee, C. (2010). *Sedimentation and erosion of sediment at high solids concentration*. https://www.researchgate.net/publication/295074480
- Schulte, S. A. (2013). Vertical transport methods for Deep Sea Mining Section of Dredging Engineering.
- Schwartz. Maurice L. (2005). *Encyclopedia of Earth Sciences Series Encyclopedia of Coastal Science*. Springer.
- Shakeel, A., Kirichek, A., & Chassagne, C. (2021). Rheology and yielding transitions in mixed kaolinite/bentonite suspensions. *Applied Clay Science*, *211*. https://doi.org/10.1016/j.clay.2021.106206
- van Rijn, L. C. (1993). *Principles of sediment transport in rivers, estuaries and coastal seas-Aqua Publications*. Aqua Publications .
- Vanreusel, A., Hilario, A., Ribeiro, P. A., Menot, L., & Arbizu, P. M. (2016). Threatened by mining, polymetallic nodules are required to preserve abyssal epifauna. *Scientific Reports*, *6*. https://doi.org/10.1038/srep26808
- Winterwerp, J. C., & Kesteren, G. M. van. (2004). *Introduction to the Physics of Cohesive Sediment in the Marine Environment*. Elsevier. http://www.clscvicr.com/locatc/pcrmissions
- Winterwerp, J. C., & Kranenburg, C. (2002). *Fine Sediment Dynamics in the Marine Environment*. Elsevier.

Yue, Z., Zhao, G., Xiao, L., & Liu, M. (2021). Comparative Study on Collection Performance of Three Nodule Collection Methods in Seawater and Sediment-seawater Mixture. *Applied Ocean Research*, *110*. https://doi.org/10.1016/j.apor.2021.102606

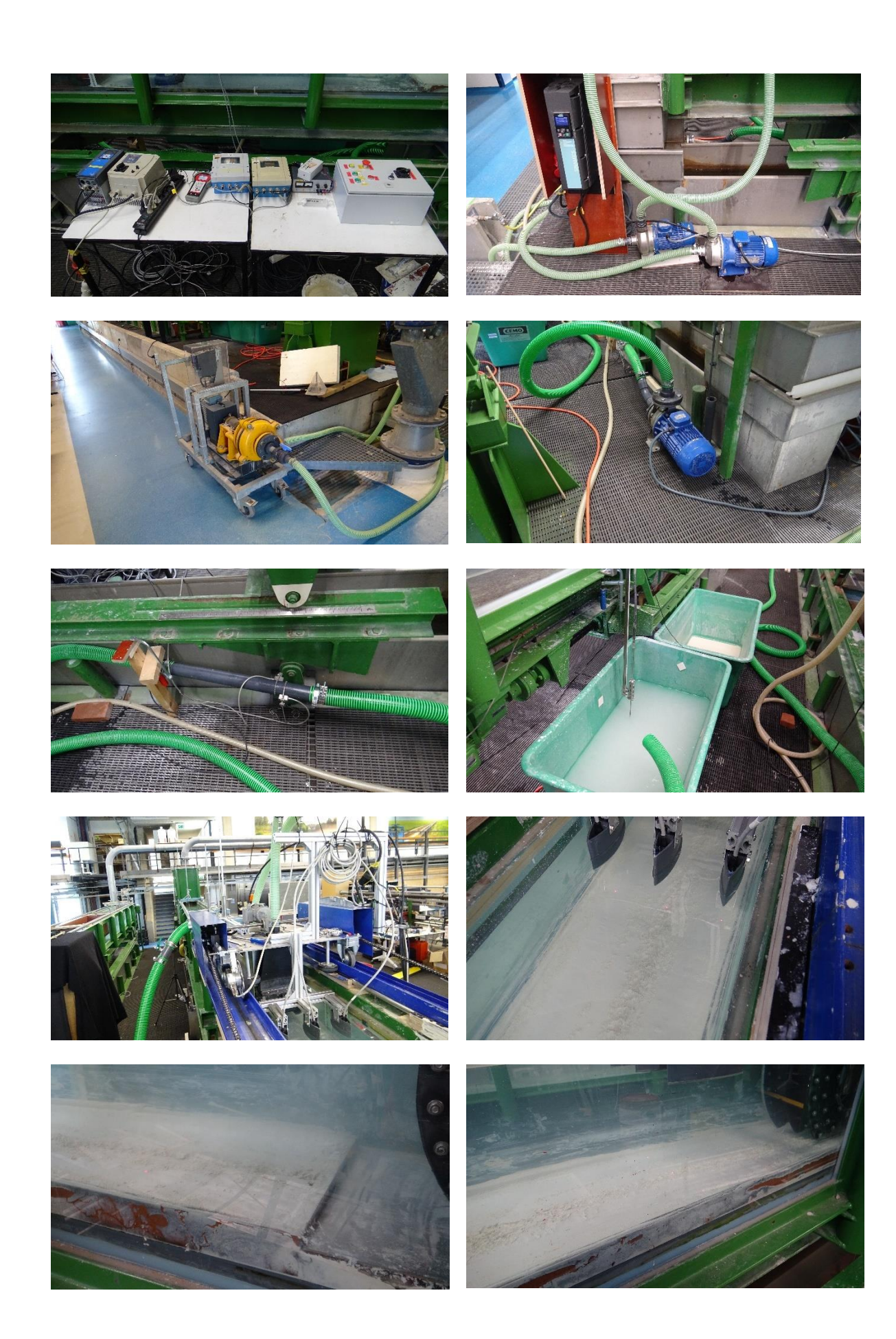
# A. Experimental Setup































## B. Water Entrainment

## B1. Influence of The Different Parameters

Table 11 A series of experiments conducted to study the water entrainment while the collector is stationary.

	Qmj [L/s]	Qsj [L/s]	c [mm]	EMS [V]	Velocity [m/s]	Velocity 45 degree [m/s]	Q [L/s]	Fv [cm/s]
Test								
1	4.0	4.70	0.0	-3.95	0.403	0.570	1.03	0
2	4.0	0.00	0.0	-1.24	0.129	0.182	0.33	0
3	4.0	3.13	0.0	-3.01	0.308	0.436	0.79	0
4	3.0	4.70	0.0	-2.40	0.246	0.348	0.63	0
5	4.4	6.00	0.0	-5.28	1.320	1.867	3.38	0
6	4.4	4.70	0.0	-4.57	1.146	1.621	2.93	0
7	4.4	5.70	0.0	-4.97	1.244	1.759	3.18	0
8	4.0	4.70	7.5	-3.12	0.319	0.451	0.82	0
9	4.0	0.00	7.5	-0.61	0.064	0.091	0.16	0
10	4.0	3.13	7.5	-2.91	0.298	0.421	0.76	0
11	3.0	4.70	7.5	-1.91	0.197	0.279	0.50	0
12	4.4	6.00	7.5	-4.62	1.159	1.639	2.96	0
13	4.4	4.70	7.5	-4.11	1.033	1.461	2.64	0
14	4.4	5.70	7.5	-4.51	1.132	1.601	2.90	0
15	4.0	4.70	13.5	-2.13	0.219	0.310	0.56	0
16	4.0	0.00	13.5	-0.00	0.002	0.003	0.01	0
17	4.0	3.13	13.5	-1.77	0.182	0.257	0.46	0
18	3.0	4.70	13.5	-0.72	0.076	0.107	0.19	0
19	4.4	6.00	13.5	-3.38	0.346	0.489	0.88	0
20	4.4	4.70	13.5	-2.68	0.275	0.389	0.70	0
21	4.4	5.70	13.5	-3.32	0.340	0.481	0.87	0

# B2. Influence of The Secondary Jet Duct

Table 12 List of tests done while maintaining the secondary jet velocity at 0.

Test #	Q <sub>mj</sub> [L/s]	Q <sub>sj</sub> [L/s]	c [mm]	v <sub>f</sub> [m/s]
1	2.0	0.0	0.0	0.000
2	3.0	0.0	0.0	0.000
3	4.4	0.0	0.0	0.000
4	2.0	0.0	0.0	0.125
5	3.0	0.0	0.0	0.125
6	4.4	0.0	0.0	0.125
7	2.0	0.0	0.0	0.250
8	3.0	0.0	0.0	0.250
9	4.4	0.0	0.0	0.250
10	2.0	0.0	10.0	0.000
11	3.0	0.0	10.0	0.000
12	4.4	0.0	10.0	0.000
13	2.0	0.0	10.0	0.125
14	3.0	0.0	10.0	0.125
15	4.4	0.0	10.0	0.125
16	2.0	0.0	10.0	0.250
17	3.0	0.0	10.0	0.250
18	4.4	0.0	10.0	0.250
19	2.0	0.0	18.0	0.000
20	3.0	0.0	18.0	0.000
21	4.4	0.0	18.0	0.000
22	2.0	0.0	18.0	0.125
23	3.0	0.0	18.0	0.125
24	4.4	0.0	18.0	0.125
25	2.0	0.0	18.0	0.250
26	3.0	0.0	18.0	0.250
27	4.4	0.0	18.0	0.250

# C. Clay Bed Erosion

### C1. Preparation of Clay

Different clay mixtures were prepared and tested.

					mm	kPa			
Test #	Betonite	Kaolinite	Water content	Fa	II cone test	Shear strength			
1	1	0	20%		-		Difficult to	mix. Swel	ls fast
2	0.42	0.85	35%		-		Difficult to	mix c	
3	0.34	0.66	45%		9	1.08			
4	0.25	0.75	35%		-		Difficult to	mix c	
5	0.25	0.75	45%		13	0.52			
6	0.17	0.83	45%		14.5	0.42			
7	0.08	0.92	45%		24	0.15			
8	0.08	0.92	55%		Too soft	-			

Experiments were conducted using batch 7, but erosion did not take place, see picture below.





Before After

Finally batch 8 was used to conduct the experiments.

### C2. Conducted Experiments

### To study the influence of the forward velocities the following tests are conducted.

Table 13 The four tests conducted to investigate the influence of the collector's forward velocity.

Test #	Q <sub>mj</sub> [L/s]	V <sub>mj</sub> [m/s]	Q <sub>sj</sub> [L/s]	V <sub>sj</sub> [m/s]	Q <sub>c</sub> [L/s]	c [mm]	V <sub>f</sub> [m/s]
1	4.4	4.4	6.1	0.976	10.5	3.0	0.5
2	4.4	4.4	6.1	0.976	10.5	3.0	0.375
3	4.4	4.4	6.1	0.976	10.5	3.0	0.25
5	4.4	4.4	6.1	0.976	10.5	3.0	0.125

#### To study the influence of the bottom clearance the following tests are conducted.

Table 14 The four tests conducted to investigate the influence of the bottom clearance under the collector head.

Test #	Q <sub>mj</sub> [L/s]	V <sub>mj</sub> [m/s]	Q <sub>sj</sub> [L/s]	V <sub>sj</sub> [m/s]	Qc [L/s]	c [mm]	V <sub>f</sub> [m/s]
4	4.4	4.4	6.1	0.976	10.5	0.0	0.125
5	4.4	4.4	6.1	0.976	10.5	3.0	0.125
6	4.4	4.4	6.1	0.976	10.5	5.0	0.125
7	4.4	4.4	6.1	0.976	10.5	8.0	0.125

#### To study the influence of the main jet velocity the following tests are conducted.

Table 15 The four tests conducted to investigate the influence of the main jet velocity.

Test #	Q <sub>mj</sub> [L/s]	V <sub>mj</sub> [m/s]	Q <sub>sj</sub> [L/s]	V <sub>sj</sub> [m/s]	Q <sub>c</sub> [L/s]	c [mm]	V <sub>f</sub> [m/s]
5	4.4	4.4	6.1	0.976	10.5	3.0	0.125
11	3.0	3.0	6.1	0.976	9.1	3.0	0.125
12	2.0	2.0	6.1	0.976	8.1	3.0	0.125
13	0.0	0.0	6.1	0.976	6.1	3.0	0.125

#### To study the influence of the main jet velocity the following tests are conducted.

Table 16 The four tests conducted to investigate the influence of the secondary jet velocity.

Test #	Q <sub>mj</sub> [L/s]	V <sub>mj</sub> [m/s]	Q <sub>sj</sub> [L/s]	V <sub>sj</sub> [m/s]	Q <sub>c</sub> [L/s]	c [mm]	V <sub>f</sub> [m/s]
8	4.4	4.4	0.0	0.0	4.4	3.0	0.125
9	4.4	4.4	3.0	0.48	7.4	3.0	0.125
10	4.4	4.4	4.7	0.752	9.1	3.0	0.125
5	4.4	4.4	6.1	0.976	10.5	3.0	0.125

#### To study the influence of the time the following tests are conducted.

Table 17 Repetition of experiment 10 after allowing the clay bed to consolidate for three days.

Test #	$Q_{mj}$ [L/s]	V <sub>mj</sub> [m/s]	$Q_{sj}[L/s]$	V <sub>sj</sub> [m/s]	Q <sub>c</sub> [L/s]	c [mm]	V <sub>f</sub> [m/s]
10	4.4	4.4	4.7	0.752	9.1	3.0	0.125
10 cons.	4.4	4.4	4.7	0.752	9.1	3.0	0.125

#### To study the reproducibility of experiments the following tests are conducted.

Table 18 Repetition of experiment 5 under the same conditions.

Test #	Q <sub>mj</sub> [L/s]	V <sub>mj</sub> [m/s]	$Q_{sj}[L/s]$	V <sub>sj</sub> [m/s]	Q <sub>c</sub> [L/s]	c [mm]	V <sub>f</sub> [m/s]
5	4.4	4.4	6.1	0.976	10.5	3.0	0.125
5 rep.	4.4	4.4	6.1	0.976	10.5	3.0	0.125

## C3. CCM Results

Test Matrix											Ve	Based on Ve	Based on CCIV	_
Test # (	Qmj [L/s]	vmj [m/s]	Qsj [L/s]	vsj [m/s]	Qc [L/s]	c[mm]	vf [m/s]	vf [m/s] Erosion depth [cm] Eroded area [cm2]	Eroded area [cm2]	Disturbance [cm2]	Erosion rate [cm3/s]	Concentration [%]	CCM[%]	area [cm2]
1	4.4	4.4	6.1	0.976	10.5	æ	0.5	0.89	3.07	9.74	154	1.15	3.87	10.33
2	4.4	4.4	6.1	0.976	10.5	e	0.375	П	3.54	0.27	133	1	3.39	12.04
3	4.4	4.4	6.1	0.976	10.5	3	0.25	1.18	5.05	0.59	126	0.95	3.84	20.48
2	4.4	4.4	6.1	0.976	10.5	e	0.125	1.76	11.09	0.78	139	1.04	3.24	34.56
4	4.4	4.4	6.1	0.976	10.5	0	0.125	2.43	14.83	1.15	185	1.39	4.36	45.52
9	4.4	4.4	6.1	0.976	10.5	2	0.125	1.6	80.6	5.71	113	0.85	4.46	47.61
7	4.4	4.4	6.1	0.976	10.5	∞	0.125	1.39	5.6	10.62	70	0.53	3.47	36.96
∞	4.4	4.4	0	0	4.4	æ	0.125	П	3.77	9.07	141	1.06	3.99	14.17
6	4.4	4.4	ĸ	0.48	7.4	33	0.125	1.16	5.75	89:0	72	0.76	3.87	29.07
10	4.4	3	4.7	0.752	9.1	e	0.125	1.61	6.62	2.52	83	0.72	3.36	31.07
2	4.4	4.4	6.1	0.976	10.5	3	0.125	1.76	11.09	0.78	139	1.04	3.24	34.56
11	3	3	6.1	0.976	9.1	Э	0.125	1.17	13.36	0	167	1.45	3.3	30.47
12	2	2	6.1	0.976	8.1	e	0.125	1.02	6.94	1.78	87	1.12	3.6	22.32
13	0	0	6.1	0.976	6.1	e	0.125	0.46	7.22	1.45	06	1.17	3.85	23.86
∞	4.4	4.4	0	0	4.4	Э	0.125	1	3.77	9.07	141	1.06	3.99	14.17
18	4.4	4.4	duct removed		4.4	3	0.125	1.85	8.28	8.6	103	1.84	6.28	28.09
19	3	3	4.4	0.704	7.4	3	0.125	0.56	2.44	7.17	30	0.32	5.92	44.49
6	4.4	4.4	3	0.48	7.4	3	0.125	1.16	5.75	0.68	72	0.76	3.87	29.07
2	4.4	4.4	6.1	0.976	10.5	3	0.125	1.76	11.09	0.78	139	1.04	3.24	34.56
5 rep	4.4	4.4	6.1	0.976	10.5	3	0.125	1.69	10.58	5.17	132	0.99	3.79	40.42
10	4.4	4.4	4.7	0.752	9.1	3	0.125	1.61	6.62	2.52	83	0.72	3.36	31.07
10 con	4.4	4.4	4.7	0.752	9.1	m	0.125	1.42	6.13	3.29	77	0.66	2.96	27.35

# C4. Pictures of Eroded Clay Bed after Experiments

Test 1





Test 2





Test 3





Test 4





Test 5





Test 6





Test 7





Test 8





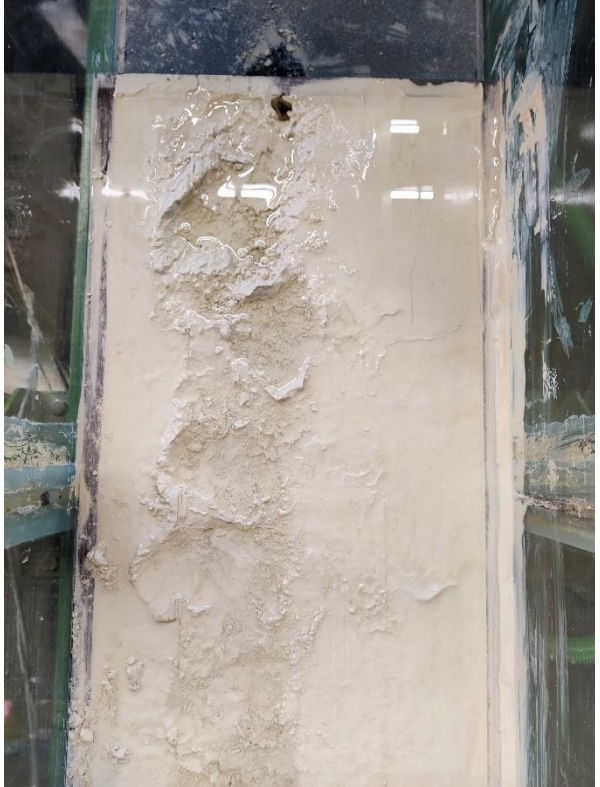
Test 9





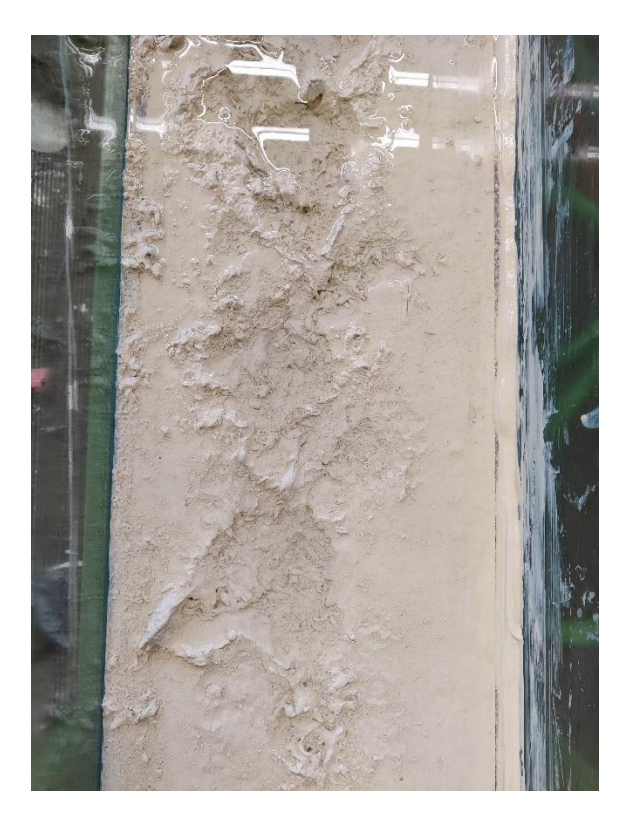
Test 11





Test 12





Test 13



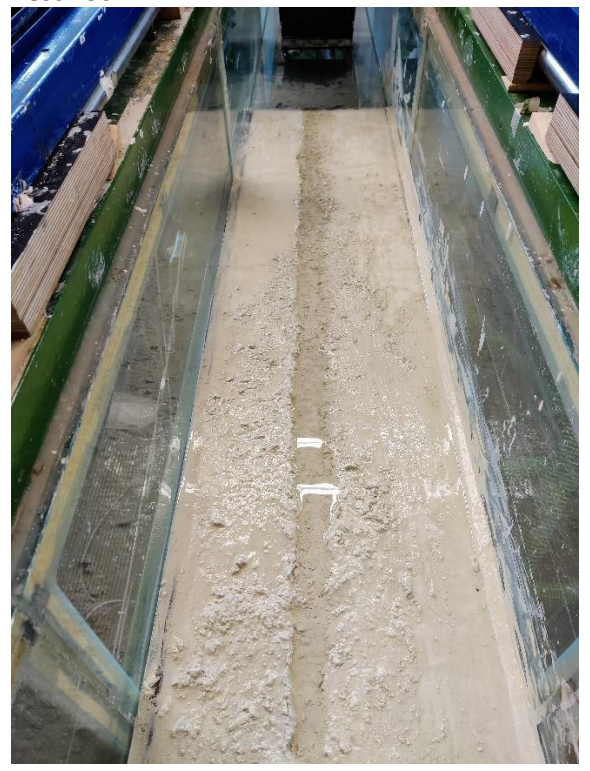


Test 5 repetition





Test 10c



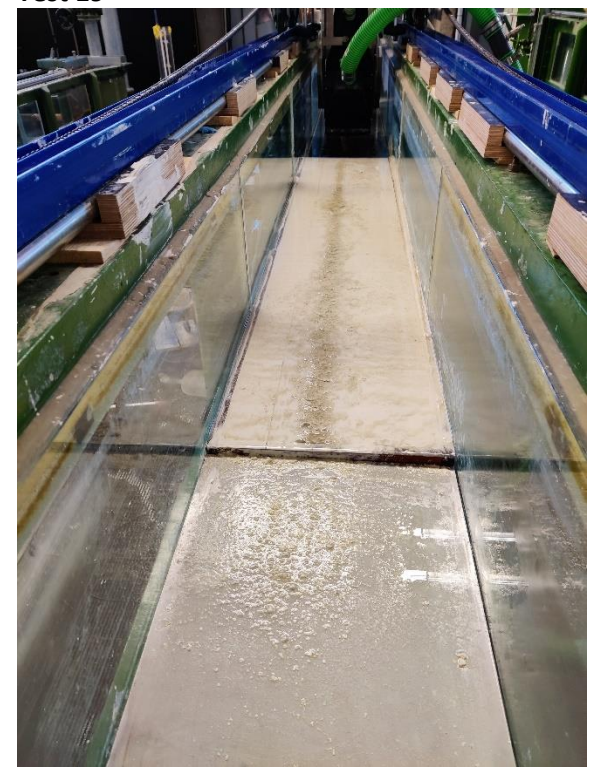


Test 18





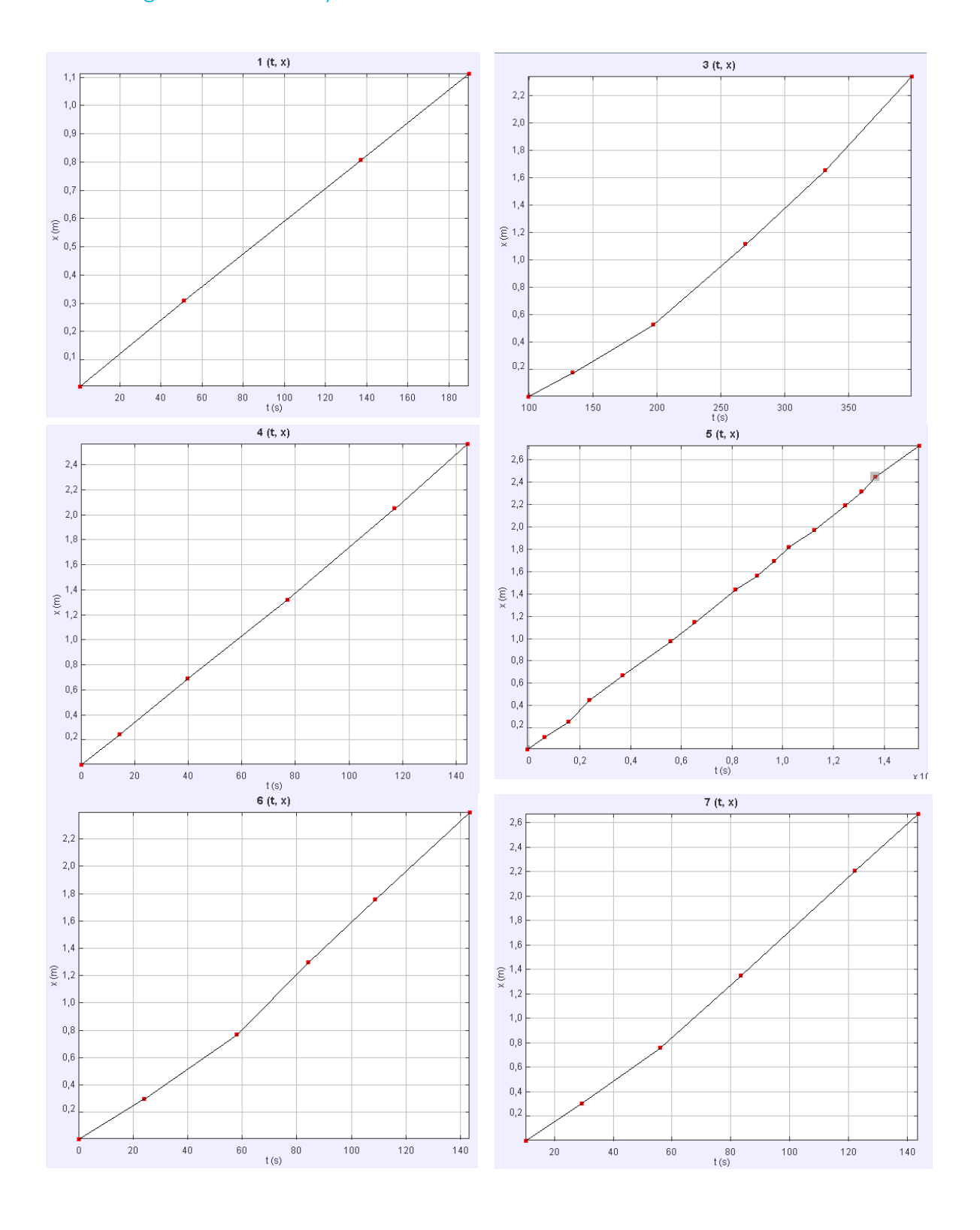
Test 19

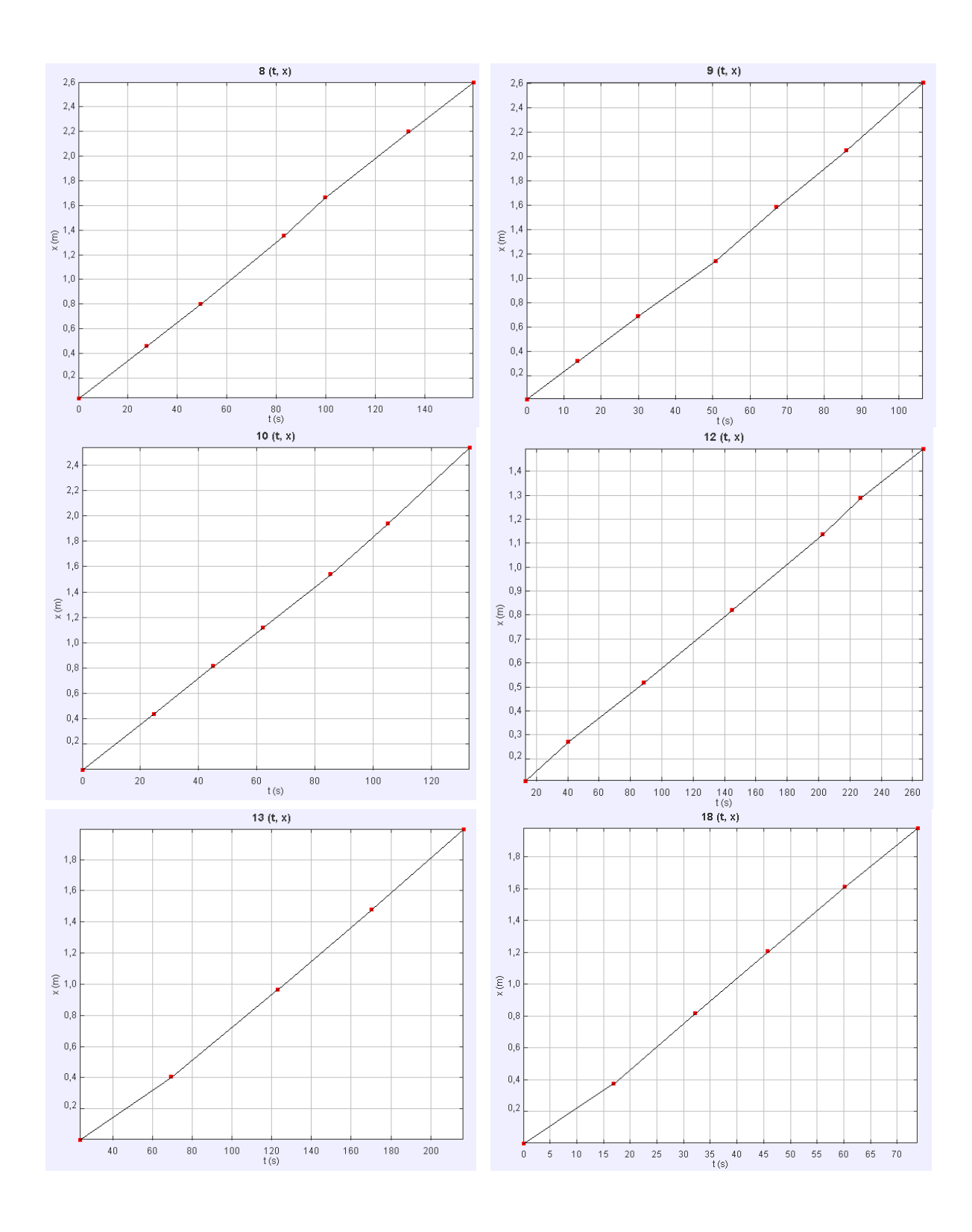


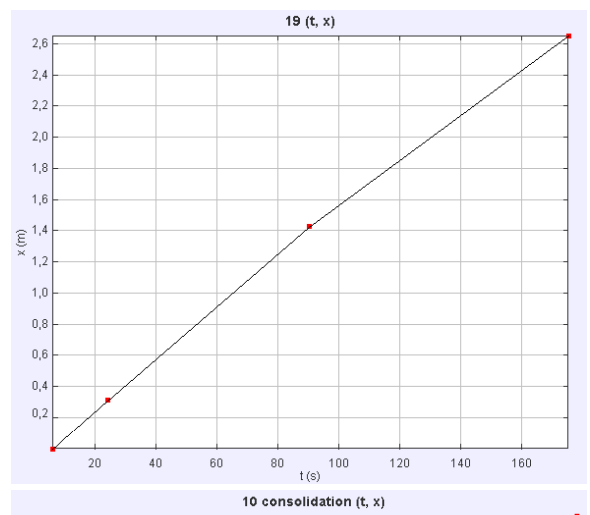


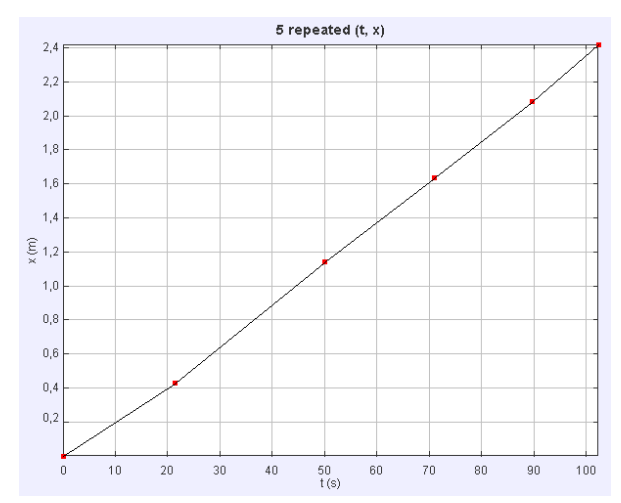
# D. Turbidity currents

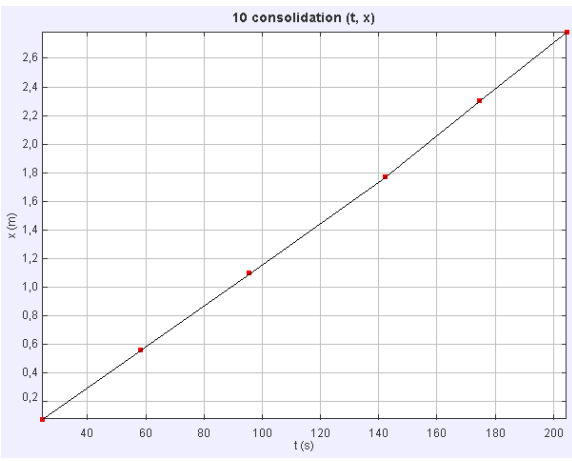
## D1. x-t Diagrams of Turbidity Currents











### D2. Vertical Velocity Profiles

